

**CONTROL STRATEGIES FOR POWER ELECTRONIC INTERFACES IN
UNBALANCED DIESEL HYBRID MINI-GRIDS WITH RENEWABLE
SOURCES AND STORAGE**

Nayeem Ahmed Ninad

A Thesis

In the Department

of

Electrical and Computer Engineering

Presented in Partial Fulfillment of the Requirements

For The Degree Of

Doctor of Philosophy (Electrical and Computer Engineering) at

Concordia University

Montreal, Quebec, Canada

May, 2013

© Nayeem Ahmed Ninad, 2013

CONCORDIA UNIVERSITY
SCHOOL OF GRADUATE STUDIES

This is to certify that the thesis prepared

By: **Nayeem Ahmed Ninad**

Entitled: **Control Strategies for Power Electronic Interfaces in Unbalanced Diesel Hybrid Mini-Grids with Renewable Sources and Storage**

and submitted in partial fulfillment of the requirements for the degree of

Doctor of Philosophy (Electrical and Computer Engineering)

complies with the regulations of the University and meets the accepted standards with respect to originality and quality.

Signed by the final examining committee:

_____	Chair
Dr. M. Pugh	
_____	External Examiner
Dr. M. Tariq Iqbal	
_____	External to Program
Dr. A. Dolatabadi	
_____	Examiner
Dr. S. Hashtrudi Zad	
_____	Examiner
Dr. S. Williamson	
_____	Thesis Supervisor
Dr. L.A.C. Lopes	

Approved by _____
Dr. J.X. Zhang, Graduate Program Director

Date: May 29, 2013

Dr. Robin A.L. Drew, Dean
Faculty of Engineering and Computer Science

ABSTRACT

Control Strategies for Power Electronic Interfaces in Unbalanced Diesel Hybrid Mini-Grids with Renewable Sources and Storage

Nayeem Ahmed Ninad, Ph. D.

Concordia University, 2013

Traditionally, remote communities worldwide consist of autonomous power systems (mini-grids) supplied almost exclusively by diesel-engine generator sets (gensets) at relatively high costs. Integration of renewable energy sources (RESs), such as, photovoltaic (PV) and wind, can substantially reduce the cost of electricity generation and emissions in these remote communities. However, the highly variable load profile typical of mini-grids and the fluctuating characteristics of the RESs, cause frequent operation of the diesel genset at low loading condition, at low efficiency points and subject to carbon build up, which can significantly affect the maintenance costs and even the life time of the genset. Another important issue that is frequently overlooked in small (< 100 kVA) mini-grids, which usually present a low number of loads thus reducing the averaging effect, is load unbalance. Diesel gensets supplying unbalanced loads experience overheating in the synchronous generator and vibration in the shaft. For efficient operation, the genset should be operated near its full capacity and also in balanced mode.

In order to address the above mentioned issues, a fast and reliable *multi-mode* battery energy storage system (BESS) employing voltage source inverter (VSI), is proposed in this thesis. In the *genset support mode*, as a basic feature, it can provide minimum

loading for the genset and supplement it under peak load conditions. In addition, it can also provide load balancing and reactive power compensation for the mini-grid system. Therefore, the genset operates in balanced condition and within its ideal power range. In cases when the power demand from the genset is low, due to high supply of RESs and/or low load consumption, the genset can be shut-down and the BESS forms the grid, regulating voltage and frequency of the mini-grid system in the *grid forming* mode. Besides, the logic for defining the operating mode of the BESS and for achieving smooth transitions between *modes* are also presented in this thesis.

The conventional approach for the control of three-phase VSI with unbalanced loads uses three-phase vector (dq) control and symmetrical components calculator which usually results in slow dynamic responses. Besides, the common power (P) vs. frequency (f) droop characteristic of the genset results in the mini-grid operating with variable frequency what further complicates the design of the controller for the VSI. Therefore, a new frequency adaptive per-phase dq-control scheme for three-wire and four-wire three-phase VSI based on the concept of fictive axis emulation is presented. It enables the control of current/voltage of each phase separately to achieve better dynamic performance in the variable frequency diesel hybrid mini-grid system. The effectiveness of the proposed techniques is demonstrated by means of simulation and experimental results.

ACKNOWLEDGEMENTS

I would like to express my deep and sincere gratitude to all people who supported me throughout the years of my Ph. D. studies and beyond. First and foremost, I am truly indebted to my thesis supervisor, Dr. Luiz Lopes, who is not only the most hard working person I have ever come across but also a dedicated and extremely helpful professor. I appreciate his critical thinking, amazing scientific knowledge, but essentially his extraordinary precision. Our discussions enabled me to develop my capabilities as a researcher and to improve my capacity to handle different tasks in a proper manner, which will also help me, for sure, in my future career. It would have been impossible for me to accomplish this endeavor without his constant support, guidance and motivations.

I thank professors Sheldon Williamson and Pragasen Pillay for allowing me to participate in a variety of activities during these four years in the Ph. D. program.

My sincere gratitude goes to all my friends and colleagues from the Power Electronics and Energy Research (PEER) group at Concordia University for their smart suggestions and valuable discussions throughout my Ph. D. I also appreciate the funding support from the Natural Sciences and Engineering Research Council (NSERC) of Canada, Quebec Funds for Research on Nature and Technology (FQRNT) and Concordia University.

Finally, my very special thanks go to my wife, Samia Enayet, and her family. She always gave me words of encouragement and strong support throughout the duration of my studies. Her patience and friendship were always present even in the most difficult moments. I would also like to thank my family, specially my father, Nazim Uddin Ahmed, and my mother, Suraiya Zaman, for their encouragement, understanding, unconditional love and support during my whole life.

TABLE OF CONTENTS

LIST OF FIGURES	X
LIST OF TABLES	XVI
NOMENCLATURE	XVII
CHAPTER 1	1
INTRODUCTION	1
1.1 Diesel Dominated Hybrid Mini-grids	3
1.1.1 The Diesel Genset	4
1.1.2 Operational Aspects of Diesel Genset	7
1.1.3 Renewable Energy Sources in Mini-grids	8
1.2 Operational and Power Quality Issues in Diesel Hybrid Mini-grid	9
1.3 Current Control of Single-Phase Inverters	17
1.4 Thesis Outline and Contributions	19
CHAPTER 2	26
VECTOR CONTROL OF SINGLE-PHASE VOLTAGE SOURCE INVERTER	26
2.1 Conventional Vector Control Approach for VSI	27
2.2 Proposed Vector Control Strategy Based on Fictive Axis Emulation	29
2.2.1 Basic Concept	29
2.2.2 Design of the Current Controller	30
2.3 Performance Verification and Comparison	33
2.3.1 Simulation Results	33
2.3.2 Experimental Results	35

2.4	Vector Controlled Single-Phase Inverters under Variable Frequency Operation in Autonomous Microgrids/Mini-Grids	41
2.4.1	Frequency Adaptive Single-Phase DQ Control Schemes.....	43
2.4.2	Simulation Results for the Proposed Method	44
2.4.3	Experimental Results	45
2.5	Summary of Chapter 2	48
CHAPTER 3		50
PER-PHASE VECTOR (DQ) CONTROLLED THREE-PHASE GRID FORMING INVERTER.....		50
3.1	Per-Phase DQ Control of a Three-Phase Three-Wire Grid Forming VSI.....	53
3.1.1	Conventional VSI Control Approach.....	54
3.1.1.1	VSI Employing Cascaded Control Loop.....	55
3.1.1.2	Extraction of the Symmetrical Components	56
3.1.2	Proposed Per-Phase DQ Control Approach.....	57
3.1.2.1	The Per-Phase Cascaded dq Control Block.....	57
3.1.3	Performance Verification.....	60
3.2	Per-Phase DQ Control of a Three-Phase Four-Wire Grid Forming VSI with Δ -Y Transformer.....	64
3.2.1	Control Strategy with the Impact of Δ -Y Transformer.....	65
3.2.2	Performance Verification.....	68
3.3	Per-Phase DQ Control of a Four-Leg Grid Forming VSI	72
3.3.1	Emulation of the Fictive Circuit in the Current Loop of a Four-Leg Inverter with Neutral Impedance	74

3.3.2	Generation of the Inverter Output Voltage	75
3.3.3	Performance Verification	77
3.3.3.1	Simulation Study	77
3.3.3.2	Experimental Study	83
3.4	Summary of Chapter 3	88
CHAPTER 4		90
BESS OPERATION IN DIESEL HYBRID MINI-GRID		90
4.1	Description of the System	91
4.2	Control Circuit of the BESS	94
4.2.1	The Per-Phase Cascaded DQ Control Block	96
4.2.2	Reference Current Generation in Genset Support Mode	98
4.2.2.1	Negative Sequence Component Extraction from Load Current	98
4.2.2.2	BESS Capacitor Current Compensation	99
4.2.2.3	Load Reactive Power Compensation	100
4.2.2.4	BESS' Active Component Current Calculation to Operate the Genset within the Desired Range	101
4.2.3	Mode Selection and Transition System (MSTS) Module	103
4.2.3.1	'mode' Signal	104
4.2.3.2	'g _{s2f} ' Signal and the Corresponding Transition Process	105
4.2.3.3	'g _{f2s} ' Signal and the Corresponding Transition Process	107
4.2.3.4	Loading & Unloading of Genset Current during Transition Processes ...	109
4.2.4	PLL+ICA Module	111
4.3	Diesel Genset Model	117

LIST OF FIGURES

Fig. 1.1. Typical diesel dominated hybrid mini-grid.	4
Fig. 1.2. Basic diagram of a diesel genset.....	4
Fig. 1.3. Isochronous operation. (a) Steady state frequency vs. load operation and (b) Dynamic response.	6
Fig. 1.4. Droop operation. (a) Steady state frequency vs. load operation and (b) Dynamic response.....	7
Fig. 2.1. Vector (dq) control applied to a three-phase inverter using standard PI controllers and feed-forward decoupling networks.	27
Fig. 2.2. Vector (dq) control applied to a single-phase inverter (original technique).....	28
Fig. 2.3. Proposed scheme for implementing vector (dq) control in single-phase inverters.	30
Fig. 2.4. Schematic of the system.	31
Fig. 2.5. Equivalent model of the power circuit in the dq (rotating) frame.	32
Fig. 2.6. Response for variation in I_d^* and I_q^* of new vector control technique for single-phase inverters.	33
Fig. 2.7. Response for variation in I_d^* and I_q^* of conventional vector control technique for three-phase inverters.	34
Fig. 2.8. Response for variation in I_d^* and I_q^* of conventional vector control technique for single-phase inverters.....	35

Fig. 2.9. Conventional vector (dq) control technique for single-phase inverters with 100 Hz PI. a) Fixed frame currents; b) Rotating frame currents; c) Harmonic spectrum of the line current.	37
Fig. 2.10. New vector (dq) control technique for single-phase inverters with 100 Hz PI. a) Fixed frame currents; b) Rotating frame currents; c) Harmonic spectrum of the line current.	38
Fig. 2.11. New vector (dq) control technique for single-phase inverters with 400 Hz PI. a) Fixed frame currents; b) Rotating frame currents; c) Harmonic spectrum of the line current.	39
Fig. 2.12. Conventional vector (dq) control technique for single-phase inverters with a 100 Hz current loop. a) Fixed frame currents; b) Rotating frame currents.....	40
Fig. 2.13. New vector (dq) control technique for single-phase inverters with a 100 Hz current loop. a) Fixed frame currents; b) Rotating frame currents.	40
Fig. 2.14. New vector (dq) control technique for single-phase inverters with a 400 Hz current loop. a) Fixed frame currents; b) Rotating frame currents.	41
Fig. 2.15. Actual dq axis currents for T/4 delay method when the frequency varies.	42
Fig. 2.16. Frequency adaptive second order generalized integrator (SOGI).	43
Fig. 2.17. d and q current waveforms and angular frequency.....	44
Fig. 2.18. Steady state results for single-phase dq control with FAE at 62 Hz. a) Fixed frame currents; b) Rotating frame currents.	45

Fig. 2.19. Transient response results for single-phase dq control with FAE at 62 Hz. a) Fixed frame currents; b) Rotating frame currents.....	46
Fig. 2.20. Response to frequency variation for single-phase dq control with FAE. a) Fixed frame currents; b) Rotating frame currents; c) Frequency.....	47
Fig. 2.21. Transient response results for single-phase dq control with two SOGI at 62 Hz. a) Fixed frame currents; b) Rotating frame currents.....	48
Fig. 3.1. Circuit diagram of a three-phase three-wire grid forming inverter operating in diesel-hybrid mini-grid with single-phase RES and unbalanced load.	53
Fig. 3.2. Circuit diagram for conventional cascaded control of grid forming inverter.....	54
Fig. 3.3. Cascaded voltage and current regulation loops for the conventional method....	55
Fig. 3.4. Schematic of the system on per-phase basis.....	57
Fig. 3.5. Schematic diagram of the per-phase cascaded control block.	59
Fig. 3.6. Waveforms for the per-phase vector control. a) Load voltages and currents; b) dq-frame reference and actual voltages for the three phases; c) dq-frame reference and actual inverter currents for the three phases	62
Fig. 3.7. Waveforms for the conventional vector control. a) Load voltages and currents; b) dq-frame reference and actual voltages; c) dq-frame reference and actual inverter currents.....	63
Fig. 3.8. Δ -Y transformer based grid forming inverter with unbalanced loads and source(s).....	65
Fig. 3.9. Three-phase Δ -Y transformer.....	66

Fig. 3.10. Reference current transformation for phase ‘a’	68
Fig. 3.11. Waveforms of the three-phase load voltages, load currents and inductor currents.....	69
Fig. 3.12. dq waveforms of the voltage and current loops with the proposed control strategy; (a) Reference and actual voltages for the three phases, (b) Reference and actual currents for the three phases.	70
Fig. 3.13. Secondary side dq reference current waveforms for the three phases (before the current transformation & applied to the current controllers).....	72
Fig. 3.14. Schematic diagram of a grid forming four-leg inverter with unbalanced load and source.	73
Fig. 3.15. Emulation of the fictive circuit with neutral impedance.	74
Fig. 3.16. Carrier based PWM method for four-leg inverter. [83].....	76
Fig. 3.17. Schematic diagram of the PV-hybrid system used in the simulation studies. ..	77
Fig. 3.18. Waveforms of the output voltages and currents of the grid forming inverter for varying load conditions. a) Conventional SCC-based control scheme; b) Proposed per-phase control scheme.	79
Fig. 3.19. Waveforms of the voltage and current loops of the grid forming inverter in dq coordinates. a-b) Reference and actual voltages for the conventional and proposed control schemes respectively; c-d) Reference and actual currents for the conventional and proposed control schemes respectively.....	81

Fig. 3.20. Waveforms of the output voltages and currents of the grid forming inverter with unbalanced and non-linear load for the proposed per-phase control strategy.	83
Fig. 3.21. Steady state load voltages and currents of the grid forming inverter for different loads. a) Balanced load; b-d) Unbalanced load #1, #2 and #3 respectively.	85
Fig. 3.22. Transient response of the grid forming inverter. a) abc-frame load voltages and currents; b) dq-frame reference and actual voltages and currents for the three phases. ...	87
Fig. 4.1. Circuit diagram of a three-phase three-wire diesel-hybrid mini-grid with battery inverter, single-phase RES and unbalanced load.	92
Fig. 4.2. Schematic diagram of the proposed control circuit for the BESS.	95
Fig. 4.3. Schematic diagram of the per-phase cascaded control block for the BESS.	97
Fig. 4.4. Flow chart for the transition from genset support to grid forming mode.	106
Fig. 4.5. Flow chart for the transition from grid forming to genset support mode.	108
Fig. 4.6. Generation of positive sequence active power command for the BESS.	110
Fig. 4.7. Frequency adaptive SOGI block diagram for generation of an orthogonal component.	113
Fig. 4.8. Basic components of the PLL+ICA module.	114
Fig. 4.9. SIMULINK implementation of diesel generator.	118
Fig. 4.10. SIMULINK implementation of genset controller.	119

Fig. 4.11. Waveforms for the genset support mode. (a) Genset shaft speed, mini-grid frequency and peak value of the positive seq. voltage; (b) Real and reactive power of the genset, load and BESS.	121
Fig.4.12. Steady-state waveforms of the PCC voltages, genset currents, load currents and BESS currents for different loads.	124
Fig. 4.13. Output voltages and currents of the grid forming BESS for varying loads....	125
Fig. 4.14. Waveforms of the control loops of the grid forming BESS in dq frames. a) Reference and actual voltages; b) Reference and actual currents.	126
Fig. 4.15. Waveforms during transition between the modes. (From top to bottom: Frequency of the genset and BESS; Peak value of the PCC phase voltage; Active power of the genset, BESS and load.).....	128
Fig. 4.16. Waveforms during the transitions. (Top to bottom: PCC voltage, difference between genset voltage and PCC voltage, genset current, load current and BESS current)	130
Fig. 4.17. Dq current waveforms for the three phases of the BESS during the transitions.	132

LIST OF TABLES

Table 2.1. Harmonics for the New dq Technique with a 400 Hz Current Loop.....	37
Table 3.1. System Parameters for the Experimental Study.	84
Table 3.2. Experimental Results of Steady State Performances.	86
Table 4.1. Look-Up Table Used for the Parameters' Value of DSOGI-FLL.	116
Table 4.2. Loads in Diesel Mini-Grid during Genset Support Mode of BESS.	120

NOMENCLATURE

3-D SVM	Three-Dimensional Space Vector Modulation
APF	All-Pass Filter
AVR	Automatic Voltage Regulator
BESS	Battery Energy Storage System
DG	Distributed Generation
DSOGI	Dual Second Order Generalized Integrator
FF	Feed Forward
FAE	Fictive Axis Emulation
FLL	Frequency Locked Loop
FC	Fuel Cell
ICA	Intelligent Connection Agent
IGBT	Insulated-Gate Bipolar Transistor
LPF	Low Pass Filter
MSTS	Mode Selection and Transition System
PVUR	Phase Voltage Unbalance Rate
PV	Photovoltaic
PI	Proportional Integral
PLL	Phase Locked Loop
PCC	Point of Common Coupling
PSC	Positive Sequence Components
PR	Proportional Resonant
PWM	Pulse Width Modulation

RES	Renewable Energy Source
RET	Renewable Energy Technology
S&H	Sample and Hold
SPWM	Sinusoidal Pulse Width Modulation
SOGI	Second Order Generalized Integrator
SOC	State-of-Charge
SCC	Symmetrical Components Calculator
SG	Synchronous Generator
THD	Total Harmonic Distortion
UC	Ultra-Capacitor
UPF	Unity Power Factor
VSI	Voltage Source Inverter

CHAPTER 1

INTRODUCTION

Energy plays an important role in the development of any nation. Traditional electricity infrastructure in most countries is based on bulk centrally located power plants connected to highly meshed transmission networks. Due to a number of economic, logistical, safety, environmental, geographical and geological factors, these plants are usually built far from large centers of consumption. The generated power is then transported to the consumers over long transmission lines and distribution systems.

It is also very important to make better use of the available resources. Typically, 20% of the generation capacity is used only to meet peak demand which occurs only during 5% of the time [1]. Also, almost 8% of the generation output is lost in long transmission systems [1]. Besides, environmental issues are major problems for the conventional fossil fuel based power generation plants as these are the major emitters of greenhouse gases, which are the main contributors to global warming. Furthermore, these plants consume non-renewable energy to produce electricity which may cause energy shortage in the future.

The energy demand in the world is steadily increasing. The conventional generation, transmission and distribution are becoming utilized to their maximum capacity. The increased load demand requires increased generation as well as expansion of transmission and distribution infrastructure. All these factors have made the system planners to look for alternative approaches for the future electrical grid. One favored

approach is the use of distributed generation. Distributed generation (DG) is defined as small-scale power generation, usually in sizes ranging from a few kW to a few MW [2]. The DGs are located on the utility system, at the site of the utility customers, or at an isolated site not connected to the utility grid. The distributed generation with "green power" (renewable) such as wind turbines, solar photovoltaic (PV) systems, solar-thermo power, biomass power plants, fuel cells, gas micro-turbines, hydropower turbines, combined heat and power (CHP) micro-turbines and hybrid power systems can provide a significant environmental benefit and can reduce transmission line losses, congestion and expansion costs, which greatly increases DG systems' overall efficiency and economic advantages.

Microgrids are locally-controlled clusters of distributed energy resources that, from the grid's perspective, behave electrically as a single producer or load, and are also capable of islanding. They are semi-autonomous systems, that use DG and distributed storage, and that can operate in either the grid-connected mode or the autonomous islanding mode and benefits both utilities and customers in terms of efficiency, reliability, and power quality [3, 4].

The impact of microgrid technology can be even more important for remote stand-alone systems. Canada has over 300 remote communities which are not connected to the main electricity grid and usually depend on oil for heating and electricity [5]. Electricity generation costs in these communities are considerably higher than the national average, e.g., the cost in the Northwest Territories varies in between C\$0.13/kWh to C\$2.45/kWh [5]. Therefore, even small improvements in the utilization of the fuel consumption of the remote electric power system can have substantial economic benefits by reducing

operating costs. Electricity generation from grid connected PV costs roughly C\$0.38/kWh to C\$0.75/kWh and has been decreasing steadily [5]. Therefore, one option is to use renewable energy technologies (RETs), i.e., PV and wind, which can substantially reduce the cost of electricity generation and emissions in these remote communities.

These autonomous local electrical networks which are not connected to the main grid are called mini-grids [6] and are usually based on diesel power plants. When mini-grids use multiple types of energy sources, i.e. diesel gensets (diesel engine-generator sets) and photovoltaic (PV) systems or diesel gensets and storage systems, they are called hybrid mini-grids.

The main focus of this Ph. D. thesis is on diesel hybrid mini-grids. Techniques capable of reducing operational cost and increasing system's power quality and reliability will be investigated and assessed in this research work. For that, a brief background is first provided in this chapter to explain the operational aspects and the main issues in diesel dominated hybrid mini-grids, leading to the definition of the research objectives. Finally the chapter ends with the key steps used to accomplish the objectives, the new contributions of the research and the outline of the thesis.

1.1 Diesel Dominated Hybrid Mini-grids

Diesel dominated hybrid mini-grids are formed by a diesel power plant consisting of one or more diesel units which serves multiple residential and commercial loads. Fig. 1.1 shows a typical diesel dominated hybrid mini-grid. RETs such as solar PVs, small wind turbines, and/or run-off river hydro power sources may also be used to supply part of the load [7]. In principle, at least one of the diesel generators should operate

continuously in the mini-grid while other(s) can be dispatched based on variations in load demand and DG availability.

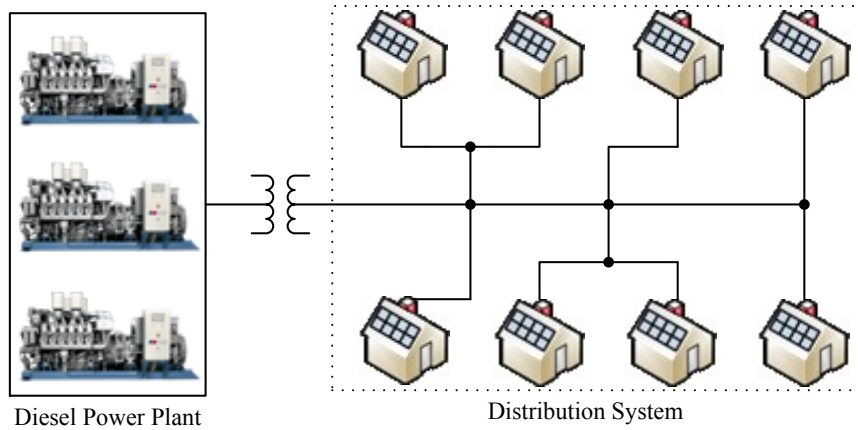


Fig. 1.1. Typical diesel dominated hybrid mini-grid.

1.1.1 The Diesel Genset

A diesel genset (diesel engine-generator set) consists of two main components coupled by a common shaft: the diesel prime mover and the electrical generator. Fig. 1.2 shows the basic block diagram of a diesel genset.

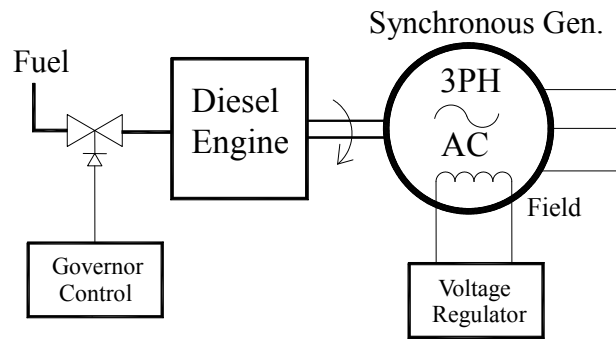


Fig. 1.2. Basic diagram of a diesel genset.

The diesel engine converts chemical energy of the fuel to the kinetic energy of the rotating shaft to drive a synchronous machine. The fuel injection is controlled by a governor to regulate the speed of the engine. Thus it regulates the output electrical

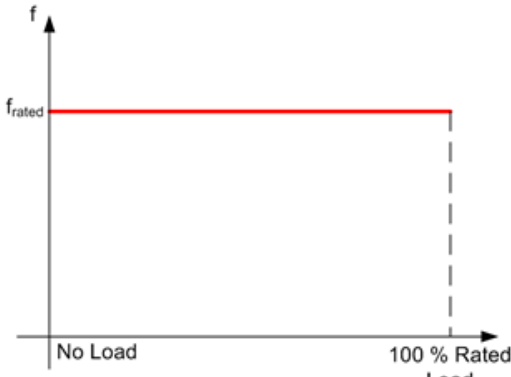
frequency of the generator, since the shaft speed (ω) is related with the electrical frequency (f) and the number of poles (P) of the synchronous machine as,

$$\omega = \frac{120f}{P} \quad (1.1)$$

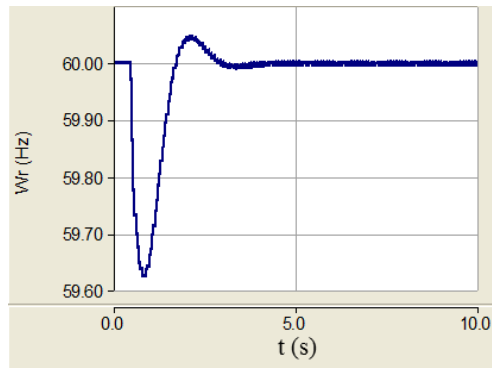
Generally, governor systems are categorized according to the type of controls and feedback signals used for the speed regulation [8]. The governor may operate in two main modes. These are: (i) “isochronous” or constant speed governor, and (ii) “speed-droop” governor.

Isochronous or constant-speed governor is commonly used for constant frequency control of a single genset unit. The operation of the genset in isochronous mode is shown in Fig. 1.3. The genset runs at constant speed/frequency, in steady state, regardless of the load as shown in Fig. 1.3(a). Fig. 1.3(b) shows the genset frequency for a step change in load. After a transient, the frequency returns to the desired (constant) value.

In the speed-droop governor, the speed/frequency of the genset varies according to the load. Fig. 1.4 shows the operation of the genset in droop mode. The relation between steady state frequency and load in droop operation mode is shown in Fig. 1.4(a). The generator speed and power frequency are reduced in response to load increase in the droop mode. Droop factor is defined as the frequency/speed difference between the no load condition and the full load. The frequency-droop control is commonly used for governor controls to provide power dispatch capability and parallel operation of multiple units without a communication link. Fig. 1.4(b) shows a sketch of the response of the genset frequency for a step increase in load. After a transient, the genset frequency operates in a lower value according to the new load as set by the droop characteristic.



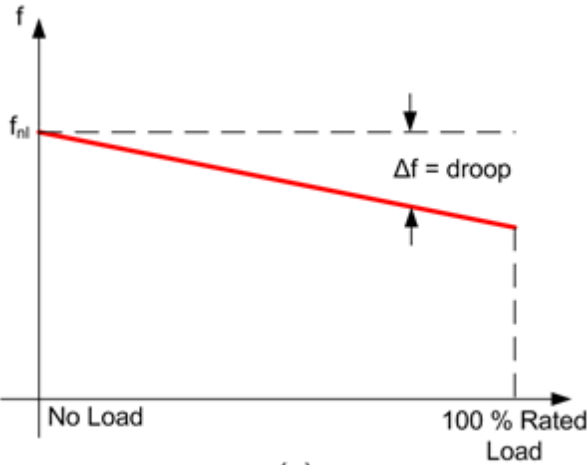
(a)



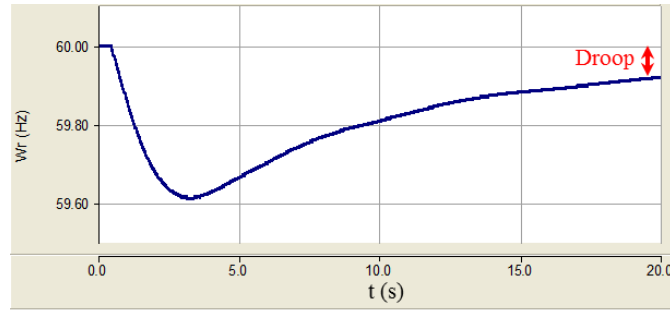
(b)

Fig. 1.3. Isochronous operation. (a) Steady state frequency vs. load operation and (b) Dynamic response.

The synchronous machine has an excitation system to control the output voltage of the genset. The excitation system generates the rotor magnetic field. This field may be provided by means of permanent magnets or by a DC source that feeds the field windings. Normally the diesel genset uses an Automatic Voltage Regulator (AVR) to adjust the generator field voltage and/or the field current according to the variations in the output terminal voltage.



(a)



(b)

Fig. 1.4. Droop operation. (a) Steady state frequency vs. load operation and (b) Dynamic response.

1.1.2 Operational Aspects of Diesel Genset

The diesel power plant can operate with multiple gensets of same size or different sizes. Optimal unit sizing of a diesel power plant requires detailed knowledge about several factors, i.e., daily and seasonal load profile of the mini-grid, annual load growth etc. Sizing of gensets based on yearly peak and/or average load values, with some safety margins and additional capacity for future expansion, results in an oversized plant, as remote community loads are highly variable with the peak load as high as 5 to 10 times the average load [9]. Besides, in a multi-genset system, multiple instances of unit cycling should be avoided for maintenance and expected life considerations [7].

Considering the fuel consumption characteristics of the gensets and the load profile of remote communities, the use of different size gensets is very attractive, which in turn can reduce the fuel consumption rate under low load conditions and can ensure optimal dispatch of the genset units to match load demand. Some basic requirements for sizing gensets in isolated diesel power plant are [7]:

- The diesel power plant should have at least two gensets in order to account for risk of a unit failure or maintenance requirements.
- The average load of the diesel plant should be greater than the suggested minimum loading of a single unit (40-50%).
- The combined capacity of the diesel power plant, with one unit out of service, should be capable of supplying about 110% of the forecast peak load.
- To provide spinning reserve, each unit in operation should not be loaded to more than 85% of its rated power.

Another very particular requirement for autonomous power systems is that many three-phase gensets might need to operate in a single-phase connection where only two of the three outputs of the genset are used. In practice it means that only $\frac{2}{3}$ of the generator power is available.

1.1.3 Renewable Energy Sources in Mini-grids

Diesel units are traditionally used to supply electricity in remote mini-grids due to the low initial cost and reliability of the technology. The integration of renewable energy sources (RESs) into such systems can reduce the operating cost, fuel consumption and environmental impact. Nowadays, some diesel hybrid mini-grid systems include renewable energy technologies and/or storage systems and fossil fuelled systems [7], e.g.,

PV-diesel hybrid mini-grid in Namiah Valley of British Columbia (Canada) and King's Canyon (Australia), wind-battery-diesel hybrid mini-grid in Canary Island (Spain), etc.

PV technology is widely used in hybrid mini-grids. 84% of PV systems installed in Canada are for stand-alone applications which mean that the systems use PV arrays as a single generator or with a diesel genset or small wind turbine in hybrid mini-grid systems [10]. In 2007, Most of domestic module sales (66% of total market share) occurred for off-grid applications (both residential and non-residential) [10].

Among the RESs, PV arrays and wind turbines are considered uncontrollable sources due to the stochastic nature of wind and solar irradiance. They usually operate as current sources and inject as much power as possible into the diesel based mini-grid. Distributed integration of these RESs may help off-set the load locally and reduce the fuel cost and distribution losses in low voltage mini-grids. However during the high penetration of distributed non-controllable RESs with low load, the mini-grid can be subject to over-voltage/over-frequency. Besides, the inherent fluctuating and intermittent power characteristics of solar and wind energy, can have a significant impact on the economical operation of the diesel genset(s), which already has to deal with the highly variable mini-grid load, and also has its own operating constraints for safe and reliable operation. Therefore, the control structure of the mini-grid plays an important role to overcome these issues.

1.2 Operational and Power Quality Issues in Diesel Hybrid Mini-grid

Many of the hybrid mini-grids found in remote communities, consist of a diesel power plant, with two or more gensets and RESs such as wind and PV. The diesel genset usually performs the grid forming task, regulating the voltage and frequency and

matching supply and demand of active and reactive power in the mini-grid. However, the diesel based remote mini-grid systems are characterized by high costs and a high degree of dependence on fossil fuels. The use of RETs to meet part of energy needs offer good potential for reducing fuel consumption and carbon di-oxide emission in diesel based hybrid mini-grids. Normally the RETs do not participate in the control strategy of the mini-grid and usually inject maximum amount of power available from the solar or wind energy. However, the inherent fluctuating and intermittent power characteristics of solar and wind energy, can deteriorate the power quality and reliability in the diesel dominated hybrid mini-grid.

Despite being a mature technology, the optimization of the operation of the diesel power plant in mini-grids for reduced fuel consumption and maintenance costs is not straightforward. Remote communities are characterized by highly variable load profiles with the peak load as high as 5 to 10 times the average load [11]. Normally the genset(s) are sized for the peak load condition of the mini-grid. In such a case, a diesel genset might need to operate for some time at low load conditions. The fuel efficiency of diesel engine decreases substantially at light load [12, 13]. Besides, all the fuel is not burnt completely by the diesel engine for light load operation and it results in carbon build up in the diesel engine [12, 14]. This increases the maintenance cost for the diesel engine and also significantly affect the life time of the genset [15]. In order to improve the efficiency and avoid carbon build up, a minimum load of about 40% to 50% is usually recommended by the manufacturers [14]. If the light load operation of the genset cannot be avoided in the mini-grid, then the genset should run close to full load for 1-2 hours to get rid of the carbon accumulated during the day. This leads to high costs in fuel.

If the diesel plant consists of gensets of different sizes, these can be dispatched more efficiently to meet the variable load demand of the mini-grid. Nonetheless, the improvements are relatively moderate because the gensets still need to provide the spinning reserve to account for the possibility of sudden load increase and should not be cycled frequently as frequent unit cycling also increases the operational cost of the system [15] and should be avoided for maintenance and expected life considerations [7]. The main issue with spinning reserve is that it forces genset to operate with spare power capacity what can mean operating below the highest possible efficiency point.

Though RETs can reduce the fuel cost and environmental impact in diesel hybrid mini-grid, during the high penetration of RETs, still the genset may need to operate below minimum loading limit resulting in the aforementioned problems. In some cases, a significant part of the renewable energy might need to be either curtailed or dissipated in dump loads not only to prevent operation of the genset(s) under low load conditions but also to keep the voltage and frequency of the system within given limits [16]. As a result, the displacement of fossil fuels with RETs in hybrid mini-grids is usually modest, even with relatively large installed capacities of RESs.

One of the objectives of this research work is to address the above mentioned issues. These issues can be mitigated with the use of energy storage units and/or controllable loads. Load management is an interesting effective option for energy management, at the expense of more elaborate coordination and control systems [17]. Small (short term) battery energy storage system (BESS) can relieve the gensets from the spinning reserve task as well as can ensure operation above a minimum loading condition for some time in the *genset support mode* and larger ones operating in the *grid forming*

mode can allow the mini-grid to operate without the diesel gensets during high supply of RESs and/or low load consumption. In such a case, the BESS will regulate the voltage and frequency, until the load increases beyond a certain value or its state-of-charge (SOC) reaches a minimum value. At this point, the genset can be re-started assuming the grid forming task and the BESS goes back to the support mode. Besides, BESS can also support the genset with reactive power compensation of the mini-grid distribution system. Therefore the genset can operate with unity power factor. Besides, this also facilitates the operation of the genset by operating with only real power and does not need to allocate any capacity for reactive power supply.

Another important aspect to consider in small diesel based hybrid mini-grids with high penetration of renewables is the load unbalance. In general, the three-phase distribution system of the mini-grid allows connection of small loads and RESs in single-phase mode and the larger ones in three-phase mode depending on their number of phases and power ratings. These are usually arranged in order to result in a balanced power distribution across the three phases. However, in small (< 100 kVA) mini-grids with a relatively small number of loads and RESs, it is more likely that load unbalances will occur leading to unbalanced mini-grid voltages. This can result in increased losses and heating in rotating machines, saturation of transformers as well as malfunction of protection devices [18]. Besides, the unbalanced load will result in unbalanced current flow in the synchronous generator and as a consequence it will result in vibration in the shaft and overheating in the machine [19]. It can require the derating of the output power of synchronous generators up to 10% [19]. Operation under unbalanced conditions can have a significant impact on the efficiency and life time of the generator. To assure safe

operation of the diesel genset, the ANSI standard specifies general-purpose multifunctional generator protective device with the maximum limit of 2% voltage unbalance and 10-20% current unbalance [7, 19]. Therefore, it is desirable that the synchronous generator of the diesel genset operates with balanced load. In this case, the BESS can help minimize this problem and also provide additional ancillary services to reduce operating costs and increase power quality. Besides, it is also expected that the BESS should be able to form the grid regulating voltage and frequency across the unbalanced load when the genset is ‘off’. Therefore, another objective of this work is to achieve these functions using the BESS to improve these power quality issues.

Utility grids ideally provide reliable and uninterrupted service with constant voltage and frequency to the consumer loads. In practice, voltage and frequency variation are allowed within a “normal range” giving some flexibility for the system operator. According to the IEEE Standard for Interconnecting Distributed Resources with Electric Power Systems (IEEE Std. 1547), distributed resources smaller than 30 kW should cease to energize the area electric power system (EPS) when the voltage goes out of the *normal* range, typically 88% to 110% of the nominal voltage and the frequency goes out of range, 59.3 Hz to 60.5 Hz [20]. The European Standard EN-50160 requires that for a non-interconnected (i.e. autonomous) power system, voltage and frequency should be within certain ranges [21]:

1. 230 V \pm 10% (i.e. 207 – 253 V) during 95% of a week;
230 V – 15% or + 10% (i.e. 195.5 – 253 V) during 100% of a week; and
2. 50 Hz \pm 2% (i.e. 49 – 51 Hz) during 95% of a week;
50 Hz \pm 15% (i.e. 42.5 – 57.5 Hz) during 100% of a week;

Isolated microgrid or mini-grid systems can use droop characteristics for parallel operation of distributed generation. Paralleling of power sources and storage units with physical interconnections of control and synchronization signals, pose a restriction on the locations of these components. In order to avoid a dedicated communication channel, the droop method is usually applied [22]. Therefore, the mini-grids usually operate with wider frequency/voltage ranges than conventional grids. One of the benefits is that frequency is used for conveying, without a dedicated communication channel, information of the shortage (low frequencies) or surplus (high frequencies) of power/energy in the mini-grid to distributed controllable sources and loads [7]. Therefore the BESS should be capable of working with both voltage and frequency variation in grid forming and genset support modes in the diesel hybrid mini-grid.

Therefore, BESS is a good alternative which can be employed in the diesel hybrid mini-grid to achieve the objectives discussed above. However, in this regard, the BESS system should be equipped with a frequency adaptive control strategy that allows operation in both genset support and grid forming modes and also during the transition between the modes. Diesel hybrid mini-grids with BESS, RETs and three-phase unbalanced loads have been discussed in the literature but only for the BESS supporting the genset [23-27]. The BESS control logic was limited to load balancing and power factor correction only in the genset support mode. The issue of light load operation of the genset, which leads to operation with low efficiency and increased maintenance costs, was not addressed. The operation of a BESS in grid forming mode and also the transition between the two modes with unbalanced load has not been addressed in those studies.

The operation of a BESS in the grid forming mode supplying balanced voltages to unbalanced loads in a stand-alone system was discussed in [28-39]. However, the impact of small unbalanced (single-phase) renewable supply, commonly based on single-phase inverters, and the possibility of operating with variable frequency have not been considered. Due to the relatively larger impedances of the low-pass output filter of the inverters, unbalanced inverter currents create larger voltage unbalances. Thus, the control strategy of the inverter should be such that it can keep the voltage balanced while sourcing or sinking unbalanced currents in a variable frequency diesel hybrid mini-grid.

Regarding the control scheme for balancing the output voltages of the grid forming inverter operating with unbalanced loads in stand-alone hybrid system or mini-grid, there are also many choices [28-41]. Some are based on vector (dq) control, which is an elegant technique frequently employed in high-performance three-phase inverters [42]. By converting AC into DC quantities, simple PI-type controllers can be employed to obtain zero error in steady-state and fast transient response [43]. However, in the presence of unbalances, the quantities in the rotating frame are not pure DC anymore, containing a double line frequency component due to the negative sequence components and a line frequency component due to the zero sequence components. These components, when present at the output of the PI controllers, will interact with the rotating frame yielding non-zero steady-state errors [44]. This problem can be mitigated by employing low pass filters (LPFs) as shown in [40, 41]. The problem is that they introduce delays and slow down the dynamic response of the system.

The usual control approach for operation with unbalance system is to use dq (vector) control, extracting the symmetrical components (positive, negative and zero

sequence components) and designing the controllers for each of the symmetrical sequence decomposed circuit [35-39, 45]. The 90° phase shift required for a realization of the symmetrical components calculator (SCC) was implemented with a fixed quarter cycle delay in [38, 45] and with an all-pass filter (APF) in [35-37, 39]. However, the SCCs are implemented for a specific desired frequency (which is not realistic in variable frequency mini-grid) and the dynamics of the SCC has been neglected in all cases above, but the crossover frequency of the control loops has been selected lower than typical. Therefore the dynamic response of the system is quite slow for a specific desired frequency and also the system is not suitable for operation with variable frequency.

Some different techniques without using the SCC have been proposed in [29, 30, 32, 34]. [32] employs rotating frame controllers to eliminate positive and negative sequence distortions and stationary frame controllers to attenuate the zero sequence distortion due to the neutral current. However, it only presented simulation results under steady-state conditions and zero steady-state error was not truly achieved for the zero sequence components. This idea has been extended in [29] with the use of notch filters in the positive and negative sequence rotating frames and resonant controller for the zero sequence component, however still the use of filters cause the dynamic response to be slow and restrict the operation to a fixed frequency system. A stationary frame per-phase voltage loop only control approach for a grid forming inverter with unbalanced loads was proposed in [34], but the control strategy was shown to be robust for a specific range of unbalanced load which does not include the highly unbalanced load (i.e. single-phase load). A technique with a sliding mode controlled inner current loop and a servomechanism controlled outer voltage loop, was reported in [30] for unbalanced

operation of distributed generation units, but the transient response was relatively slow (typically more than 3 line cycles).

The desired control strategy of the BESS should be fast and frequency adaptive with zero error in steady-state for operation with unbalanced load in diesel hybrid mini-grid. The control strategy for the grid forming operation should also be able to work in genset support mode to avoid switching between different controllers designed for different modes. Besides, depending on the status of the system (i.e., low load condition in diesel grid forming mode, sufficient energy available in the battery to supply the distribution load etc.) the BESS operates in two different modes, therefore, a means of smooth transition is required which will ensure minimal disturbance to the mini-grid system. These objectives will be addressed in this Thesis.

Finally, another important aspect to consider in diesel hybrid mini-grid is the current control of single-phase PV inverter. Usually the PVs are connected to the mini-grid through voltage source inverters to supply part of the demand. Single-phase inverters are frequently employed to connect residential roof-top PVs (capacity below 10 kW) to the utility or microgrid/mini-grid system. The inverters should present fast dynamic current control even in case of grid frequency variation that occurs in the mini-grid for power management purpose. Therefore, current control of inverter is inevitable for PV power generation systems.

1.3 Current Control of Single-Phase Inverters

Single-phase voltage source inverters (VSIs) are widely utilized in many applications, i.e., photovoltaic (PV) power generation [46], active power filters [47], power factor controllers (PFC) [48], distributed generation [33], etc. The high depth of

penetration of distributed energy resources has recently intensified the demand for such inverters. Full-bridge VSIs are employed in such systems and a current regulation strategy is usually adopted for control purposes [49].

There has been considerable research on the current regulation of VSIs and various approaches have been proposed [36, 42, 50-53]. The most common ones are the hysteresis current controllers (HCC) and the sinusoidal pulse width modulator (SPWM) with a linear controller. The first is well known for excellent transient response, inherent peak current limiting capability and their stability and robustness under varying load conditions, but the problem is that it gives a variable switching frequency what complicates the filter design [50]. The second one yields a fixed switching frequency and can be classified into two major classes: (i) stationary frame and (ii) synchronous frame controllers. Simple linear proportional integrator (PI) controllers are commonly used in stationary frame controllers [42, 51]. Its main issue is that it cannot provide zero error in steady state for a non-DC reference signal, since its gain is only “infinite” at zero Hz. Recently, other approaches such as proportional resonant (PR) [51, 52] controllers have been proposed, which can track AC reference in the stationary frame with zero steady-state error. The PR controller provides infinite gain at the target frequency (resonant frequency) for eliminating steady-state error, which is virtually similar to the infinite gain of a PI controller at DC. However, the PR controller suffers from several drawbacks, e.g., sensitivity to small variations in the interfaced grid frequency, exponentially decaying transients during step changes, and being pushed toward instability margins even by a small phase shift introduced by the current sensors [51].

Among synchronous frame controllers, PI regulators are widely utilized for both single- and three-phase systems [50, 53]. This scheme is also known as vector (dq) control. In a synchronous reference frame usually referred to as dq-frame, AC (time varying) quantities appear as DC (time invariant) quantities allowing the controller to be designed as for DC-DC converters presenting infinite control gain at the steady-state operating point for zero steady-state error. Vector (dq) control is a well-known technique used in three-phase inverters for high dynamic performance, however, it is not straight forward to implement for the single-phase systems. Several literatures have proposed techniques to implement the vector control in single-phase inverters [54-60], but they were not able to demonstrate the expected high dynamic performance of vector controlled single-phase inverters, similar to that of three-phase inverters. Besides, all these techniques are for operation with fixed frequency and cannot operate with a variable frequency, a condition that can be found in PV-hybrid mini-grid systems. Therefore, one of the objectives of this research work is to develop a new frequency adaptive vector control scheme for single-phase VSIs for PV power generation in diesel hybrid mini-grid.

1.4 Thesis Outline and Contributions

The objectives of this thesis are to investigate techniques that allow reliable and efficient operation of the diesel hybrid mini-grids with good power quality, reduced fuel consumption and maintenance costs of the grid forming gensets. In this regard, the main issues associated with the operation of the system and the objectives of this research work are presented in details in sections 1.2 and 1.3.

In order to reduce fuel consumption and environmental impact of diesel genset, roof-top type PVs can be incorporated into the mini-grid system to supply part of the

load. Current controlled single-phase VSIs are used for PV power generation in the mini-grid. Conventional vector current control strategy can provide regulated current to the fixed frequency grid. However, the dynamic response is quite slow and the control strategy is not suitable for variable frequency mini-grid. Therefore, a new vector current control strategy for single-phase inverters is presented in Chapter 2 that can be used for PV inverters operating in diesel hybrid mini-grids. The proposed vector current control strategy is based on a fictive axis emulation (FAE) which provides regulated current with high dynamic performance like the three-phase one and is also capable of operating in variable frequency mini-grid [61, 62]. This is the main contribution of this chapter. The fictive axis circuit emulation, modeling and controller design is presented in Chapter 2. Moreover, simulation and experimental results for a single-phase inverter operating with the conventional delay based and new emulated imaginary circuit based vector control techniques are presented to show the superior performance of the latter. Besides, this proposed idea also serves as the basis for the per-phase dq control of three-phase grid forming inverter for operation with unbalanced system.

Load unbalance is quite common in stand-alone hybrid systems. As mentioned earlier, a BESS system should be capable of operating with unbalance voltage/current in the variable frequency diesel hybrid mini-grid system. The conventional grid forming inverter system can provide balanced regulated voltage across the unbalanced load in steady-state. However, the dynamic response is slow and the control strategies are not suitable for operation with variable frequency. The desired control strategy of the BESS should be fast and frequency adaptive with zero error in steady-state for operation with unbalanced load. The control strategy should also be capable of working in both grid

forming and genset support modes to avoid switching between different controllers designed for different modes.

Chapter 3 will present a new frequency adaptive per-phase vector (dq) control strategy for three-phase grid forming inverters that can provide balanced voltage to highly unbalanced load with enhanced dynamic response even when it has to supply active power in two phases and absorb in the other one, due to the presence of a single-phase RET. The proposed per-phase dq control strategy employs fictive axis circuit emulation in the inner current loop and frequency adaptive second order generalized integrator (SOGI) in the outer voltage loop to obtain the orthogonal components. Therefore, the proposed per-phase control strategy can operate with variable frequency unlike the conventional control methods. These are the main contributions in this chapter. The use of cascaded control loops also allows such system to be used as BESS in a three-phase hybrid mini-grid system. Besides, the three-phase distribution system can be either three-wire or four-wire system. The complexity of the control strategy increases with the four-wire system. Therefore, appropriate per-phase control strategies have been developed for different configurations of the grid forming inverters [63-66]. The proposed per-phase control strategy is compared with the conventional SCC based control strategy. Simulation and experimental results are presented to ensure better dynamic response of the proposed control strategy in case of operation of the grid forming system with highly unbalanced load.

A complete multi-mode control system of a BESS operating in variable frequency diesel hybrid mini-grid with high penetration of RESs and highly unbalanced loads is presented in Chapter 4. In the genset support mode when the genset forms the grid, the

BESS operates as a three-phase independently controllable current source and it balances the load by injecting the negative sequence of the load current, provides load reactive power so that the genset operates with unity power factor (UPF), supplies the reactive current for the output filter capacitors of the BESS and controls active power so as to provide minimum loading for the genset to avoid carbon build up and supplement it under peak load conditions. If the load demand is below the minimum loading limit (typically 40% of its capacity) of the genset, the BESS absorbs power from the genset while the genset operates at its minimum loading point. Conversely, the BESS can supplement the genset by supplying part of the peak load demand. Again to overcome the impact of unbalance operation of the genset in diesel hybrid mini-grid, the BESS does the load balancing for the genset. Besides, the BESS can also support the genset with reactive power compensation of the mini-grid system. Therefore the genset can operate with unity power factor which in turn also facilitates the operation of the genset by operating with only real power and does not need to allocate any capacity for reactive power supply.

Again, in cases when the power demand from the genset is low, due to high supply of RESs and/or low load consumption, the genset can be shut-down and the BESS forms the grid, regulating voltage and frequency. In this second mode, the BESS forms the grid what requires operation as a three-phase voltage source. One major challenge in this case is to provide balanced voltage to an unbalanced load. The proposed per-phase dq control strategy has been adopted for the grid forming BESS. During the grid forming mode, the BESS employs the cascaded control scheme to provide balanced regulated voltage across the unbalanced distribution system, while during the genset support mode, it employs only the inner current loop to provide the desired compensation currents of the mini-grid.

What is more, a logic for defining the mode of operation of the BESS, and when a transition is needed is also presented in Chapter 4. For instance, if the genset operates under light load condition, and the BESS becomes fully charged while operating in the genset support mode, a transition to the grid forming mode, with the genset off might be advantageous. This and other management tasks are carried out by a proposed Mode Selection and Transition System (MSTS). It operates the BESS either in genset support or in grid forming mode, depending on the status of the system and directly controls the genset breaker in this regard. It also coordinates the smooth transition between the modes. For this, the load power is transferred smoothly between the genset and the BESS during the transition while ensuring slow loading/unloading of the genset.

The synchronization of the BESS with the genset and the disconnection process of the genset are done by a proposed PLL+ICA (Phase Locked Loop + Intelligent Connection Agent) module; the control signals generated by the MSTS are used to perform these processes. The PLL+ICA system has been proposed to extract or generate the phase angle, frequency and reference voltage for the per-phase controllers and reference current generator during the genset support or grid forming mode. For the BESS, it acts as a PLL during the genset support mode, while it acts as a reference voltage generator during the grid forming mode. The performance of the proposed multi-functional BESS in diesel hybrid mini-grid is verified by time domain simulation results.

Finally Chapter 5 presents the conclusion and future prospects of the research work.

Therefore, in summary, the main contributions of this research work are:

Chapter 2:

- A new vector current control strategy based on fictive axis circuit emulation for single-phase inverter is proposed which provides regulated current with high dynamic performance like the three-phase one.
- The proposed strategy allows operation with high bandwidth control loop, which reduces the total harmonic distortion for the output current.
- The application of a second order generalized integrator (SOGI) in the proposed control strategy allows operation in variable frequency mini-grid.

Chapter 3:

- A new frequency adaptive per-phase vector control strategy of three-phase grid forming inverter for operation with unbalanced load is proposed.
- FAE in the inner current loop and frequency adaptive SOGI in the outer voltage loop to obtain the orthogonal components are proposed which makes the control strategy fast and frequency adaptive, with zero error in steady-state unlike the conventional control methods.
- A new control strategy for Δ -Y transformer based grid forming inverter is developed. Control strategy with a new current and voltage transformation is proposed to overcome the impact of transformer phase shift.
- A new coupled fictive axis emulation based per-phase control strategy for the three-phase four-leg inverter is proposed to compensate the impact of the zero sequence current components in the four-wire unbalanced system.

Chapter 4:

- In order to address the low loading and unbalance operations of the diesel genset, a multi-functional battery energy storage based solution is proposed.
- In the *genset support* mode, it does load balancing, reactive power compensation and active power control of the genset. So the genset operates in balanced condition without carbon build up in the diesel engine and thus reduces the operational and maintenance cost of the diesel genset.
- During light load condition, the BESS acts as an *grid forming* unit for the unbalanced mini-grid distribution system, while the genset is ‘off’ which also reduces the operational cost and environmental impact of the genset.
- Methods for operating mode selection for energy management purpose and also to make smooth transitions between the modes are presented in this Thesis. These are achieved by the proposed MSTS and PLL+ICA modules.

CHAPTER 2

VECTOR CONTROL OF SINGLE-PHASE VOLTAGE SOURCE INVERTER

Vector (dq) control is a powerful technique used in high dynamic performance three-phase inverters. The transformation of AC into DC quantities allows one to get zero steady-state error for AC currents and voltages with simple PI-type controllers. It can be easily implemented for three-phase inverters but presents some challenges for single-phase ones. The orthogonal component (β) required for the stationary to rotating frame transformation is usually created by phase shifting the real one (α) by $\frac{1}{4}$ of a line cycle, what deteriorates the dynamic response. The emulation of a fictive orthogonal circuit for obtaining the β current component has been shown to yield enhanced transient response. This chapter shows that the dynamic response of vector controlled single-phase inverters implemented with orthogonal circuit emulation is identical to that of a three-phase inverter. This concept is then extended for operation with variable grid frequencies, a condition that can be found in PV hybrid autonomous microgrids/mini-grids, where the grid frequency variation is used for energy management purposes. Experimental results for a single-phase inverter operating with the conventional delay based and the new emulated imaginary circuit based vector control techniques are presented to show the superior performance of the latter.

2.1 Conventional Vector Control Approach for VSI

Vector (dq) control is a well-known technique used in three-phase inverters for high dynamic performance [50, 53]. As shown in Fig. 2.1, the abc (stationary frame) quantities are converted into orthogonal $\alpha\beta$ coordinates (stationary frame) and then into dq coordinates (rotating frame). The latter are DC components, what allow the use of simple PI controllers for achieving zero steady-state error for the fundamental AC components. The modulating signals for the carrier based sinusoidal pulse width modulation (SPWM) are obtained with the inverse transformations, dq- $\alpha\beta$ and $\alpha\beta$ -abc.

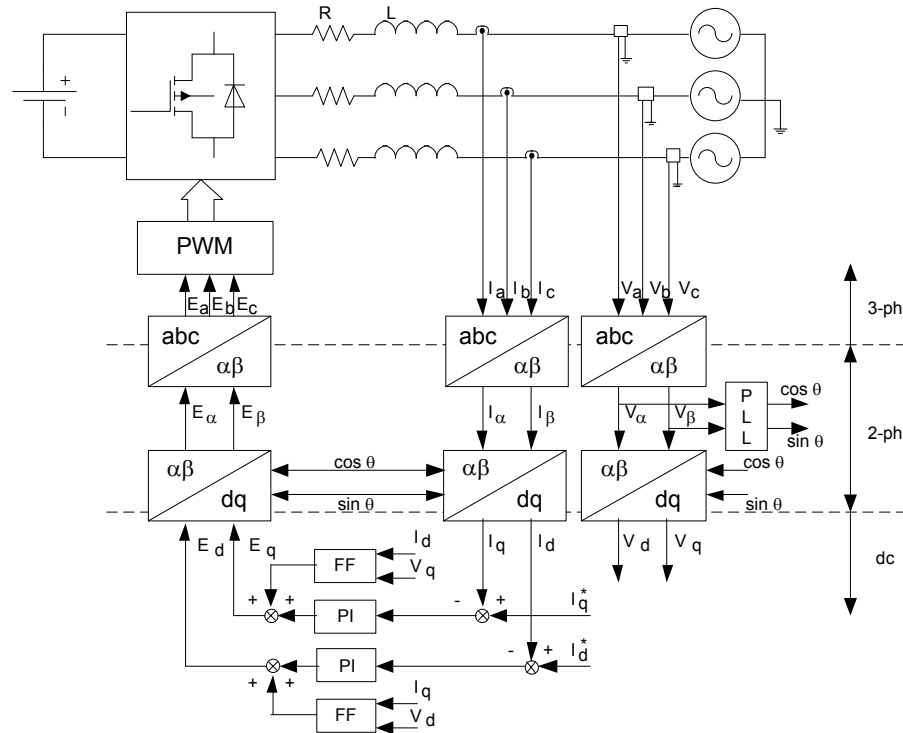


Fig. 2.1. Vector (dq) control applied to a three-phase inverter using standard PI controllers and feed-forward decoupling networks.

The application of vector (dq) control in single-phase inverters is not straightforward due to the existence of a single AC quantity (voltage or current). The idea

behind the approach proposed in [54] is based on an imaginary circuit, identical to the actual one, but with the waveforms orthogonal to those of the real circuit. It is used to generate steady-state DC components using the $\alpha\beta$ -dq transformation. In practice, this concept was implemented by delaying the real quantities (α) by $1/4$ of a line cycle to create the imaginary orthogonal quantities (β) as shown in Fig. 2.2.

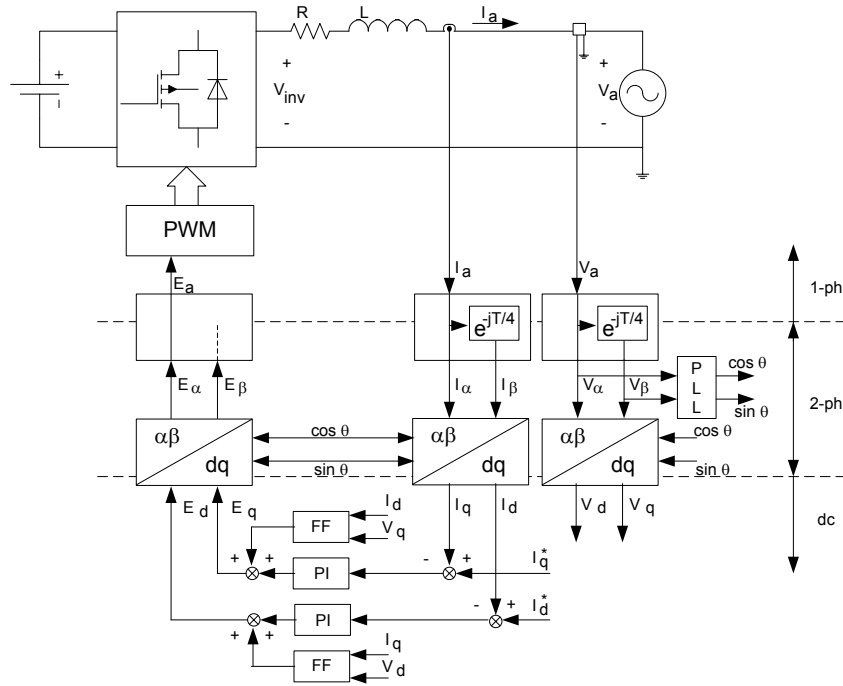


Fig. 2.2. Vector (dq) control applied to a single-phase inverter (original technique).

Two DC control loops are used for regulating the magnitude of the current component in phase (d axis) and in quadrature (q axis) with the grid voltage. The outputs of the d and q controllers are passed through a dq- $\alpha\beta$ transformation block. The α coordinate signal is used for controlling the real inverter while the β coordinate signal, related to the imaginary circuit is discarded. This approach allows the controllers to be designed in the rotating frame, for regulating DC quantities, as for three-phase inverters. Thus, high dynamic performance with zero steady-state error, similar to that of the three-

phase circuits, would be expected. The first part, unlike the second, was not clearly demonstrated in [54]. The introduction of the delay in the system tends to deteriorate the dynamic response, which becomes naturally slow.

A number of papers followed up discussing different strategies, i.e., differentiation method, all-pass filter method, observer based method, etc. for obtaining the orthogonal (β) quantity for the $\alpha\beta$ -dq transformation [55-60]. However, they were not able to demonstrate the expected high dynamic performance of vector controlled single-phase inverters, similar to that of three-phase inverters. Besides, all these techniques are for operation with fixed frequency utility grid and cannot operate with a variable frequency, a condition that can be found in PV-hybrid autonomous microgrid/mini-grid systems.

2.2 Proposed Vector Control Strategy Based on Fictive Axis Emulation

2.2.1 Basic Concept

The key point in this new approach is that the orthogonal current of the imaginary circuit, required for the $\alpha\beta$ -dq transformation, is not obtained by phase-shifting the real quantity. The imaginary circuit is emulated and the β coordinate control signal, obtained from the dq- $\alpha\beta$ transformation, is not discarded. It is used to regulate the inverter current in the imaginary circuit [61, 62, 67], which in turn is used to accurately calculate the d and q components of the inverter current. The implementation of the vector (dq) control for a single-phase inverter with fictive axis emulation (FAE) is shown in Fig. 2.3. The orthogonal current component (I_β) is obtained using the β coordinate control signal (E_β) from the dq- $\alpha\beta$ transformation, the fictive grid voltage (V_β) and the coupling impedance, R and L, of the real circuit. V_β is obtained by phase-shifting the grid voltage by a quarter line cycle. However, for this quantity, the use of a $\frac{1}{4}$ line cycle delay does not

significantly affect the transient response for variations in the reference currents (I_d^* and I_q^*). It has been shown in [67] that the sensitivity of this control scheme to changes in parameters R and L is small (a mismatch of 50% between the actual and fictive circuit parameters was considered).

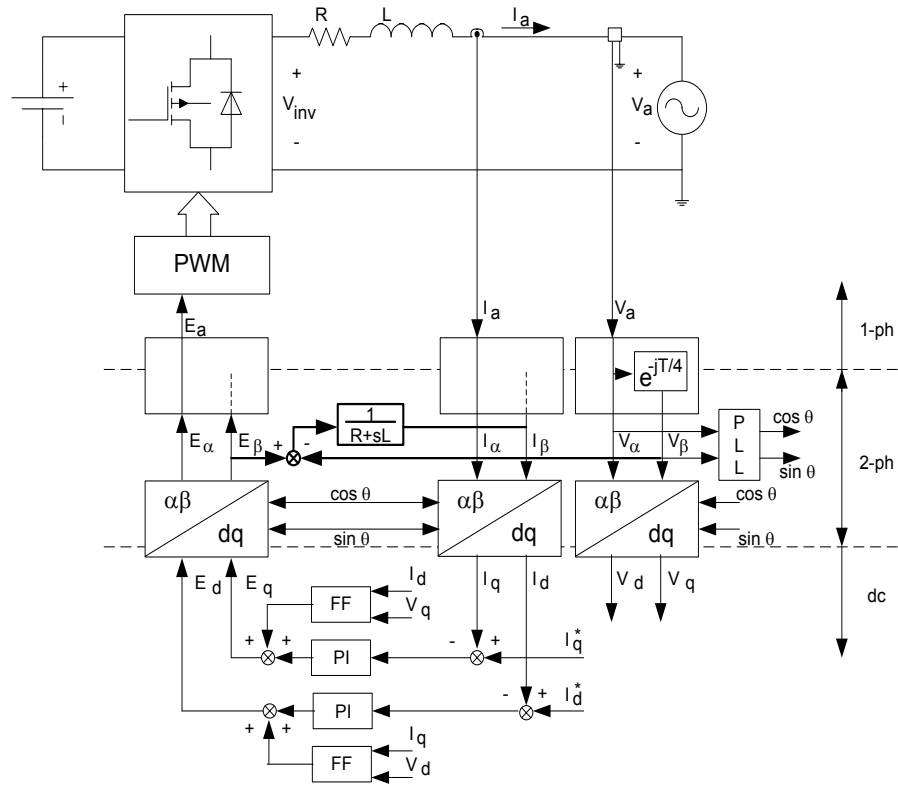


Fig. 2.3. Proposed scheme for implementing vector (dq) control in single-phase inverters.

2.2.2 Design of the Current Controller

The fundamental component of the switched voltage of a single-phase VSI can be modeled as an ideal controlled voltage source ($E_{inv\alpha}$) as shown in Fig. 2.4. The inverter is connected to the grid through an L filter where R represents the internal resistance of the filter. The inverter inductor current and grid voltages are $I_{L\alpha}$ and $V_{g\alpha}$ respectively.

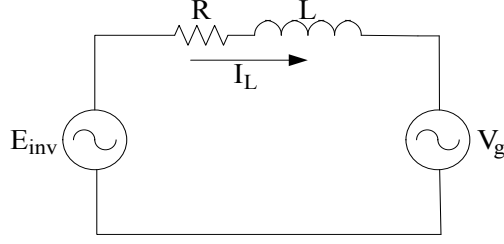


Fig. 2.4. Schematic of the system.

For representing voltages and currents of a single-phase system in a rotating reference frame, that is, with dq coordinates, one needs first to create a two-phase system with orthogonal components. The α components are obtained and measured from the real single-phase circuit. The β components are obtained from a virtual circuit where all voltages and currents are phase-shifted by 90° with respect to the real (α -coordinates) voltages and currents.

The system model of Fig. 2.4 in $\alpha\beta$ -frame is,

$$L \frac{di_{L\alpha\beta}}{dt} = e_{inv\alpha\beta} - i_{L\alpha\beta}R - v_{g\alpha\beta} \quad (2.1)$$

The state space model has been developed. The Park's transformation matrix represented by equation (2.2) was applied to derive the system in dq-frame.

$$T_{\alpha\beta-dq} = \begin{bmatrix} \cos(\omega t) & \sin(\omega t) \\ -\sin(\omega t) & \cos(\omega t) \end{bmatrix} \quad (2.2)$$

In such a case, equation (2.3) represents the dq circuits and can be represented as shown in Fig. 2.5.

$$\begin{bmatrix} e_d \\ e_q \end{bmatrix} = L \begin{bmatrix} \frac{di_d}{dt} \\ \frac{di_q}{dt} \end{bmatrix} + \begin{bmatrix} R & -\omega L \\ \omega L & R \end{bmatrix} \begin{bmatrix} i_d \\ i_q \end{bmatrix} + \begin{bmatrix} v_d \\ v_q \end{bmatrix} \quad (2.3)$$

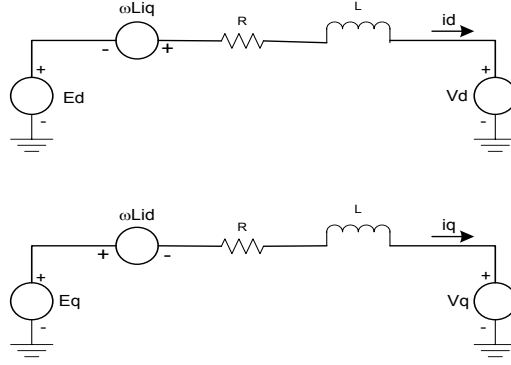


Fig. 2.5. Equivalent model of the power circuit in the dq (rotating) frame.

The coupling between the d and q equivalent circuits and variations in the magnitude of the grid voltage are considered as disturbances and are compensated by means of a feed-forward network [68]. The transfer function of the decoupled system for the design of the current controller becomes,

$$G(s) = \frac{K_s}{1 + sT_s} \quad (2.4)$$

where, $K_s = 1/R$ and $T_s = L/R$.

Thus, a simple PI controller can be used for controlling the DC current flowing through a simple RL circuit with zero error in the steady-state for step variations in the reference (dq) signal. Assuming that the inverter operates with unipolar SPWM with a 20 kHz carrier, and that the current and voltage sensors are ideal with a unity gain, the controller is designed as described in [68]. The inductance and resistance of the AC side inductor are equal to 5 mH and 0.1 Ω . The PI controllers were designed for a bandwidth (f_x) of 5 kHz and damping factor (ζ) of 1.2, yielding proportional and integral gain of $k_p = 377$ and $k_i = 4.9 \times 10^6$ respectively. It should be noted that the use of high bandwidth for the current loop also facilitates the design of cascaded control loop for the grid forming inverters as will be shown later in Chapter 3, as the inner current loop has to be fast to

regulate the output voltage of the grid forming inverter. Besides, high bandwidth current control loop is also desirable for other applications, i.e., power factor correction, two-stage PV power generation, active power filter, etc.

2.3 Performance Verification and Comparison

2.3.1 Simulation Results

The performance of the proposed technique is verified by means of simulation using PSIM[®] for a single-phase inverter connected to a 120 V, 60 Hz grid. The DC bus is represented by a 400 V source and the other parameters are as described in the previous section. Fig. 2.6 shows the response of the proposed system for variation in I_d^* and I_q^* . Initially, the inverter was operating with $I_d^* = 2$ A and $I_q^* = 0$ A. Then, a step change is applied in I_d^* to 4 A at 0.05s and 50 ms later a step change is applied in I_q^* to -2 A. The response is fast and well damped. The impact of a step variation of I_d^* (I_q^*) on I_q (I_d) is virtually inexistent. Besides, one can see that the waveform of I_β is not merely a $\frac{1}{4}$ line cycle phase shifted version of I_α following step variation in I_d^* and I_q^* .

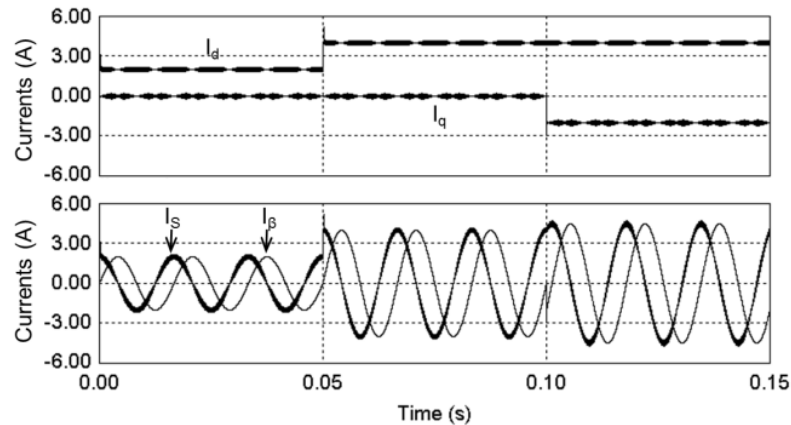


Fig. 2.6. Response for variation in I_d^* and I_q^* of new vector control technique for single-phase inverters.

The simulation results of an equivalent three-phase vector controlled inverter are presented next. This way, one can compare the $\alpha\beta$ and dq waveforms obtained for the single-phase inverter using the new dq control scheme with those of the three-phase inverter in $\alpha\beta$ coordinates. It is equivalent to the single-phase inverter in the sense that it operates with the same values of voltages in the $\alpha\beta$ coordinates, and power. Its DC bus voltage is equal to 800 V and it is connected to a 208 V three-phase grid through the same coupling impedances of the single-phase inverter. The same PI controllers are used in this case. Fig. 2.7 shows the same waveforms of Fig. 2.6 for the equivalent three-phase vector controlled inverter. There one sees that they are virtually identical to those obtained for the single-phase inverter with the new dq control scheme.

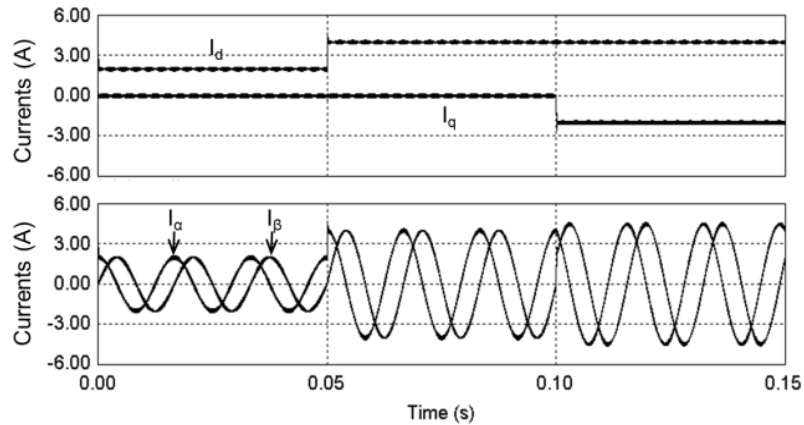


Fig. 2.7. Response for variation in I_d^* and I_q^* of conventional vector control technique for three-phase inverters.

Fig. 2.8 shows the results obtained with the conventional implementation of vector (dq) control for single-phase inverters using the $\frac{1}{4}$ cycle delay for obtaining the orthogonal component. These results were obtained for $f_x = 100$ Hz and $\zeta = 1.2$ where $k_p = 7.44$ and $k_i = 2 \times 10^3$. It should be noted that the system was unstable for $f_x > 180$ Hz,

probably due to the fact that the $\frac{1}{4}$ line cycle delay, used for obtaining I_β and then I_d and I_q , is not taken into consideration when designing the current controller [54]. The response is much slower than for the new approach and also there exists coupling between the dq currents. One can also see in Fig. 2.8 that I_β is essentially I_α phase shifted by $\frac{1}{4}$ cycle, as per the means employed for obtaining the imaginary component. This is unlike the case of three-phase inverter and single-phase inverter with the new technique.

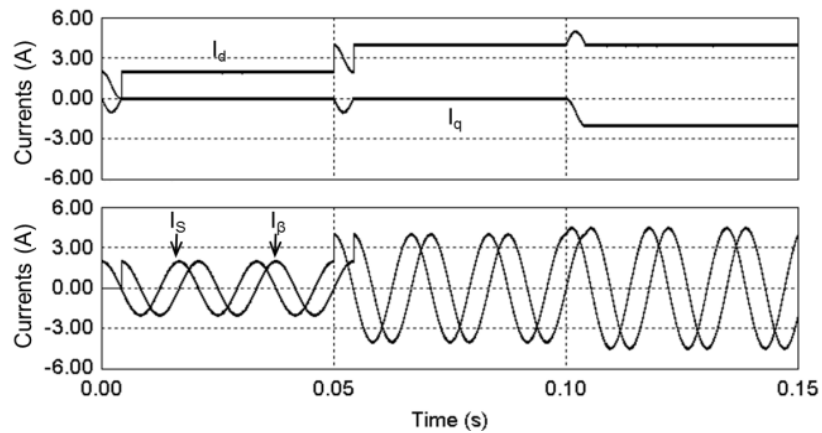


Fig. 2.8. Response for variation in I_d^* and I_q^* of conventional vector control technique for single-phase inverters.

2.3.2 Experimental Results

A laboratory prototype of a single-phase inverter was implemented with SEMIKRON IGBTs (SKM50GB123B) and gate drive circuits (SKHI22) to verify the simulation results. The control algorithm for both the new and the delay based technique were implemented in a dSPACE DS-1103 board. The inverter was connected to a 120 V, 60 Hz grid through an 80 V : 120 V single-phase transformer. The DC link voltage is 145 V and the AC side filter inductance and resistance are equal to 5 mH and 0.1 Ω . The carrier frequency used in the unipolar SPWM scheme was selected as 5 kHz because of

the dead-time of 4.8 μs in the SKHI22 gate driver circuit. A dead-time compensation logic was used to minimize the distortion, and consequent THD (total harmonic distortion), on the current created by this relatively large dead-time [69]. The results were captured in the control desk of dSPACE[®] and finally plotted using MATLAB[®].

Two PI controllers were designed for the single-phase dq controlled inverter. One for $f_x = 100$ Hz and the other for $f_x = 400$ Hz while $\zeta = 1.2$ was used for both. They can be used with the new dq control scheme but only the first one can be used for the conventional scheme due to stability reasons. The PI gains were calculated as $k_p = 30$ and $k_i = 31 \times 10^3$ and $k_p = 7.44$ and $k_i = 2 \times 10^3$, respectively. Tests with these two PIs are carried out to identify what is gained with the new dq control scheme and what is due to a current loop with a higher bandwidth.

Fig. 2.9, Fig. 2.10 and Fig. 2.11 show the steady state responses for the delay based dq control technique with the 100 Hz current loop and for the new dq control technique with the 100 Hz and 400 Hz current loops, respectively. In all cases, $I_d^* = 6$ A and $I_q^* = 2$ A. There one can see that there is zero error in steady-state in all cases. Regarding harmonic distortion in the line current, it seems to be more dependent on the bandwidth of the current loop than on the method used to implement dq control. However, since the new dq control technique allows the use of a higher bandwidth, it is advantageous in terms of low THD and fast response with respect to the conventional method. For instance, for a current loop with a 400 Hz bandwidth the magnitude of the lower order harmonics are as shown in Table 2.1, what complies with the IEEE 1547-2003 requirements [20].

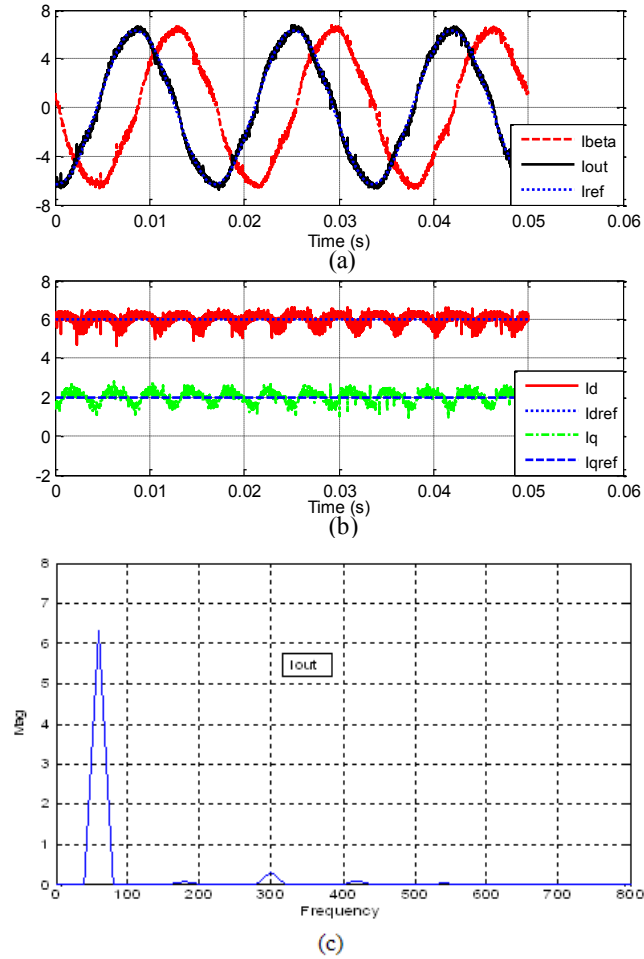


Fig. 2.9. Conventional vector (dq) control technique for single-phase inverters with 100 Hz PI. a) Fixed frame currents; b) Rotating frame currents; c) Harmonic spectrum of the line current.

Table 2.1. Harmonics for the New dq Technique with a 400 Hz Current Loop.

Fundamental	3rd harmonic	5th harmonic	7th harmonic	9th harmonic
6.35 A	85.2 mA	55.4 mA	49.4 mA	24.5 mA
100 %	1.34 %	0.87 %	0.78 %	0.39 %

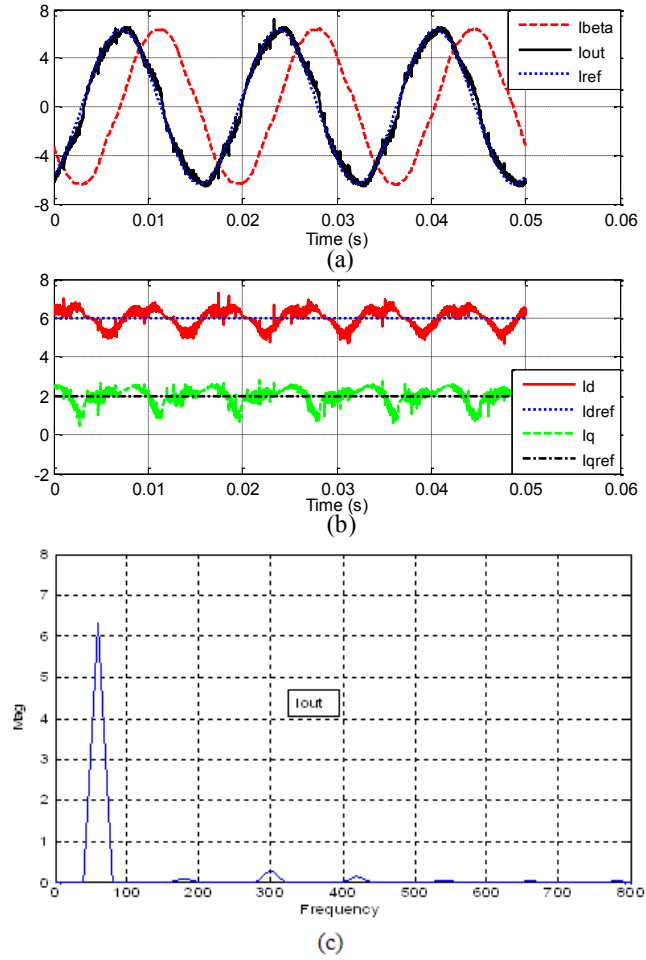


Fig. 2.10. New vector (dq) control technique for single-phase inverters with 100 Hz PI. a) Fixed frame currents; b) Rotating frame currents; c) Harmonic spectrum of the line current.

Fig. 2.12, Fig. 2.13 and Fig. 2.14 show the transient responses for the delay based dq control technique with the 100 Hz current loop and for the new dq control technique with the 100 Hz and 400 Hz current loops, respectively. Initially, the inverter was operating with $I_d^* = 4$ A and $I_q^* = 0$ A. Then, a step change is applied in I_d^* to 6 A and 45 ms later a step change is applied in I_q^* to 2 A. There, one sees that the response time of the conventional method and of the new method with a 100 Hz current loop is very similar to step variations in the reference signals. On the other hand, despite the ripple

components on the waveforms, one can clearly see the coupling between the d and q circuits for the conventional method, following a reference signal variation, what does not occur for the new method. The best result, faster and without coupling, is obtained for a 400 Hz current loop that can be used with the new method but not with the conventional one based on the $\frac{1}{4}$ line cycle delay due to stability issues.

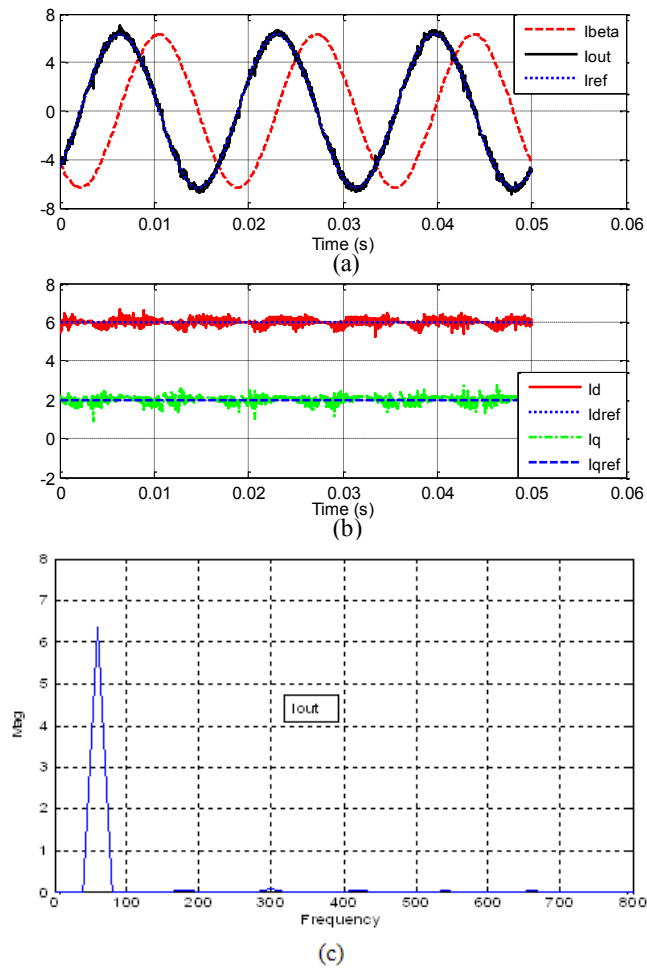


Fig. 2.11. New vector (dq) control technique for single-phase inverters with 400 Hz PI. a) Fixed frame currents; b) Rotating frame currents; c) Harmonic spectrum of the line current.

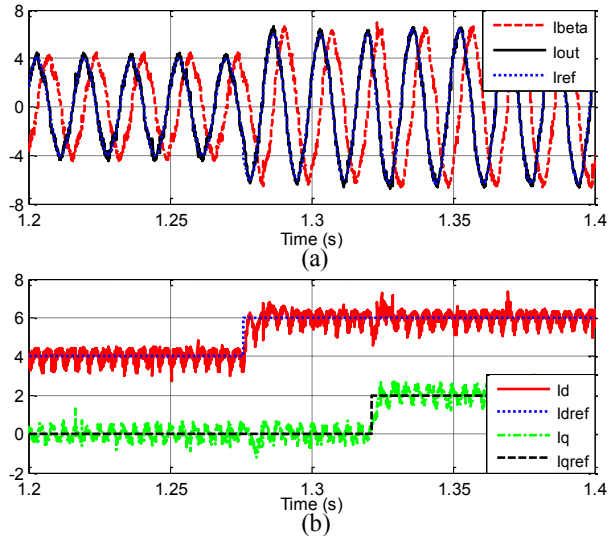


Fig. 2.12. Conventional vector (dq) control technique for single-phase inverters with a 100 Hz current loop. a) Fixed frame currents; b) Rotating frame currents.

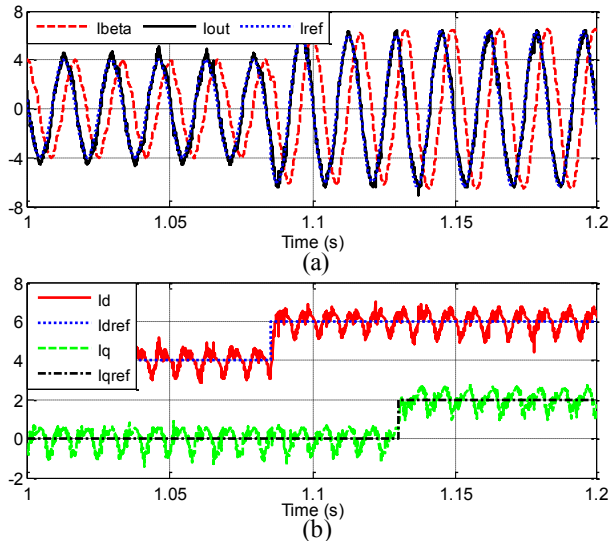


Fig. 2.13. New vector (dq) control technique for single-phase inverters with a 100 Hz current loop. a) Fixed frame currents; b) Rotating frame currents.

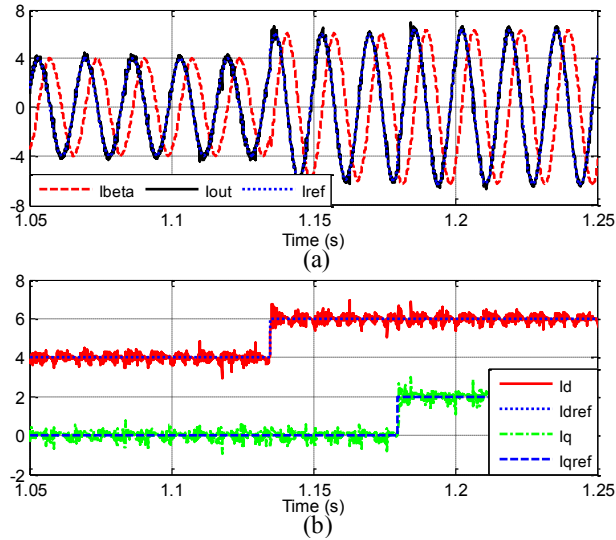


Fig. 2.14. New vector (dq) control technique for single-phase inverters with a 400 Hz current loop. a) Fixed frame currents; b) Rotating frame currents.

2.4 Vector Controlled Single-Phase Inverters under Variable Frequency Operation in Autonomous Microgrids/Mini-Grids

Microgrids/Mini-grids allow the integration of high levels of distributed and renewable generation sources into the grid and also increase grid reliability and power quality [3]. In such systems, parallel operation of the distributed generators are becoming more and more popular in order to distribute the total loads to various sources according to their availability and operating costs [70]. Paralleling of power sources with physical interconnections of control and synchronization signals, pose a restriction on the locations of the sources. In order to avoid a dedicated communication channel, the droop method is usually applied [22]. The frequency of the system is varied depending on the load demand; therefore, frequency is used for conveying information of the shortage (low frequencies) or surplus (high frequencies) of power/energy in the microgrid/mini-grid to distributed controllable sources and loads. Standards like the European EN50160 only

require the frequency in autonomous power systems (autonomous microgrid/mini-grid) to be within $\pm 2\%$ of the rated value (50 Hz) during 95% of the week and within 15% during 100% of the week [21], while IEEE Standard for such autonomous power system allows a frequency variation in a narrower range between 59.3 Hz and 60.5 Hz [20].

The PV sources are connected to the microgrid/mini-grid through VSIs. Single-phase inverters are frequently employed to connect residential roof-top PV sources (capacity below 10 kW) to the utility or microgrid/mini-grid system. The inverters should present fast dynamic current control even in case of grid frequency variation that occurs in the system for power management purpose. If one wishes to employ dq control in this application, the dq-control technique should be frequency adaptive. Fig. 2.15 shows what happens to the dq current components of a single-phase inverter operating with the conventional dq control designed for 60 Hz operation (Fig. 2.2) when the grid frequency changes from 60 Hz to 62 Hz at $t = 0.15$ s with $I_d^* = 6$ A and $I_q^* = 2$ A. The results obtained with the proposed scheme shown in Fig. 2.3 are similar to this. Therefore, a means for obtaining the orthogonal component for variable frequency conditions is required.

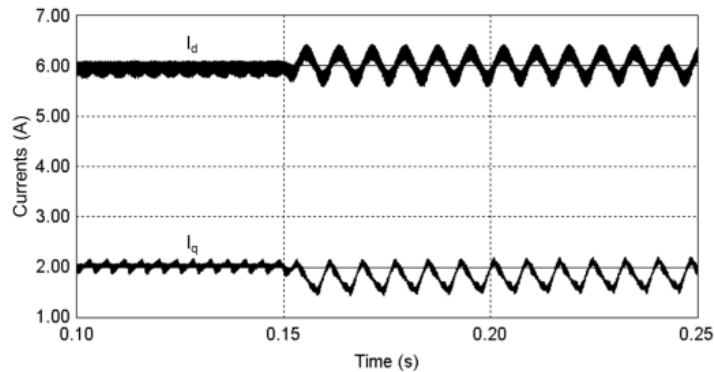


Fig. 2.15. Actual dq axis currents for T/4 delay method when the frequency varies.

2.4.1 Frequency Adaptive Single-Phase DQ Control Schemes

The various techniques discussed in section 2.1 for creating an orthogonal (β) component from a single-phase quantity are only suited for constant frequency conditions. For variable frequency conditions, one can employ a second order generalized integrator (SOGI) [71, 72] which is frequency adaptive. A possible implementation is shown in Fig. 2.16. It should be noted that this scheme requires the instantaneous angular frequency (ω) which can be obtained from the grid voltage using an adaptive PLL [72] which is based on SOGI-FLL (Frequency locked loop). This element will also provide the sine and cosine terms required for the $\alpha\beta$ -dq and dq- $\alpha\beta$ transformations. The dynamics and stability of the SOGI-FLL has been presented in [71, 72] for different adverse grid condition. In principle, large sudden variations of frequency could be an issue, but this does not occur in stand-alone systems which usually employ a rotating electro-mechanical generator as the grid forming (master) unit.

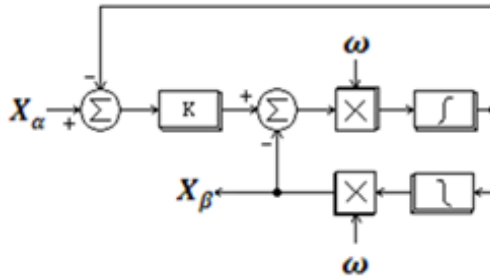


Fig. 2.16. Frequency adaptive second order generalized integrator (SOGI).

By replacing the fixed frequency $\frac{1}{4}$ line cycle blocks for the voltages shown in Fig. 2.2 and Fig. 2.3 with the SOGI of Fig. 2.16, frequency adaptive dq control schemes are obtained. Their performance will be assessed in the following sections to demonstrate the

benefits of using the fictive axis emulation in single-phase systems that operate with variable frequency.

2.4.2 Simulation Results for the Proposed Method

Simulation results for the d and q current components of a single-phase inverter with the proposed frequency adaptive FAE dq control scheme are shown in Fig. 2.17. It employs the 400 Hz PI controllers used in section 2.3.2. The grid frequency is initially at 60 Hz and the reference currents for the inverter are $I_d^* = 4$ A and $I_q^* = 0$ A. Then, a step change is applied in I_d^* to 6 A at 0.1 s and 50 ms later a step change is applied in I_q^* to 2 A. One can see from the figure that one achieves zero steady-state error and fast transient response without coupling between the d and q circuits. Then, starting at $t = 0.2$ s, the grid frequency varies every 0.05 s from 60 Hz with a step of 2 Hz. One can clearly see that frequency variations had no impact on the regulation of the d and q current components for the proposed vector current control.

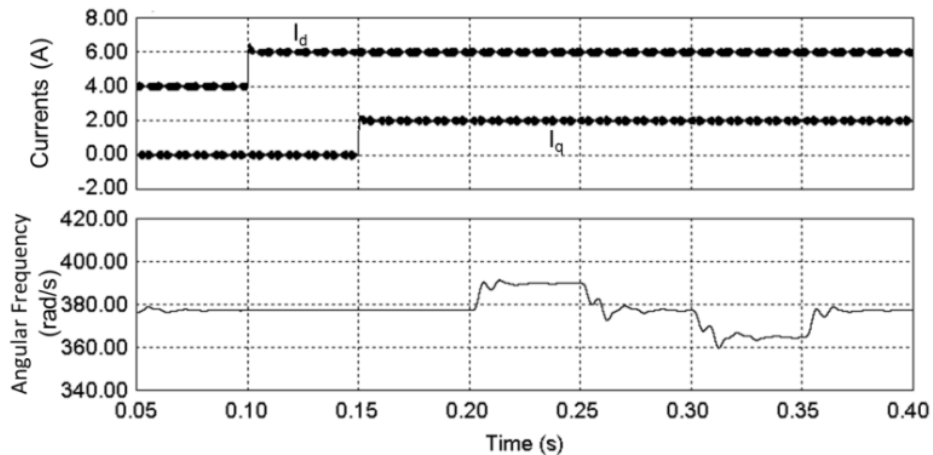


Fig. 2.17. d and q current waveforms and angular frequency.

2.4.3 Experimental Results

A programmable 4.5 kVA AC power supply from California Instruments (Model 4500 iL), which allows step changes in amplitude as well as in frequency, was used to verify the performance of two frequency adaptive single-phase dq control schemes. The same laboratory prototype of a single-phase inverter as described in section 2.3.2 was used and the control algorithm was implemented in a dSPACE DS-1103 development kit.

The performance of the proposed dq control scheme with fictive axis emulation is presented first. The PI controller was designed for $f_x = 400$ Hz and $\zeta = 1.2$ as mentioned in section 2.3.2. The steady state response with $I_d^* = 6$ A and $I_q^* = 2$ A for a grid frequency of 62 Hz is shown in Fig. 2.18. There one can see that the error is zero in steady-state.

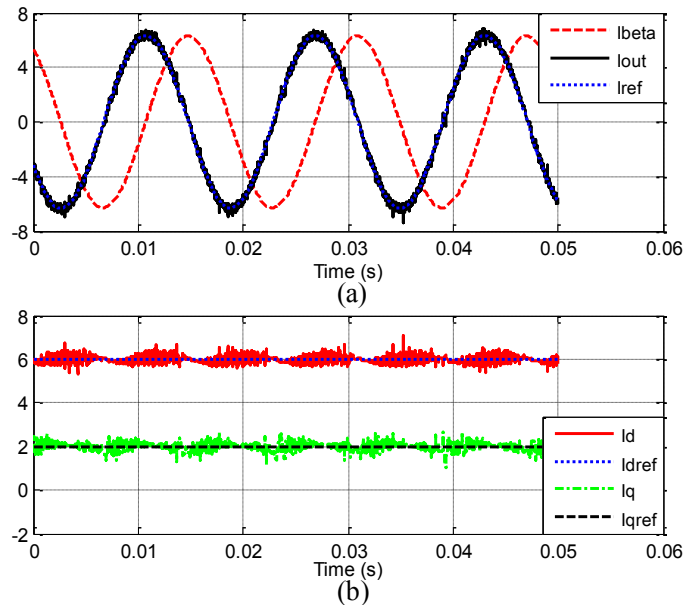


Fig. 2.18. Steady state results for single-phase dq control with FAE at 62 Hz. a) Fixed frame currents; b) Rotating frame currents.

Fig. 2.19 shows the transient response to reference current variations for a grid frequency of 62 Hz. Initially, the inverter operates with $I_d^* = 4$ A and $I_q^* = 0$ A. Then, a step change is applied in I_d^* to 6 A and 45 ms later a step change is applied in I_q^* to 2 A. The transient response is very fast and there is no coupling between d and q circuits. Fig. 2.20 shows the impact of frequency variation, from 60 Hz to 62 Hz, when the inverter operates with $I_d^* = 6$ A and $I_q^* = 2$ A. The frequency variation is tracked by the PLL and the d and q currents are regulated properly.

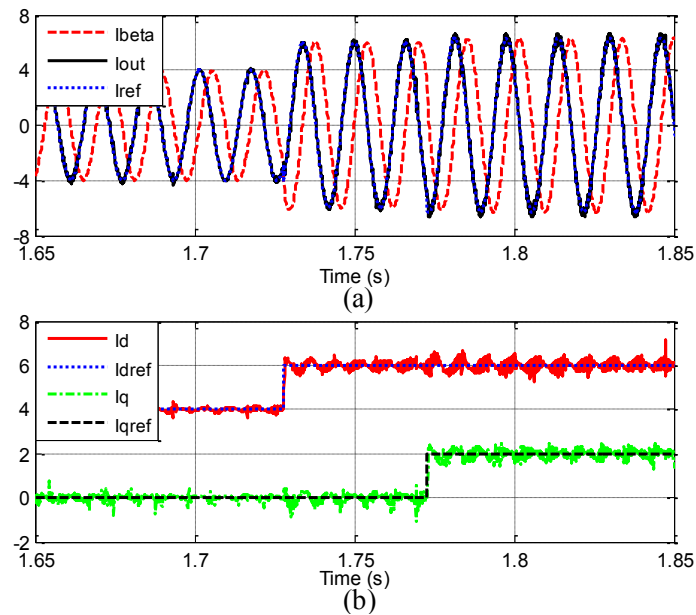


Fig. 2.19. Transient response results for single-phase dq control with FAE at 62 Hz. a)

Fixed frame currents; b) Rotating frame currents.

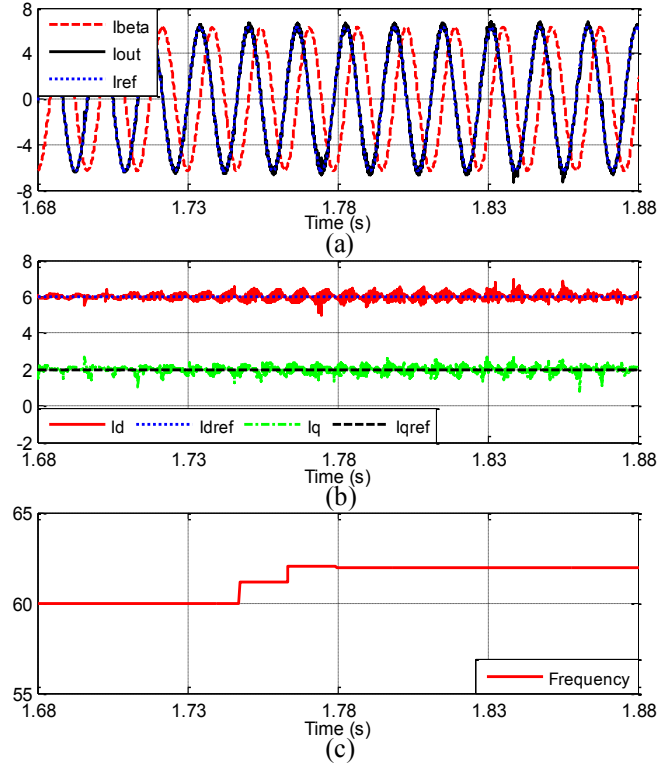


Fig. 2.20. Response to frequency variation for single-phase dq control with FAE. a) Fixed frame currents; b) Rotating frame currents; c) Frequency.

The final tests are conducted for a frequency adaptive single-phase dq control scheme that employs SOGI blocks for obtaining the β components for the grid voltage and inverter current waveforms. When the PI controller designed for $f_x = 400$ Hz and $\zeta = 1.2$ and employed successfully for the FAE scheme was used, the system became unstable. To obtain a stable and acceptable result, a new PI controller with $f_x = 250$ Hz and $\zeta = 1.2$ was designed. The PI gains were $k_p = 18.75$ and $k_i = 12.3 \times 10^3$. Fig. 2.21 shows the transient responses to reference current variations for a grid frequency of 62 Hz. Initially, the inverter operates with $I_d^* = 4$ A and $I_q^* = 0$ A. Then, a step change is applied in I_d^* to 6 A and 45 ms later a step change is applied in I_q^* to 2 A. There one sees

that the response is slower than when the fictive axis emulation is used for obtaining the β component of current (Fig. 2.20) and that there is coupling between the dq currents.

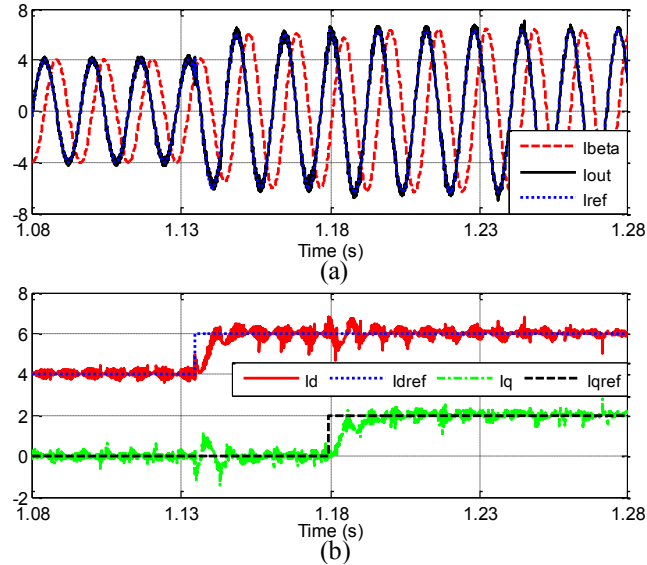


Fig. 2.21. Transient response results for single-phase dq control with two SOGI at 62 Hz.

a) Fixed frame currents; b) Rotating frame currents.

2.5 Summary of Chapter 2

This Chapter discusses additional features of a vector (dq) current control technique for single-phase inverters based on the emulation of an orthogonal circuit. It is shown that, like for a three-phase inverter, this method results in an orthogonal current component, used in the calculation of the dq components, that is not merely the α (real) component phase-shifted by 90° during transients, as obtained with previous implementations based on delaying the real component by $\frac{1}{4}$ of a line cycle. As a result, the dq components of the inverter current can be accurately calculated during transients without unnecessary delays. In this way, the current loop can be designed with a higher bandwidth, resulting in lower current harmonic distortion in the steady-state and faster

dynamic response. What is more, this approach can also be used for operation under variable frequency, a condition that can be found in photovoltaic hybrid autonomous microgrids/mini-grids, where the grid frequency is used for energy management purposes. Simulation and experimental results are provided to demonstrate the effectiveness of the proposed technique.

CHAPTER 3

PER-PHASE VECTOR (DQ) CONTROLLED THREE-PHASE GRID FORMING INVERTER

Hybrid stand-alone power systems (mini-grids) are usually based on diesel power plants. In such systems, the use of renewable energy sources (RES) and energy storage units can decrease the cost and environmental impact of electricity production. The ideal case would be to run the mini-grid with all diesel generators off, what would require a battery inverter, usually voltage source inverter type, to form the grid, balancing active and reactive power, and the RESs would operate at their maximum power point [73].

Generally, electrical distribution systems are of the three-phase type, allowing loads and RESs to be connected either in three-phase or single-phase, depending on their number of phases and power ratings. These loads/sources are usually arranged in order to result in a balanced power distribution across the three phases. However, in mini-grids with a relatively small number of loads, it is more likely that “load unbalances” will occur, leading to unequal voltage drops in the low-pass filter of the grid forming inverter and unbalanced output voltages. This can result in increased losses and heating in rotating machines, saturation of transformers as well as malfunction of protection devices [18]. Therefore, it is important that the grid forming inverter presents a suitable control scheme to supply balanced voltages to an unbalanced distribution grid while sourcing or sinking unbalanced currents. Besides, since frequency variation is frequently used for

active power sharing among battery inverters as well as for energy management, the inverter should be able to perform these tasks under variable frequency conditions.

There are a number of voltage source inverter (VSI) topologies suitable for operation in three-phase systems. For a three-phase three-wire system, the conventional widely employed three-leg VSI can be used as grid forming unit. While for the three-phase four-wire system, there are several choices. The three-leg inverter with a split DC link capacitor is the simplest one but capacitor voltage balancing can be an issue in the presence of zero sequence current components [39, 74]. Alternatively one can use a three-leg inverter with a Δ -Y transformer [75-77]. The zero sequence current component would be trapped or “circulating in the Δ winding” and the control circuit of the inverter would only have to compensate for the voltage drops of the positive and negative sequence currents on the output filter of the inverter, in the primary of the transformer. Another sophisticated and flexible topology is the four-leg inverter, where an additional leg is used for the zero sequence current components [54, 78].

Regarding the control scheme for balancing the output voltages of the grid forming inverter operating with unbalanced loads, there are also many choices as discussed in section 1.2. A common inverter control approach to provide balanced fixed frequency voltages to unbalanced loads is first to obtain the (balanced) symmetrical components and then use the classical three-phase dq control to avoid the first and second order ripple components in the dq signals [35-39, 45]. The 90° phase shift required for a realization of the symmetrical components calculator (SCC) introduces a significant delay in the system, difficult to be compensated for. Some other solutions based on low-pass/notch filters have been proposed in [29, 32, 40, 41, 44] for dq control of grid forming inverter.

However, the use of filters results in slow dynamic response. Besides, all these methods are not suitable for variable frequency operation. Some SCC-less techniques have been proposed in [30, 34], however, they have limitations (i.e., operate with specific range of unbalanced load, slow dynamic response, etc.) as discussed in section 1.2. Finally, the impact of unbalanced renewable supply, commonly based on single-phase inverters, and the possibility of operating with variable frequency have not been considered in any of the cases above.

The control approach proposed in this chapter for a three-phase grid forming inverter capable of supplying highly unbalanced loads with balanced voltages is based on the use of per-phase dq control with fictive axis emulation in the inner current loop [62, 64, 67]. In this way, one can avoid the use of the SCC block which introduces delays in the feedback signals and complicates the design of the PI-type controllers. Besides, since second order generalized integrators (SOGIs) are only used in the outer voltage loop, the system response to load variations is very fast. The superior performance of the proposed technique is demonstrated by means of simulations and experimental results.

As mentioned earlier in this section, there can be different topologies for the grid forming inverters. Therefore, at first the proposed topology is developed for the three-phase three-wire grid forming inverter. Then, the control strategies for three-leg inverter with Δ -Y transformer and four-leg inverter are presented for application in three-phase four-wire systems.

3.1 Per-Phase DQ Control of a Three-Phase Three-Wire Grid Forming VSI

The concept of per-phase dq control of a three-leg inverter for a three-phase three-wire unbalanced system has been presented in [64, 79]. In the absence of a neutral wire, the load currents do not present zero sequence components and a per-phase dq-controlled three-leg inverter can be used to indirectly regulate the positive sequence component of the output voltage and cancel the negative sequence voltage drop on the inverter output filter. Fig. 3.1 shows a generic three-phase three-wire diesel-PV-battery hybrid mini-grid. In this study, the diesel genset is assumed to be off, disconnected from the mini-grid. The three-phase battery inverter forms the grid, balancing supply from the single-phase PV inverter, connected between two lines and demand from the unbalanced loads. The three phase legs of the battery inverter are connected to the distribution feeder through LC filters, with the resistance of the inductor modeled and that of the capacitor neglected.

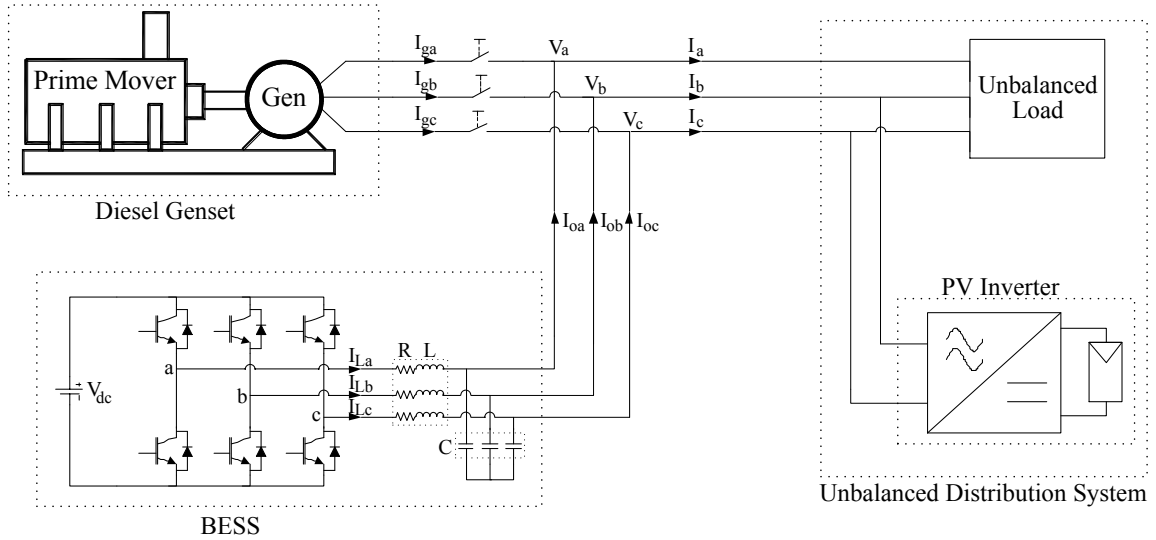


Fig. 3.1. Circuit diagram of a three-phase three-wire grid forming inverter operating in diesel-hybrid mini-grid with single-phase RES and unbalanced load.

3.1.1 Conventional VSI Control Approach

Fig. 3.2 shows the block diagram of the control circuit of a conventional three-leg grid forming VSI supplying a three-phase unbalanced load. Since the zero sequence component is not present in the three-phase three-wire system, so the voltage drops across the output filter of the inverter is only due to the positive and negative sequence current components, what makes it actually possible for the control circuit of the inverter to balance and regulate its output voltage.

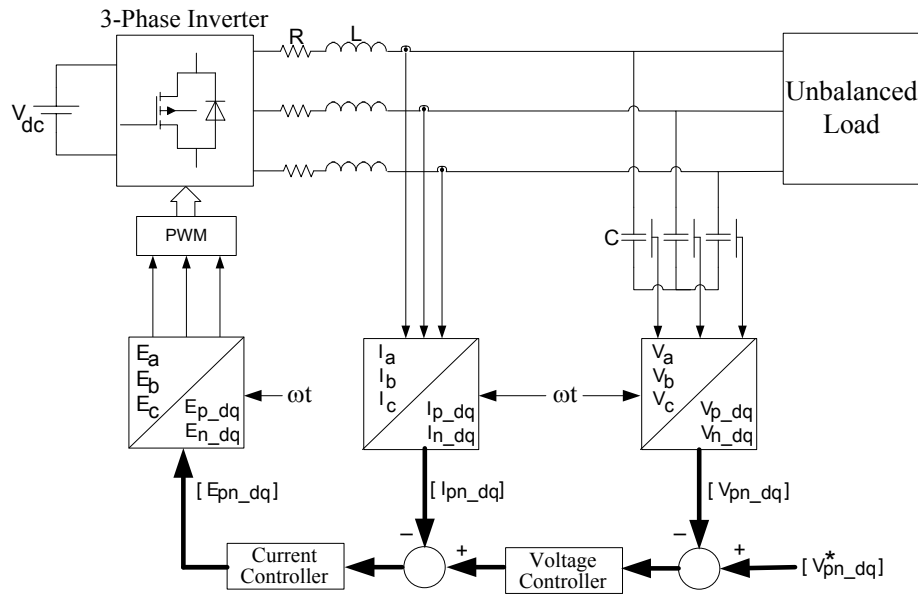


Fig. 3.2. Circuit diagram for conventional cascaded control of grid forming inverter.

The control circuit of the VSI is based on dq (vector) control following the extraction of the symmetrical components from the unbalanced voltages and currents and conversion into dq frames. Since the symmetrical components are balanced, there will be no double line frequency components in the dq signals. The dq control loops are employed in two similar channels: One for controlling positive sequence components and the other for controlling the negative sequence components [35-39, 45].

3.1.1.1 VSI Employing Cascaded Control Loop

The detailed circuit diagram for cascaded control of an inverter feeding an unbalanced load through an LC filter is shown in Fig. 3.3. The output of the outer voltage loops for all channels provide the reference signals for the inner current loops. Simple PI-type controllers are used to regulate the positive and negative sequence dq voltage components. The q-component of the positive sequence reference voltage is set to the peak value of the desired phase voltage. The other reference voltages are set to zero since the inverter is expected to supply balanced voltages.

Simple PI-type controllers are also used in the inner current loops. Their design can be done following the conventional approach for vector control of three-phase VSIs. Appropriate feed-forward (FF) of the current and voltage is adopted to decouple dq-axis dynamics. The output of the current control loops (E_{pd} , E_{pq} , E_{nd} and E_{nq}) are converted to positive and negative sequence components in the rotating frame (abc) and then added to serve as the modulation signals in the SPWM block.

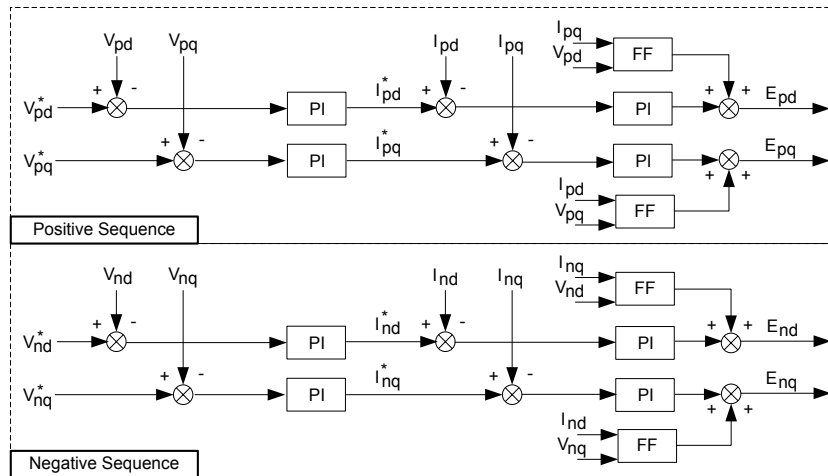


Fig. 3.3. Cascaded voltage and current regulation loops for the conventional method.

3.1.1.2 Extraction of the Symmetrical Components

In order to apply the dq control without the double line frequency component, one needs to obtain the positive and negative sequences of the output capacitor voltage and inverter inductor current. Recall that there are no zero sequence components in a three-phase three-wire system. Any unbalanced quantities (x_a , x_b and x_c) can be decomposed into positive and negative sequence symmetrical components by using the following equations.

$$\begin{bmatrix} x_{a+} \\ x_{b+} \\ x_{c+} \end{bmatrix} = \frac{1}{3} \begin{bmatrix} 1 & -1/2 & -1/2 \\ -1/2 & 1 & -1/2 \\ -1/2 & -1/2 & 1 \end{bmatrix} \begin{bmatrix} x_a \\ x_b \\ x_c \end{bmatrix} - \frac{1}{j2\sqrt{3}} \begin{bmatrix} 0 & 1 & -1 \\ -1 & 0 & 1 \\ 1 & -1 & 0 \end{bmatrix} \begin{bmatrix} x_a \\ x_b \\ x_c \end{bmatrix} \quad (3.1)$$

$$\begin{bmatrix} x_{a-} \\ x_{b-} \\ x_{c-} \end{bmatrix} = \frac{1}{3} \begin{bmatrix} 1 & -1/2 & -1/2 \\ -1/2 & 1 & -1/2 \\ -1/2 & -1/2 & 1 \end{bmatrix} \begin{bmatrix} x_a \\ x_b \\ x_c \end{bmatrix} + \frac{1}{j2\sqrt{3}} \begin{bmatrix} 0 & 1 & -1 \\ -1 & 0 & 1 \\ 1 & -1 & 0 \end{bmatrix} \begin{bmatrix} x_a \\ x_b \\ x_c \end{bmatrix} \quad (3.2)$$

where, operator j corresponds to a 90° phase shift. This has been implemented in [38, 45] with a quarter cycle delay and with an all-pass filter (APF) in [35-37, 39]. In both cases, the response of the entire systems due to variations in the reference signals or to load variations was relatively slow. Besides, they are designed for a particular frequency, therefore cannot be used with variable frequency mini-grid system. In this research work, a SCC based on a first order APF was implemented and used in the conventional scheme to provide a means of comparison with the proposed technique. Its transfer function is,

$$APF(s) = \frac{s\tau - 1}{s\tau + 1} \quad (3.3)$$

where, $\tau = 2.6525 \times 10^{-3}$ for operation at 60 Hz.

3.1.2 Proposed Per-Phase DQ Control Approach

One alternative for doing away with the SCC used in the previously mentioned three-phase dq control scheme is to employ per-phase dq control, regulating the output voltage of each phase of the VSI, individually. In such a case, the reference signals for the three phases would have the same magnitude but would be phase shifted by 120° . The main challenge is to be able to achieve the fast dynamic response of three-phase dq control in a per-phase basis, what has been shown to be possible with the fictive axis emulation discussed in Chapter 2. The following sections describe how this can be done.

3.1.2.1 The Per-Phase Cascaded dq Control Block

On a per-phase basis, the fundamental component of the switched voltage of one phase of the inverter can be modeled as an ideal controlled voltage source (E_{inv}). The inverter inductor current and capacitor voltages are I_L and V_C respectively. The load connected to that phase of the grid forming inverter can be represented by a current source (I_o) as shown in Fig. 3.4.

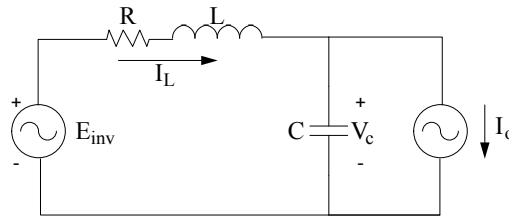


Fig. 3.4. Schematic of the system on per-phase basis.

For representing voltages and currents of a single-phase system in dq frame, one needs first to create a two-phase system with orthogonal components. The α components are obtained and measured from the real single-phase circuit. The β components are

obtained from a fictive circuit where all voltages and currents are phase-shifted by 90° , in steady-state, with respect to the real voltages and currents.

Equations (3.4) and (3.5) represent the system model of Fig. 3.4 in $\alpha\beta$ frame. By applying Park transformation in (3.4)-(3.5) one gets the well-known model of the system in dq frame, given by (3.6) and (3.7).

$$L \frac{di_{L\alpha\beta}}{dt} = e_{inv\alpha\beta} - i_{L\alpha\beta} R - v_{C\alpha\beta} \quad (3.4)$$

$$C \frac{dv_{C\alpha\beta}}{dt} = i_{L\alpha\beta} - i_{o\alpha\beta} \quad (3.5)$$

$$\begin{bmatrix} \frac{di_d}{dt} \\ \frac{di_q}{dt} \end{bmatrix} = -\frac{R}{L} \begin{bmatrix} i_d \\ i_q \end{bmatrix} + \frac{1}{L} \begin{bmatrix} e_d \\ e_q \end{bmatrix} - \frac{1}{L} \begin{bmatrix} v_d \\ v_q \end{bmatrix} + \omega \begin{bmatrix} i_q \\ -i_d \end{bmatrix} \quad (3.6)$$

$$\begin{bmatrix} \frac{dv_d}{dt} \\ \frac{dv_q}{dt} \end{bmatrix} = \frac{1}{C} \begin{bmatrix} i_d \\ i_q \end{bmatrix} - \frac{1}{C} \begin{bmatrix} i_{od} \\ i_{oq} \end{bmatrix} + \omega \begin{bmatrix} v_q \\ -v_d \end{bmatrix} \quad (3.7)$$

The use of dq control in single-phase inverters with regulated output voltage has been addressed by several literatures [54, 58, 60]. A common approach is to use cascaded inner current and outer voltage loops. This is also used in this research work as shown in Fig. 3.5. In the inner current loop, V_{Ca} and I_{La} represent “a” phase voltage at the output filter capacitor and the current in the output filter inductor, respectively. V_β , the orthogonal component to V_{Ca} (V_α), required for computing the dq components of the single-phase system is obtained with a second order generalized integrator (SOGI) which is described in more details in Section 2.4.1. Since the SOGI output was 90° lagging, therefore, a gain of -1 is used to make the β -component 90° leading as required for the

Park transformation. It should be noted that due to the relatively slow response of the SOGI, it is not the best choice to compute the β component of the output filter inductor current, which should be varied very fast in order to respond to load current variations and keep the capacitor voltage regulated. Instead, the orthogonal current component (I_β) can be obtained by emulating a fictive circuit as shown in Fig. 3.5, in bold lines. More details on this technique are presented in [61, 62, 67]. Then using Park transformation the $\alpha\beta$ components (stationary frame) are transformed to dq components (rotating frame). In addition, feed-forward (FF) loops are also used to compensate for the coupling between the dq equivalent circuits created by the output filter inductor in the actual AC circuit. The $\sin\theta$ and $\cos\theta$ terms required for the Park and inverse Park transformations are obtained from the output reference voltage with a simple PLL.

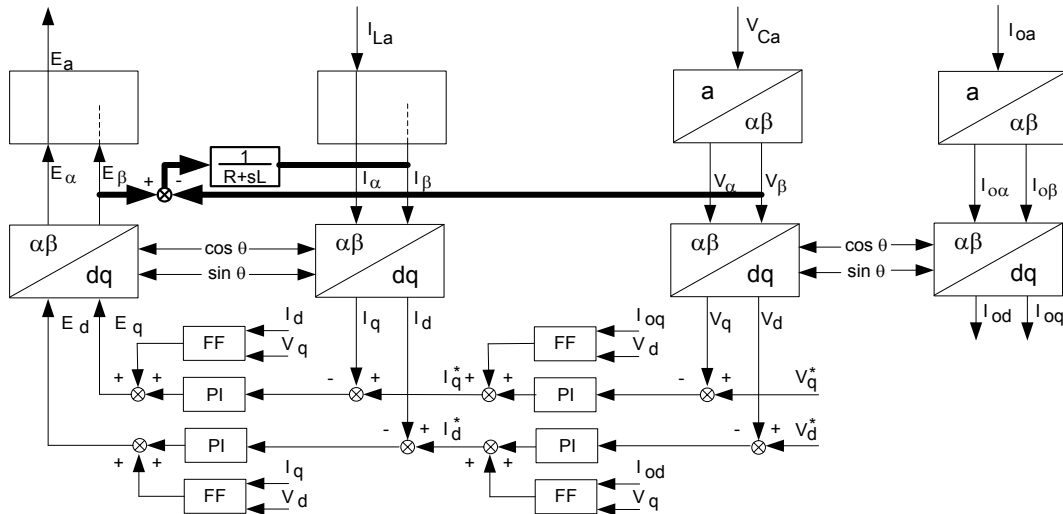


Fig. 3.5. Schematic diagram of the per-phase cascaded control block.

Regarding the outer voltage loop, the orthogonal components of phase ‘a’ actual output phase voltage (V_{Ca}) and the respective inverter output current (I_{oa}) are obtained using SOGIs. Feed-forward loops are also used to compensate for the coupling between

the dq equivalent circuits created by the output filter capacitor in the actual AC circuit. The PI-type controllers for the current and voltage loops are designed in the conventional way, for regulating DC signals, with the outer voltage loop 10 times slower than the inner current loop. V_q^* is set at the peak value of the reference phase voltage while V_d^* is set at 0V. Similar per-phase controllers also apply for phase 'b' and phase 'c' with the three θ angles being 120° apart.

3.1.3 Performance Verification

The performance of the proposed technique is compared to that of the conventional three-phase dq control with symmetrical components calculator by simulation using PSIM[®]. The three-phase grid forming inverter operates with SPWM at 6 kHz from a 460 V DC bus. The desired load voltage is 220 V (L-L) at 60 Hz. The current and voltage sensors are assumed to be ideal with a unity gain. The inductance and resistance of the output filter inductor are equal to 3 mH and 0.1 Ω . The capacitance is 25 μ F.

The PI controllers were designed as described in [68]. The inner current control loop was designed for a bandwidth (f_x) of 1200 Hz and damping factor (ζ) equal to 1.2, yielding $k_p = 3.6$ and $k_i = 120$. This inner current loop was used for the proposed per-phase vector control and for the conventional three-phase cascaded control. The outer voltage loop for the proposed per-phase vector control was designed for a bandwidth of 120 Hz and damping factor (ζ) of 0.707, yielding $k_p = 0.027$ and $k_i = 14.21$. When this controller was used in the conventional three-phase cascaded control, the system became unstable. The solution employed was to increase the ζ to 0.9, yielding $k_p = 0.034$ and $k_i = 14.21$ and resulting in a stable response. Lower values of damping result in instability. It

may be due to the dynamics presented by the SCC in the feedback path, which was not taken into account in the design of the controllers.

Fig. 3.6 shows the results for the per-phase vector control of the grid forming inverter under unbalanced load conditions. Initially it supplies a 4.5 kW balanced resistive load and the dq components of the voltage and currents for each phase have the same magnitude as they are supplying the same power to the load. At $t = 0.3$ s, a 20Ω resistance is applied between lines A-B. At $t = 0.4$ s, an inductive load ($R = 10 \Omega$, $L = 150$ mH) is applied between lines C-A. It is evident from the results that whenever a load change occurs, it only affects the corresponding phases while the remaining 3rd phase is not affected as can be seen in Fig. 3.6(b) and Fig. 3.6(c). It also settles down quickly to the new desired value within less than a half-cycle.

Fig. 3.7 shows the simulation results for the conventional vector control of the grid forming inverter using cascaded control loops. The load variations for this case are identical to those used for the inverter controlled with the per-phase dq control. There one can see that it exhibits invariably slower transient response than that achieved with the proposed technique. In case of balanced load the dq axis negative sequence current components are zero and when the load becomes unbalanced then it supplies the required negative sequence current components as seen in Fig. 3.7(c). Similarly, for the positive sequence current components, the q-axis current component increases at 0.4 s as the load active power demand increases, while the d-axis current is not affected as seen in Fig. 3.7(c).

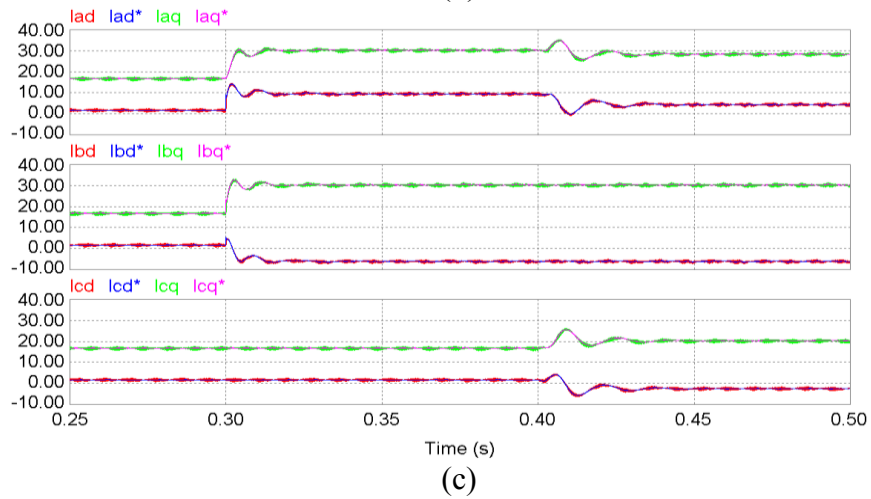
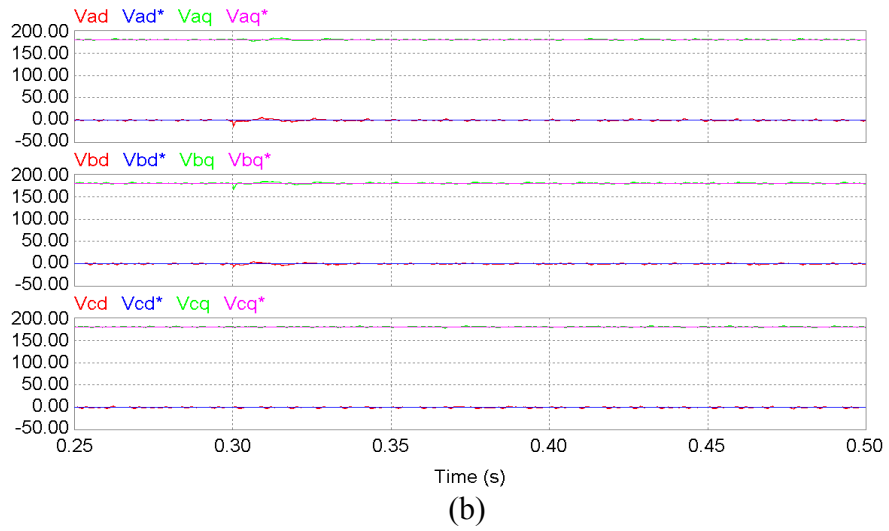
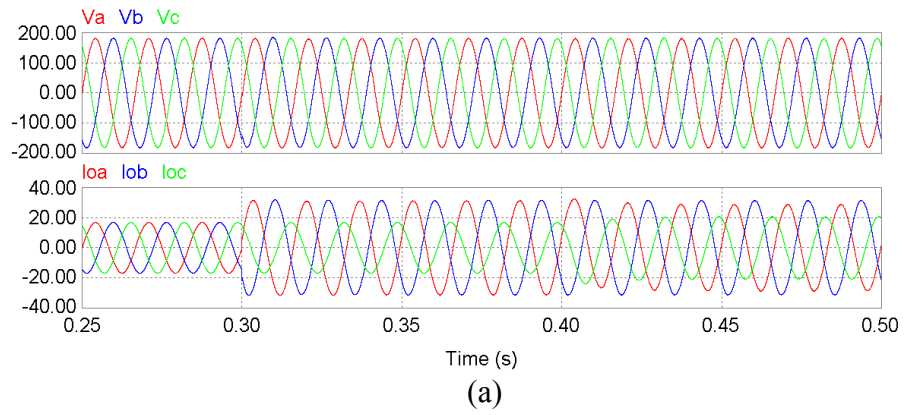
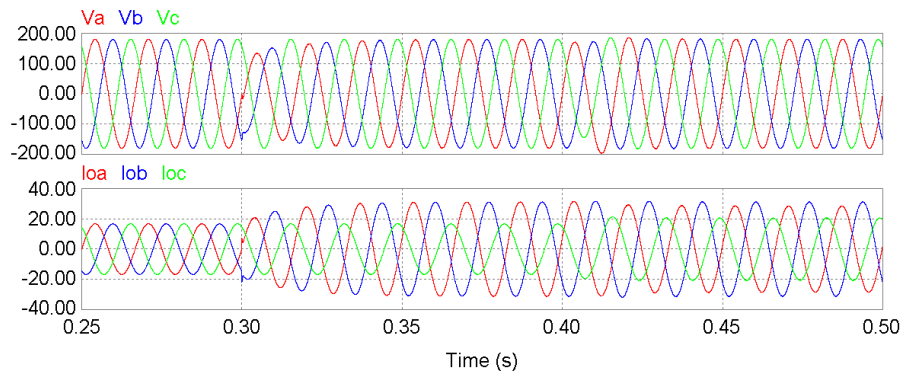
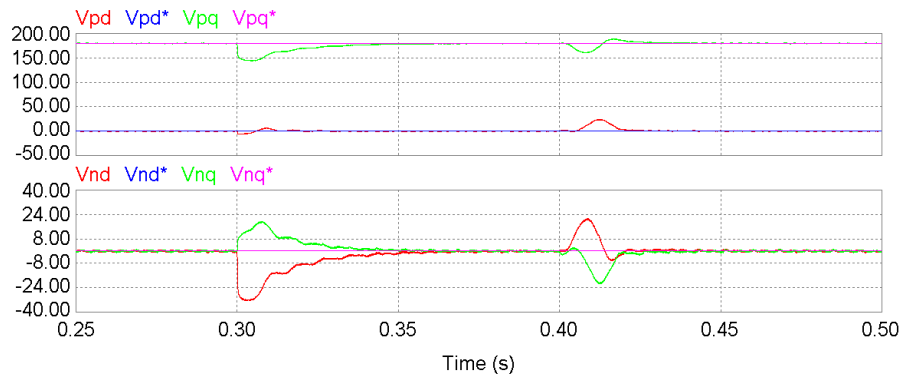


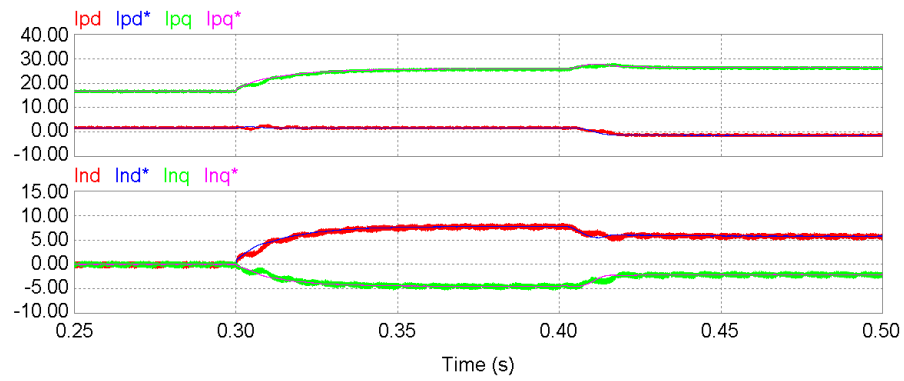
Fig. 3.6. Waveforms for the per-phase vector control. a) Load voltages and currents; b) dq-frame reference and actual voltages for the three phases; c) dq-frame reference and actual inverter currents for the three phases



(a)



(b)



(c)

Fig. 3.7. Waveforms for the conventional vector control. a) Load voltages and currents; b) dq-frame reference and actual voltages; c) dq-frame reference and actual inverter currents.

3.2 Per-Phase DQ Control of a Three-Phase Four-Wire Grid Forming VSI with Δ -Y Transformer

Three-leg voltage source inverters (VSIs) with a Δ -Y transformer between the inverter/filter and distribution system are used frequently for three-phase four-wire systems [35, 76, 77]. The transformer provides isolation, prevents DC injection from the inverter system and also allows operation with low DC link voltage for the storage battery [76]. With the Δ -Y transformer, the zero sequence component of the distribution feeder current is trapped or “circulates in the Δ winding”. Therefore, the control scheme for the grid forming inverter only needs to consider the voltage drops of the positive and negative sequence components across the output filter [76, 80].

The three-leg grid forming inverter with Δ -Y transformer in a hybrid stand-alone system is shown in Fig. 3.8. The load can include both single-phase and three-phase elements. A single-phase PV source is connected between a phase and the neutral. It is evident that this system can present severe load unbalances, requiring a grid forming inverter with a high performance control scheme to avoid voltage unbalances. The grid forming inverter is connected to the unbalanced load using LC filter and a Δ -Y transformer. The series equivalent impedance of the transformer is referred to the primary and is accounted for in the primary side filter impedance. For the LC filter, R is the resistance of the filter inductance (L) in the primary side of the transformer and C is the filter shunt capacitance in the secondary side of the transformer. The neutral point of the load is connected to the secondary side (Y-side) neutral terminal of the transformer.

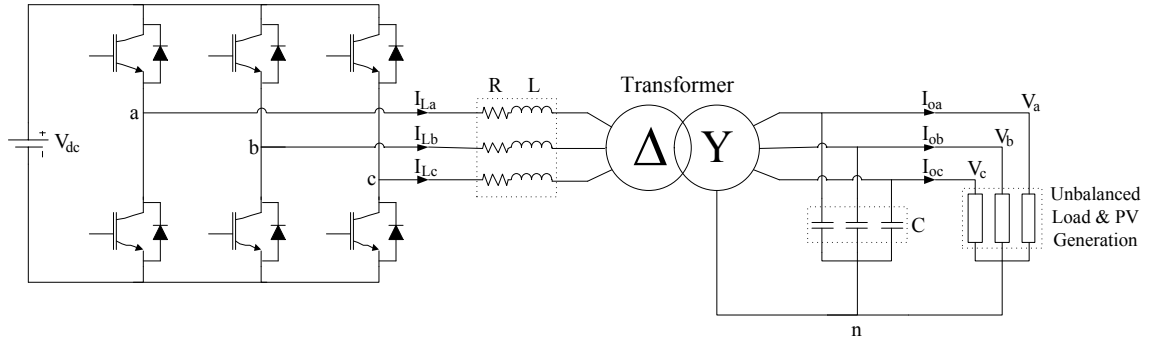


Fig. 3.8. Δ -Y transformer based grid forming inverter with unbalanced loads and source(s).

In the absence of a neutral wire as shown in section 3.1, the zero sequence component does not exist in the inductor currents and a per-phase dq-controlled three-leg inverter can be used to indirectly regulate the positive sequence component of the output voltage and cancel the negative sequence voltage drop on the inverter output filter. In principle, the same strategy can be used in a three-phase four-wire system, consisting of a three-leg inverter with a Δ -Y transformer between the inverter/filter and load. Since the zero sequence current components created by phase-to-neutral loads circulate in the Δ winding of the transformer, they would not create any additional voltage drops in the output filter inductor of the three-leg inverter. The same per-phase control strategy proposed in the previous section can be used with some modifications in the control strategy which will account for the impact of the phase shift introduced by the Δ -Y transformer, as described in the next section.

3.2.1 Control Strategy with the Impact of Δ -Y Transformer

The circuit diagram of the three-phase Δ -Y transformer is shown in Fig. 3.9 which can be represented by three single-phase transformers. The turns ratio of each single-phase unit is $n = N_p/N_s$, where N_p and N_s are the number of turns in the primary and

secondary windings respectively. The transformer impedance is approximated by the series impedance referred to the primary and is combined with the output filter inductor.

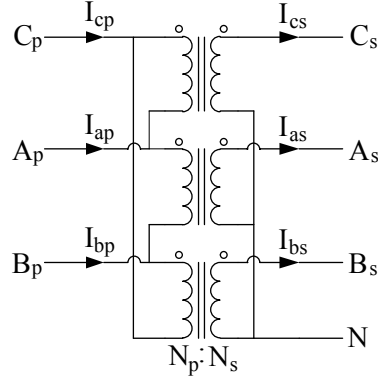


Fig. 3.9. Three-phase Δ -Y transformer.

Due to the Δ -Y connection of the isolation transformer, the voltages applied to the transformer primary (Δ) windings are reflected to the transformer secondary (Y) windings with 30° phase rotation. The stability of the closed loop control system is affected negatively when the control action is carried out without considering the phase difference between the primary and secondary winding sets of the transformer. For the connection shown in Fig. 3.9, the primary voltage lags the secondary side voltage by 30° . Again, the relation between the instantaneous primary input current and secondary output currents for the three-phase Δ -Y transformer of Fig. 3.9, is given by,

$$i_{ap} = \frac{1}{n}(i_{as} - i_{cs}) \quad (3.8)$$

$$i_{bp} = \frac{1}{n}(i_{bs} - i_{as}) \quad (3.9)$$

$$i_{cp} = \frac{1}{n}(i_{cs} - i_{bs}) \quad (3.10)$$

For the analysis of the secondary side voltage regulation, the capacitors and output current sensors are connected in the secondary side, while the inverter output L-filter is

connected in between the VSI and the primary side of the transformer. Therefore, the outer voltage control loop works in the secondary while the inner current control loop works in the primary. Due to the 30° phase shift of the transformer, since it is required to regulate the voltage across the capacitors and load, if the secondary side voltage controller for phase 'a' works with a phase angle of $\theta = \omega t$, then the primary side current controller for phase 'a' should work with a phase angle of $(\theta - 30^\circ) = (\omega t - 30^\circ)$. Similarly, the other phases will have the 30° phase shift between the voltage and current control loops.

For a three-phase three-wire system, the output of the voltage controller is the reference current for the inner current loop as shown in section 3.1.2. But in this case, the output of the voltage controller is the reference signal for the input current that has to be supplied to the common point of the capacitor and load, from the secondary side of the transformer. Since the current controller works in the primary side, so the output of the voltage controller, which is the reference current in the secondary side, should be transformed into the primary side current. So the transformation of the reference currents from the secondary to the primary should be adopted at this point. Therefore, the dq output from the voltage controller is converted to $\alpha\beta$ that corresponds to transformer secondary reference current (Park Transformation with phase angle ωt for phase 'a'). Then using the current transformation relation, it is reflected to the primary $\alpha\beta$ reference currents and then finally into dq components for the primary side (Park Transformation with phase angle $\omega t - 30^\circ$ for phase 'a') and passed to the current controller. This process for phase 'a' is shown in Fig. 3.10. Similarly, the currents of phase 'b' and 'c' can be transformed, but the phase angles (θ_b or θ_c) will be 120° shifted.

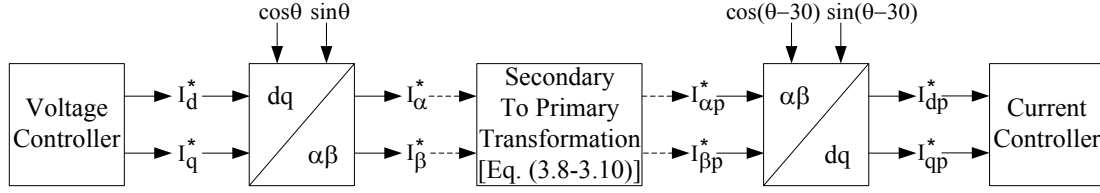


Fig. 3.10. Reference current transformation for phase ‘a’.

Similarly, the fictive axis circuit emulation is updated for the inner current loop. The fictive axis circuit is emulated with the β components of inverter output voltage and the primary side voltage of the transformer for each phase. Without loss of generality for phase ‘a’, the beta component of the inverter output voltage is generated using inverse Park transformation (using phase angle $\omega t - 30^\circ$) from the dq output of the current controller. The primary side β component of voltage can be obtained using equation (3.11). The instantaneous primary side voltage ($\alpha\beta$) for each phase can be calculated from the instantaneous secondary side voltage ($\alpha\beta$) using the following equation,

$$\begin{bmatrix} v_{\alpha p} \\ v_{\beta p} \end{bmatrix} = n \begin{bmatrix} \frac{\sqrt{3}}{2} & -\frac{1}{2} \\ \frac{1}{2} & \frac{\sqrt{3}}{2} \end{bmatrix} \begin{bmatrix} v_{\alpha s} \\ v_{\beta s} \end{bmatrix} \quad (3.11)$$

3.2.2 Performance Verification

The performance of the proposed technique is verified by simulation using PSIM[®]. The three-phase grid forming inverter operates with SPWM at 8 kHz from a 460 V DC bus. The desired load voltage is 220 V_{L-L} at 60 Hz. The inductance and resistance of the output filter inductor including the transformer series impedance are equal to 3 mH and 0.1 Ω . The filter capacitance is 25 μ F. The turns ratio of each single-phase unit of the Δ -Y transformer is $n = 1:1/\sqrt{3}$. Therefore, the magnitude of line/phase voltages is the same on both sides of the three-phase transformer. The PI controllers were designed as

described in [68]. The inner current control loop was designed for a bandwidth (f_x) of 1200 Hz while the outer voltage loop was designed for $f_x = 120$ Hz.

Initially the grid forming inverter supplies a balanced Y-connected load (10.752 Ω /ph.). At $t = 0.3$ s, a resistive load of 15 Ω is added to phase A and at $t = 0.4$ s, an inductive load ($R = 10$ Ω and $L = 15$ mH) is added to phase C. Finally, at $t = 0.5$ s a single-phase PV inverter connected between phase B and neutral, starts supplying 20 A (peak) with unity power factor. Note that this is more than the current consumed by the load(s) in this phase. The three-phase load voltages, load currents (with neutral wire current) and the inverter output currents are shown in Fig. 3.11 while the reference and actual voltages and currents in the three per-phase dq controllers are shown in Fig. 3.12.

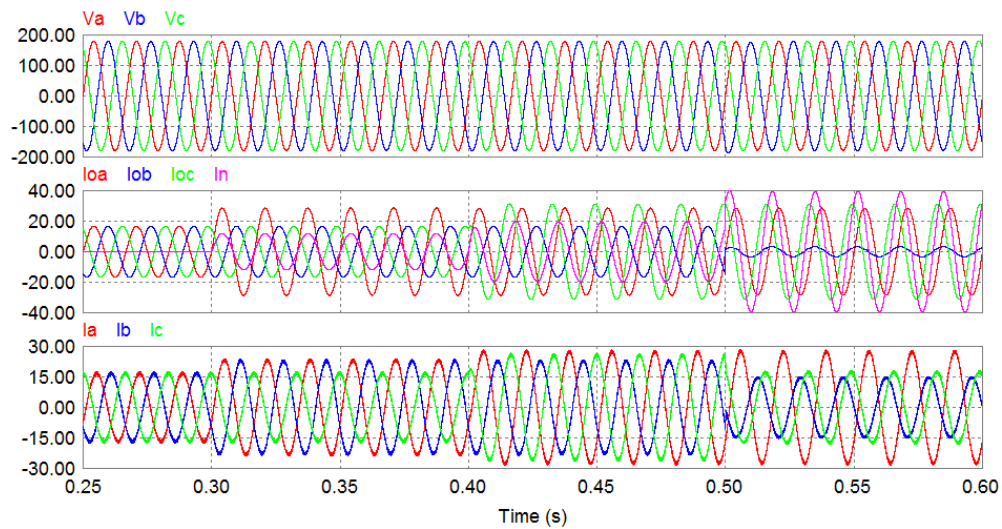
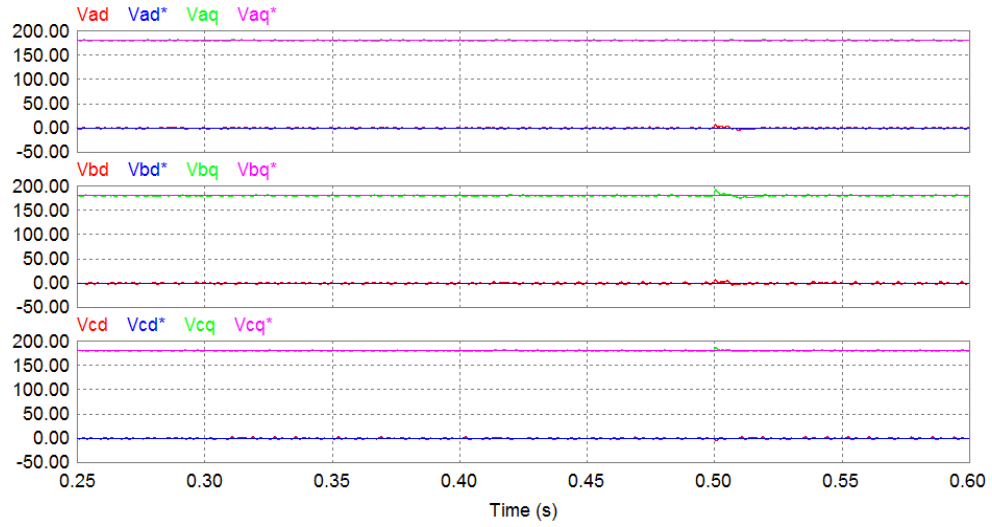


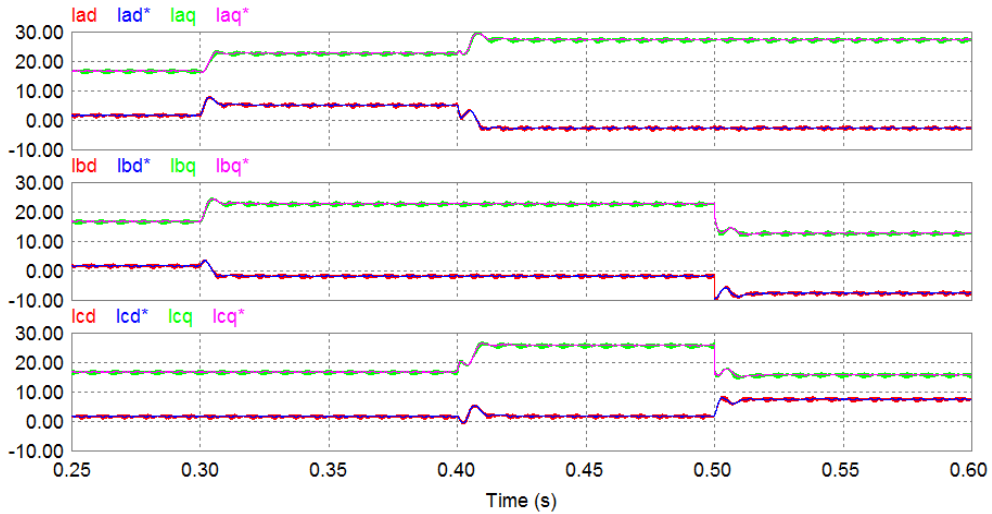
Fig. 3.11. Waveforms of the three-phase load voltages, load currents and inductor currents.

The load voltage remains virtually balanced as the load demand in each phase varies quite a bit, even when the inverter absorbs power in one phase while supplying in the other two due to the PV inverter current injection which is higher than the phase B

load current as shown in Fig. 3.11 and Fig. 3.12. Besides, when the phase current of the load changes, it affects two phases of the primary inductor current due to the Δ -Y transformer as shown in Fig. 3.11.



(a)



(b)

Fig. 3.12. dq waveforms of the voltage and current loops with the proposed control strategy; (a) Reference and actual voltages for the three phases, (b) Reference and actual currents for the three phases.

Fig. 3.13 shows the dq output of the voltage controllers for the three phases which are the reference dq currents that should be supplied to the common point of the capacitor and load in the secondary. It is shown that, whenever a load change occurs, it only affects the corresponding phase current while the others are not affected. Since these currents correspond to the secondary side of the transformer, they have been transformed to the primary as described in section 3.2.1. Therefore, the final dq reference currents for the current controllers of the three phases are different as shown in Fig. 3.12(b). The dq current waveforms are similar for the three phases, in the balanced case. However, when the active power demand in any phase is changed, the q component of the output reference current from the voltage controller also changed, while the other quantities remain unaffected as seen in Fig. 3.13. In order to visualize the transient response of the proposed per-phase dq control scheme, one can look at the variation of the reference and actual current in the filter inductor for the three phases. Fig. 3.12(b), shows that when the load demand changes, the reference current changes appropriately and reached the steady state in less than half a line cycle.

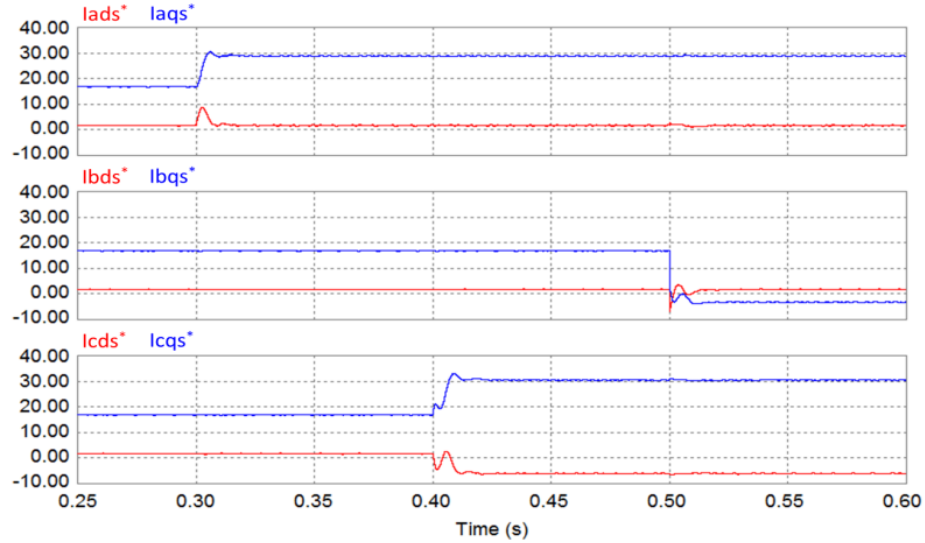


Fig. 3.13. Secondary side dq reference current waveforms for the three phases (before the current transformation & applied to the current controllers).

3.3 Per-Phase DQ Control of a Four-Leg Grid Forming VSI

Per-phase dq control strategy can be used in the grid forming inverter operating in a three-phase four-wire isolated system, consisting of a three-leg inverter with a Δ -Y transformer between the inverter/filter and load as described in the previous section. It was possible to use the three-leg inverter in the primary of the transformer for providing balanced regulated voltage across the three-phase four-wire unbalanced load; as the zero sequence current components created by phase-to-neutral loads circulate in the Δ of the transformer and they would not create any additional voltage drops in the output filter of the inverter. However, in practice, the transformer presents non-zero impedances in the Y side where the zero sequence current components produce a voltage drop. The three-leg inverter placed in the Δ side of the transformer cannot compensate this voltage drop [76]. To avoid this problem, one should use a three-phase four-leg inverter.

A four-leg grid forming inverter connected to a generic impedance block, which can include single-phase and three-phase loads and sources, in a hybrid stand-alone system is shown in Fig. 3.14. The inverter presents an LC output filter, with the resistance of the inductor modeled and that of the capacitor neglected. The neutral point of the distribution system is connected to the 4th leg (node f) of the battery inverter through a fourth inductor, identical to the other ones. It will help further reduce the switching harmonics [81] but will produce a voltage drop in the case of non-zero neutral currents to node f, making the potential at the neutral node (n) shift from zero potential. The proposed control strategy aims at preventing this problem with fast dynamic response.

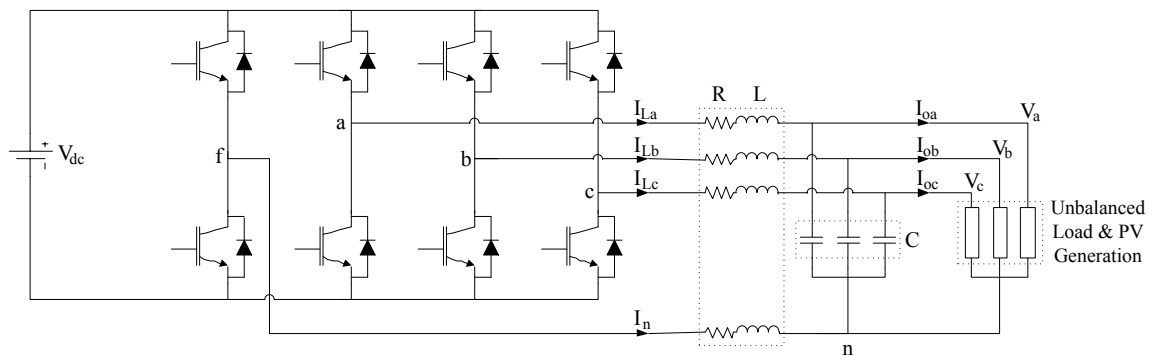


Fig. 3.14. Schematic diagram of a grid forming four-leg inverter with unbalanced load and source.

It was shown in section 3.1 that per-phase dq control using fictive axis emulation, can provide balanced voltages with faster dynamic response than the conventional three-phase dq control with symmetrical components calculator in three-phase three-wire systems. However, the application of this technique for four-wire system is not straightforward. In order to apply this technique in a four-leg inverter, one needs to include the impedance of the neutral conductor in the fictive axis emulation and generate

the gating signals for the fourth leg so as to compensate for the voltage drop across the filter inductor of that leg. These will be discussed in the following sections.

3.3.1 Emulation of the Fictive Circuit in the Current Loop of a Four-Leg Inverter with Neutral Impedance

It has been shown in section 3.1.2 that the key aspect for the implementation of single-phase dq current control with fast dynamic response is the fictive axis emulation as shown in the cascaded control scheme block diagram in Fig. 3.5. However, when this technique is considered for a four-leg inverter with a neutral wire impedance, the latter has to be included in the fictive axis circuit, which would then present a coupled configuration as shown in Fig. 3.15. It corresponds to the average model of the actual four-leg inverter with three equivalent voltage sources that was presented in [38].

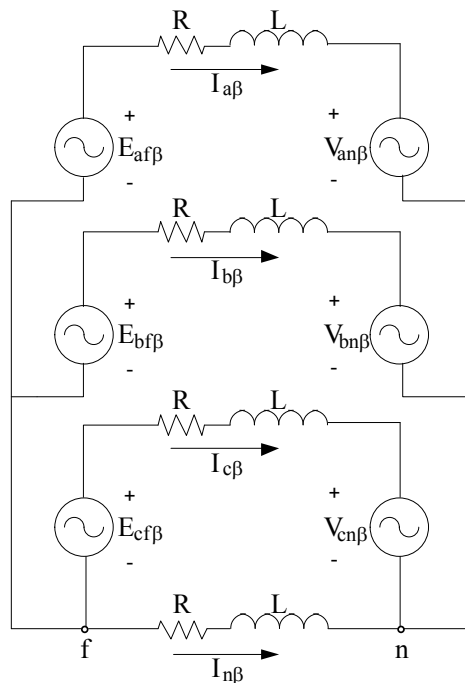


Fig. 3.15. Emulation of the fictive circuit with neutral impedance.

In Fig. 3.15 one sees the voltage sources that represent the orthogonal components of the three phases of the (switched) inverter ($E_{a\beta}$, $E_{b\beta}$ and $E_{c\beta}$) and capacitor ($V_{an\beta}$, $V_{bn\beta}$ and $V_{cn\beta}$) voltages. The former set comes from the output of the dq to $\alpha\beta$ blocks, while the latter are obtained from the actual circuit with SOGIs, as shown in Fig. 3.5. The three-phase line currents obtained from Fig. 3.15 are used for calculating the dq components of the three per-phase current control loops, similar to what is shown in Fig. 3.5. It should be noted that the neutral fictive current component ($I_{n\beta}$) is not used in any computations.

3.3.2 Generation of the Inverter Output Voltage

Various modulation techniques have been suggested for switching the four-leg inverter [81-84]. The three-dimensional space vector modulation (3-D SVM) technique was originally proposed in [81]. It employs an $\alpha\beta 0$ transformation and requires complex calculations for the selection of the switching vectors. Carrier based pulse width modulation (PWM) is another option [83]. It has been shown to be equivalent to a 3-D SVM but with an easier implementation. Because of that, it was chosen to be used in this work for converting the reference signals from the control loops into gating signals for the four-leg inverter. Its block diagram is shown in Fig. 3.16. The inputs (e_{af} , e_{bf} and e_{cf}) are the α components of the three per-phase inverter voltages obtained from Fig. 3.5 and required for balancing the output voltages of the four-leg inverter. They can be represented as,

$$\left. \begin{aligned} e_{ao} &= e_{af} + e_{fo} \\ e_{bo} &= e_{bf} + e_{fo} \\ e_{co} &= e_{cf} + e_{fo} \end{aligned} \right\} \quad (3.12)$$

with the following constraint,

$$-V_{dc} \leq e_{af}, e_{bf}, e_{cf} \leq V_{dc} \quad (3.13)$$

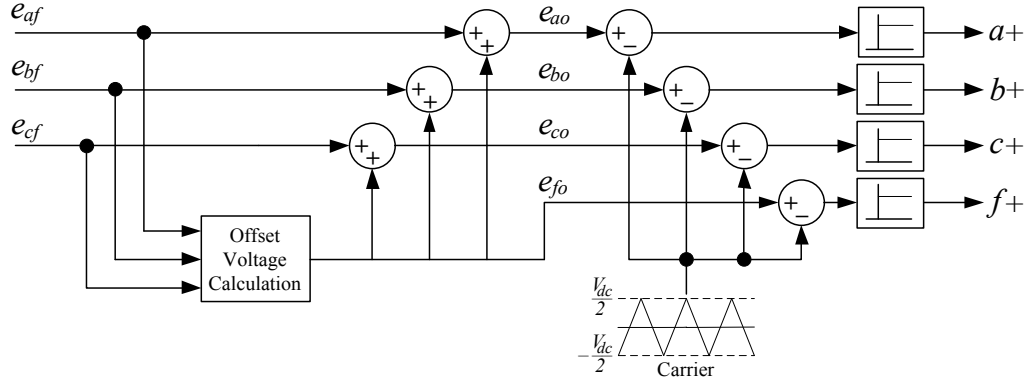


Fig. 3.16. Carrier based PWM method for four-leg inverter. [83]

In equation (3.12), ‘o’ stands for the fictive mid-point of the DC link voltage and e_{fo} is known as the offset voltage and can be calculated as,

$$e_{fo} = \text{mid} \left(-\frac{e_{max}}{2}, -\frac{e_{min}}{2}, -\frac{e_{max} + e_{min}}{2} \right) \quad (3.14)$$

Where $e_{max} = \max(e_{af}, e_{bf}, e_{cf})$ and $e_{min} = \min(e_{af}, e_{bf}, e_{cf})$. e_{max} corresponds to the maximum instantaneous value among e_{af} , e_{bf} and e_{cf} while e_{min} is the minimum value. Similarly, the function *mid* relates to the medium or intermediate value of the selected variables. The triangular carrier presents a period equal to T_s . The values of the on times of the upper switch of respective legs can be obtained from (3.15).

$$\left. \begin{aligned} T_a &= \frac{T_s}{2} + \frac{e_{ao}}{V_{dc}} T_s \\ T_b &= \frac{T_s}{2} + \frac{e_{bo}}{V_{dc}} T_s \\ T_c &= \frac{T_s}{2} + \frac{e_{co}}{V_{dc}} T_s \\ T_f &= \frac{T_s}{2} + \frac{e_{fo}}{V_{dc}} T_s \end{aligned} \right\} \quad (3.15)$$

3.3.3 Performance Verification

The performance of the proposed control strategy is verified by simulation using an average model inverter, so that one can clearly see the speed of response of the system without any switching noise and experimentally with a laboratory prototype.

3.3.3.1 Simulation Study

The simulation study was conducted using MATLAB/SIMULINK[®] and the PV hybrid system shown in Fig. 3.17. The output voltages of the inverter are the α -components of the per-phase cascaded dq control circuit shown in Fig. 3.5, one for each phase. The desired load voltage is 220 V line to line at 60 Hz. The inductance and resistance of the output filter inductor are equal to 3 mH and 0.1 Ω . The filter capacitance is 25 μ F. The PI controllers were designed as described in [68]. The inner current control loop was designed for a bandwidth of 1200 Hz while the outer voltage loop was designed for a bandwidth of 120 Hz. The performance of the proposed control strategy has been compared with a conventional SCC based control scheme [38] with the same specification for the voltage and current controllers.

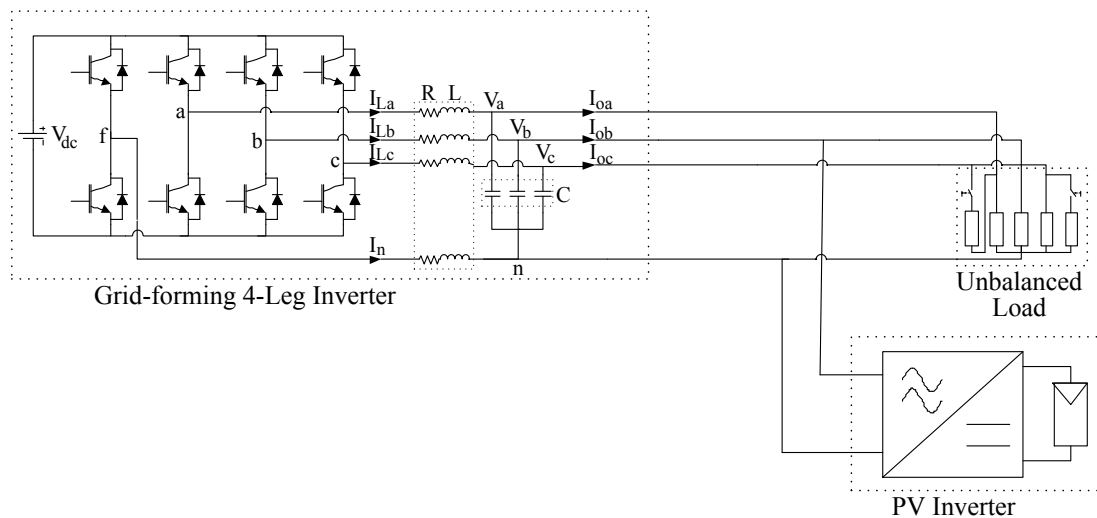


Fig. 3.17. Schematic diagram of the PV-hybrid system used in the simulation studies.

Initially the grid forming inverter is supplying a balanced load ($10.752 \Omega/\text{ph.}$). At $t = 0.3 \text{ s}$, an inductive load ($R = 30 \Omega$ and $L = 15 \text{ mH}$) is added between phases A and C and at $t = 0.5 \text{ s}$, a resistive load of 15Ω is added in phase C. Finally, at $t = 0.7 \text{ s}$ a single-phase PV inverter connected between phase B and neutral, starts supplying a current of 20 A (peak) with unity power factor. The three-phase load voltages and load currents, including neutral wire, are shown in Fig. 3.18 for both the conventional SCC based and the proposed control schemes. There one sees that the load voltages remain balanced in steady-state for both control schemes at all the various load unbalances considered in this study. However, the transient response of the SCC based control scheme was slower than the proposed one. One can observe in particular, the significant impact of reverse power flow in one of the phases when the PV inverter starts supplying active power beyond that consumed by the local load. Conversely, the proposed method presents a much faster response regulating the load voltages almost instantaneously even when the power flow in phase B of the grid forming inverter reverses.

Fig. 3.19 shows the reference and actual voltages and currents for the grid forming inverter in the dq frame with the conventional SCC based (Fig. 3.19.a & Fig. 3.19.c) and the proposed (Fig. 3.19.b & Fig. 3.19.d) control schemes. There, one clearly sees that the deviations in the voltage signals are smaller and shorter with the proposed per-phase scheme than with the conventional SCC based scheme. One reason is that the current reference signal for the proposed scheme reacts faster than the SCC based one to load variations and voltage errors. For the SCC based scheme, the positive sequence current increases as loads are added and decreases when the PV inverter starts supplying active power. Negative sequence currents appear when unbalanced loads/sources are added to

the system. As for the zero sequence currents, they are only present after $t = 0.5$ s when neutral connected unbalanced loads and sources start to operate.

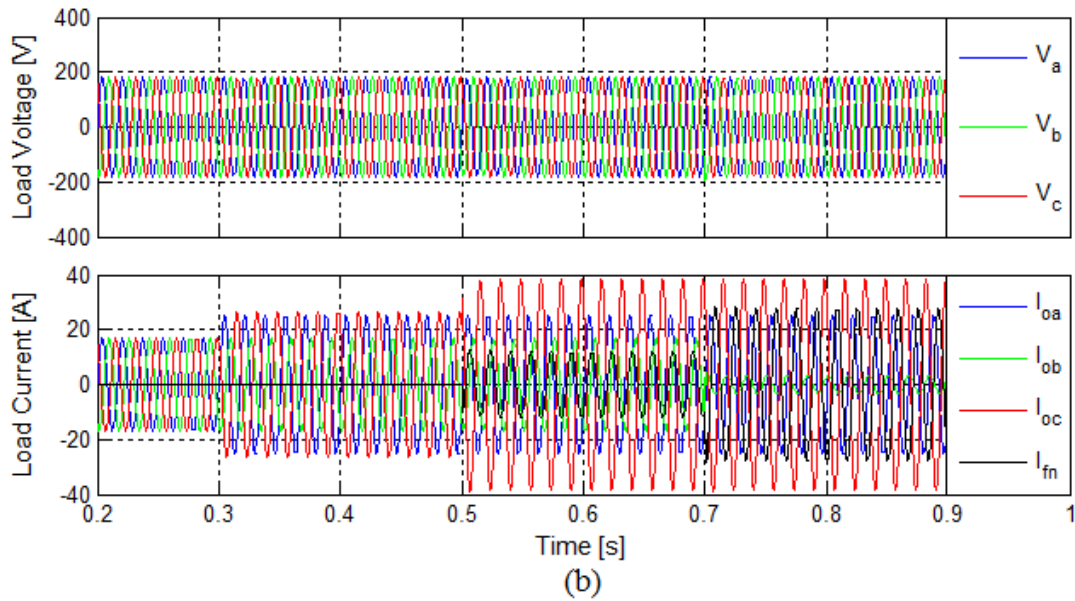
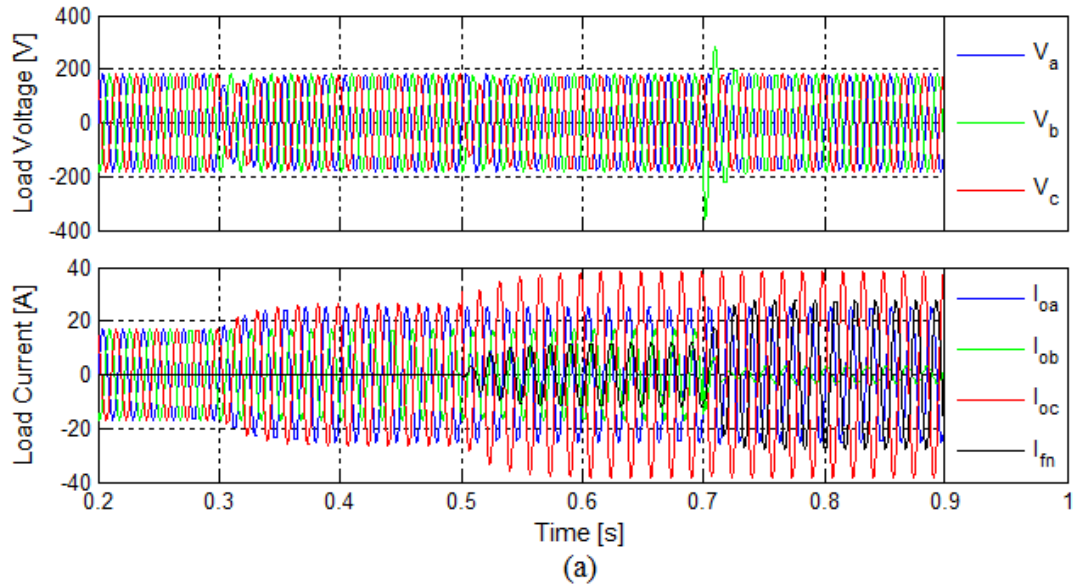
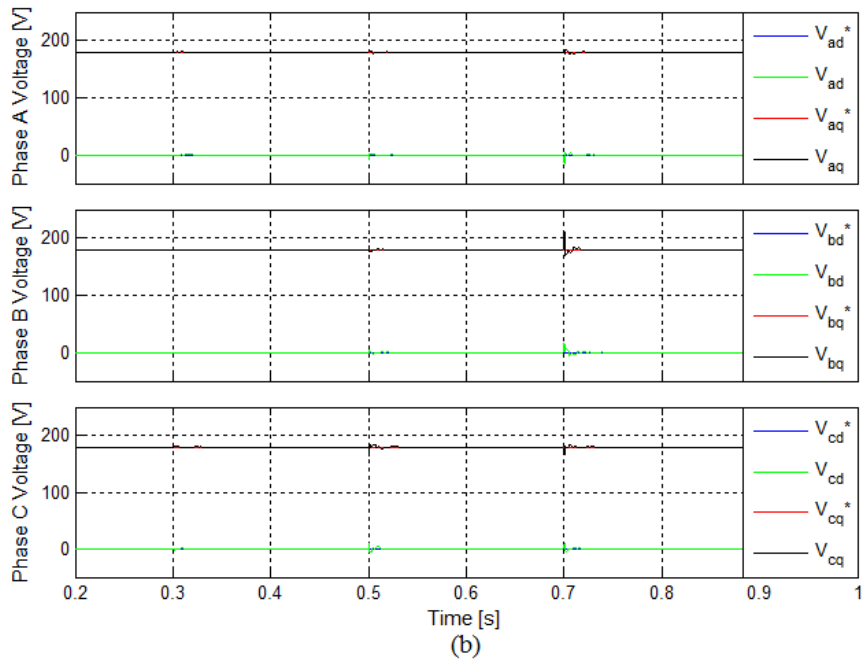
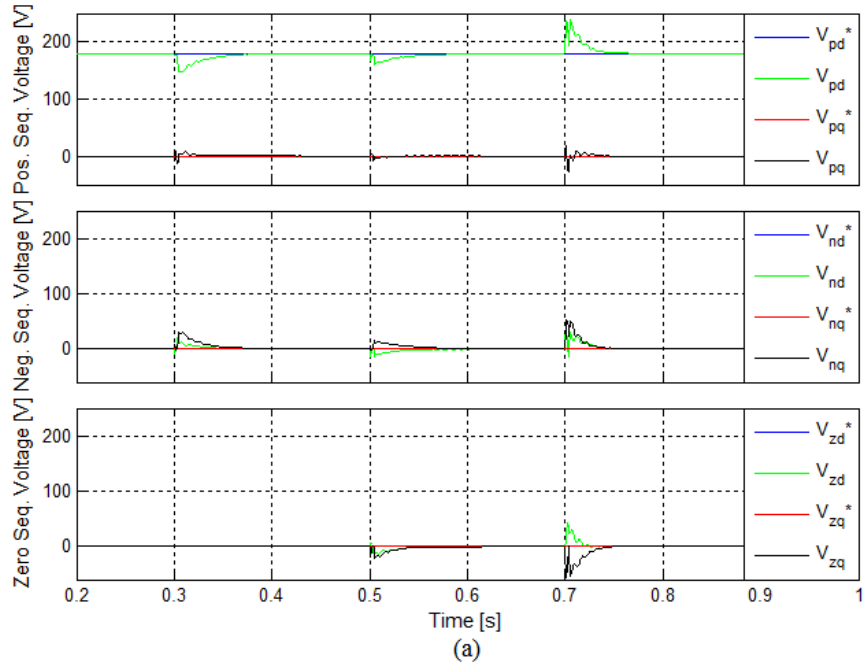


Fig. 3.18. Waveforms of the output voltages and currents of the grid forming inverter for varying load conditions. a) Conventional SCC-based control scheme; b) Proposed per-phase control scheme.



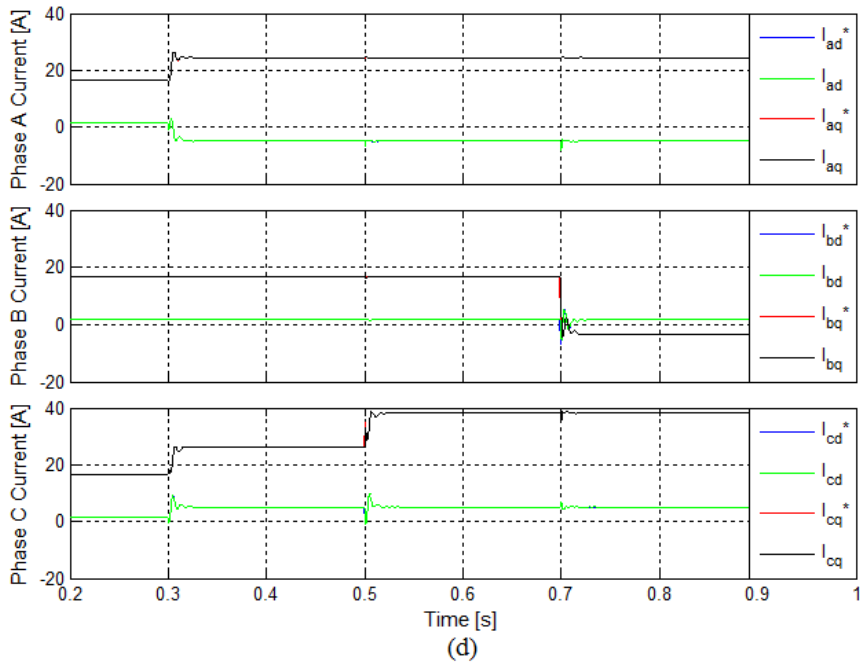
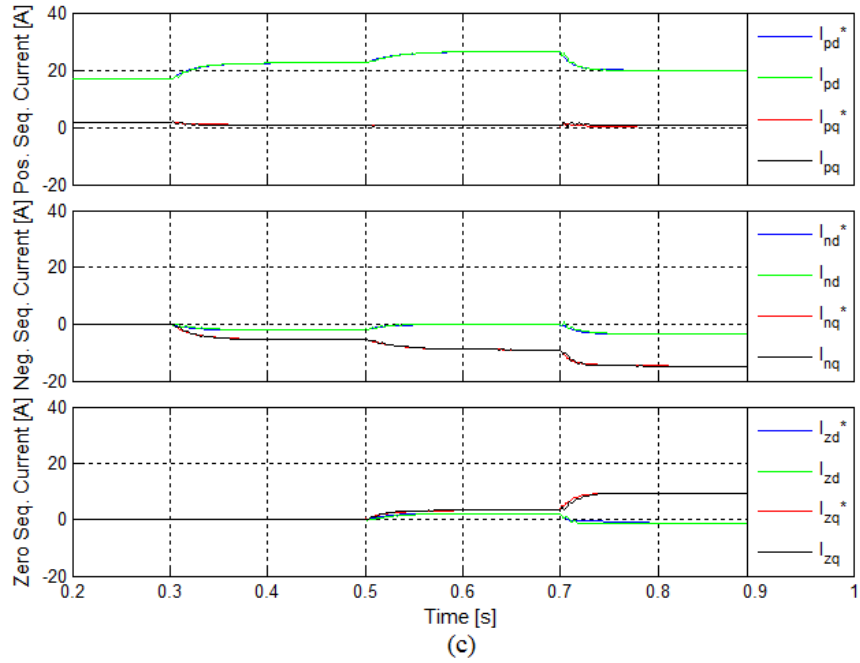


Fig. 3.19. Waveforms of the voltage and current loops of the grid forming inverter in dq coordinates. a-b) Reference and actual voltages for the conventional and proposed control schemes respectively; c-d) Reference and actual currents for the conventional and proposed control schemes respectively.

These are not explicitly seen in the per-phase scheme which does not need to compute the symmetrical components of voltages and currents, which is a slow and required process in the conventional scheme. Thus, variations in the reference currents to compensate for voltage unbalances take place faster and only in the phase(s) directly related to the load variations. Fig. 3.19(d) shows that the d component of the inductor (filter) current in phase B is small positive because of the reactive power supplied by the filter capacitor. There are no reactive power variations in that phase where a unity power factor source is connected at $t = 0.7$, making the q current in that phase become negative. Conversely, the d component of the inductor current in phase A becomes negative when an inductive load is added between phases A and C at $t = 0.3$ s and does not change at $t = 0.5$ s when a resistive load is connected between phase C and the neutral.

Finally, the performance of the per-phase dq controlled grid forming inverter has been assessed for a non-linear load. The non-linear load has been applied in parallel to the last unbalanced load, considered in the previous simulation (between 0.7 s and 0.9 s). The non-linear load is a three-phase diode rectifier loaded by a 4000 μ F capacitor and a 150 Ω resistor in parallel and the crest factor is 2.4:1, where the crest factor is equal to the peak amplitude of a waveform divided by the rms value. The three-phase load voltages and load currents, including neutral wire, are shown in Fig. 3.20 for the proposed control schemes. The current in the three phases are distorted due to the impact of non-linear load. Phase b is highly distorted with a THD of 226% since the current due to the linear load in this phase is almost zero while the THD of currents in phase a and c are 9% and 6% respectively. The output voltage is almost balanced and regulated as shown in Fig. 3.20 with THD of 1.6%.

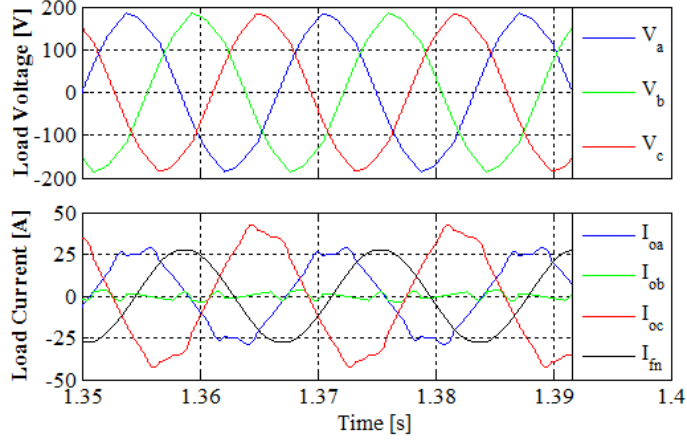


Fig. 3.20. Waveforms of the output voltages and currents of the grid forming inverter with unbalanced and non-linear load for the proposed per-phase control strategy.

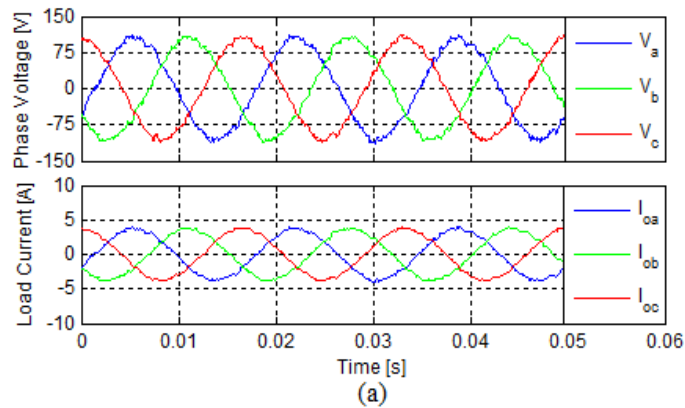
3.3.3.2 Experimental Study

The experimental study was conducted with a small-scale laboratory prototype. The four-leg inverter was realized with two SEMIKRON SEMITEACH inverters, since each one presents only three legs. The control algorithm was implemented in a dSPACE DS-1103 system. Table 3.1 shows the parameters for the experimental study of the four-leg grid forming inverter. The PI controllers have been designed as described in [68] for bandwidth of 1200 Hz and 120 Hz for the inner current control loop and outer voltage loop respectively. The DC bus of the inverter was created with the SEMITEACH's three-phase diode rectifier. A three-phase VARIAC was used to adjust the DC bus voltage to the desired value and a 8000 μF capacitor to minimize the DC bus voltage ripple. Various types of load configurations, described in Table 3.1, were considered in the tests. These include from three-phase balanced to single-phase unbalanced loads.

Table 3.1. System Parameters for the Experimental Study.

DC bus voltage		250 V
Load voltage		105 V/phase (peak) at 60Hz
Filter capacitor		10 μ F
Filter inductor		8 mH
Internal resistance of filter inductor		1 Ω
PI current controller parameters		$k_p = 120$ & $k_i = 316 \times 10^3$
PI voltage controller parameters		$k_p = 5.33 \times 10^{-3}$ & $k_i = 1.42$
Switching scheme		SPWM
Switching frequency		6 kHz
Sampling frequency of DSP		40 kHz
Load	Balanced	$R_a = R_b = R_c = 28.57 \Omega$
	Unbalanced	1. $R_a = 16.67 \Omega$ & $R_b = R_c = 28.57 \Omega$ 2. $R_b = \infty$ & $R_a = R_c = 40 \Omega$ 3. $R_b = R_c = \infty$ & $R_a = 40 \Omega$

Fig. 3.21 shows the steady-state behavior of the four-leg inverter for balanced and various unbalanced load cases as considered in Table 3.1. The four-leg inverter with the proposed control scheme was able to regulate the fundamental component of the load voltage close to the specified 105 V peak for all cases of load unbalanced including a single-phase load connected between a phase and the neutral.



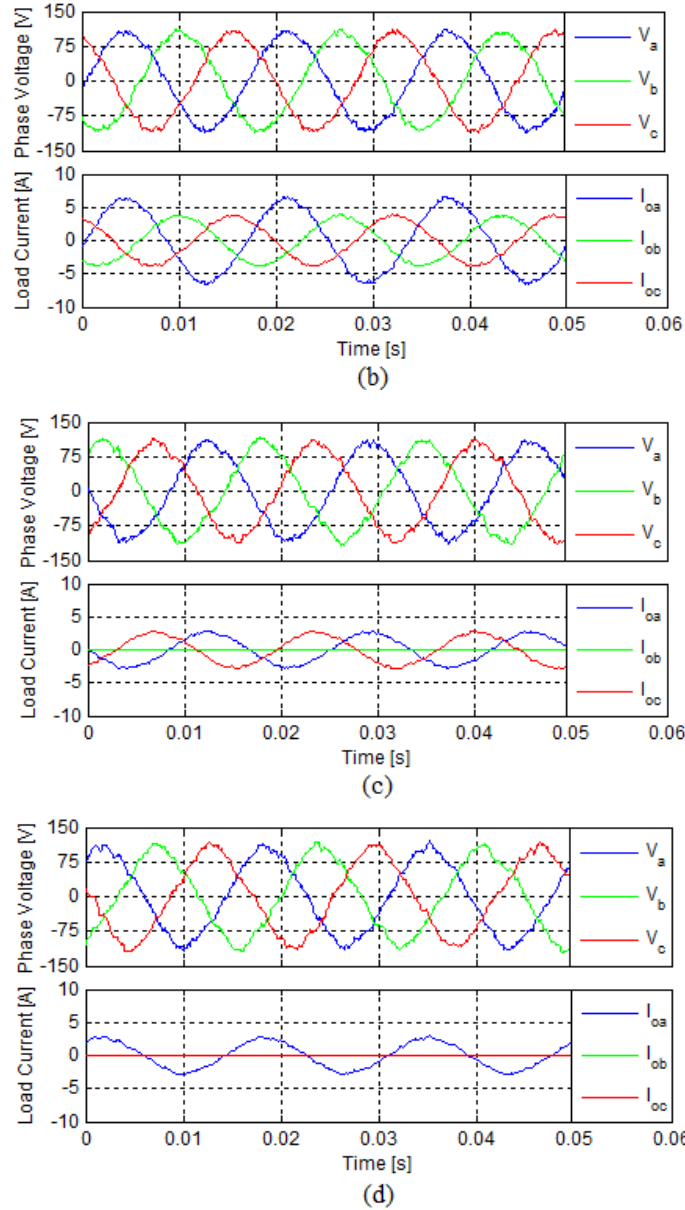


Fig. 3.21. Steady state load voltages and currents of the grid forming inverter for different loads. a) Balanced load; b-d) Unbalanced load #1, #2 and #3 respectively.

Table 3.2 shows the magnitudes of the fundamental components of the three phase voltages and the total harmonic distortion (THD) for all tested conditions in steady-state as well as the phase voltage unbalance rate (PVUR). According to IEEE, PVUR is defined as [85],

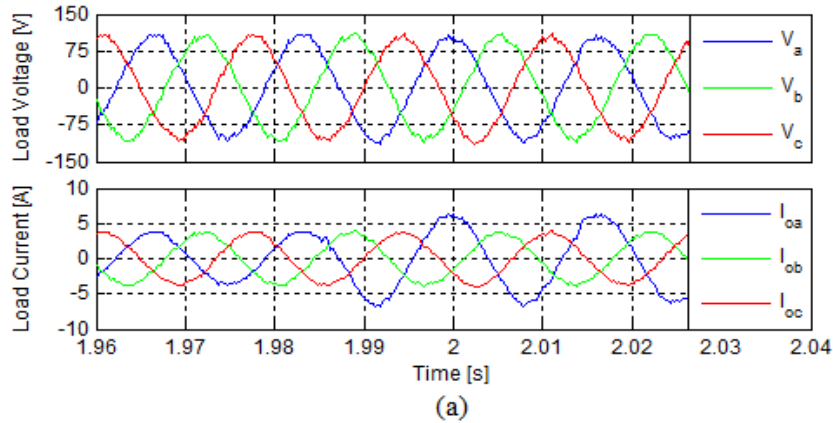
$$\%PVUR = \frac{\text{maximum voltage deviation from the average phase voltage}}{\text{average phase voltage}} \times 100 \quad (3.16)$$

IEEE recommends a value of PVUR less than 2% for the distribution system. The percentage negative and zero sequence load currents with respect to the positive sequence components are indicated for all cases, what indicates the “degree” of load unbalance. There one sees that the resulting voltage unbalances with the proposed control scheme is very small in all cases, increasing in general with the severity of the load unbalance. It should be noted that the gate drive circuit of the SEMITEACH unit uses an inherent large dead-time of 4.8 μs for each leg, what certainly increased the values of THD.

Table 3.2. Experimental Results of Steady State Performances.

Load			Load Peak Voltages (V)			THD (%)			PVUR (%)
Type	I_{neg} (%)	I_{zero} (%)	Phase A	Phase B	Phase C	Phase A	Phase B	Phase C	
Balanced	0	0	104.94	104.95	104.88	1.7	1.9	1.9	0.041
Unb. #1	100	20	104.92	104.87	105.05	1.8	1.8	1.4	0.098
Unb. #2	50	50	104.84	105.23	104.92	2.5	3.0	3.0	0.222
Unb. #3	100	100	104.96	104.77	104.69	2.8	3.9	3.9	0.146

Fig. 3.22 shows the transient response of the system. Initially the load and the inverter voltages are balanced. Then, at approximately 1.986 s, the load in phase A changes from 28.57 Ω to 16.67 Ω , making the system unbalanced.



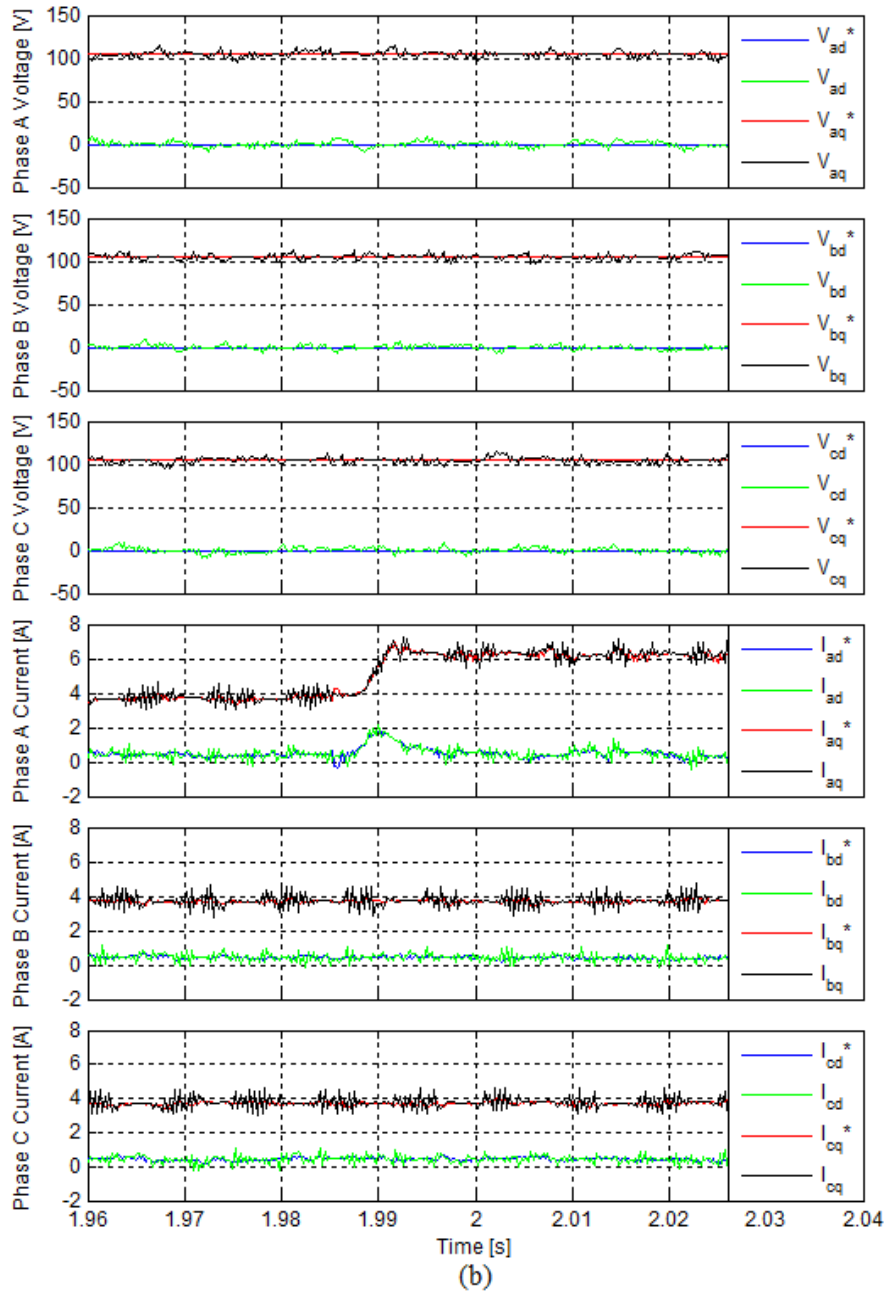


Fig. 3.22. Transient response of the grid forming inverter. a) abc-frame load voltages and currents; b) dq-frame reference and actual voltages and currents for the three phases.

In spite of the unbalanced load, the voltages in the three phases remain virtually identical as one can see from the voltage waveforms in abc and dq coordinates. The response of the system is very fast as shown by the dq coordinates of the reference and

actual currents in phase A. The currents in phases B and C remained unchanged. It should be noted that for a similar load variation it took almost 2 line cycles in [38] and [34], for the system to recover the balanced voltage condition.

3.4 Summary of Chapter 3

This chapter presents new control techniques suitable for three-phase grid forming inverters operating in stand-alone hybrid mini-grid systems with highly unbalanced loads. The conventional control methods for the grid forming inverters result in slow dynamic response and also are not suitable for variable frequency operation which is common in the autonomous systems. The speed of response achieved with this technique is very fast due to the proposed per-phase dq control strategy. Fictive axis circuit emulation was used in the inner current loop and frequency adaptive SOGI was used in the outer voltage loop to obtain the orthogonal components. Therefore, the proposed per-phase control strategy can operate with variable frequency unlike the conventional control methods.

The chapter initially presented the per-phase control strategy for the three-phase three-wire grid forming inverter employing conventional three-leg VSI. In this case, a per-phase dq-controlled three-leg inverter was used to indirectly regulate the positive sequence component of the output voltage and cancel the negative sequence voltage drop on the inverter output filter. However, the application of this technique for four-wire system is not straightforward due to the existence of the zero sequence components. Two solutions have been proposed in this regard. The first is the conventional three-leg VSI with a Δ -Y transformer between the inverter/filter and distribution system which can act as a grid forming unit for unbalanced loads. The zero sequence components do not appear in the inverter side; therefore, the per-phase control strategy of the three-leg inverter with

some modification in the control strategy to take account the impact of Δ -Y transformer was proposed. The second solution for the four-wire application was to use the four-leg inverter with per-phase dq control strategy. A new coupled fictive axis emulation for the inner current loop of four-leg grid forming inverter has been proposed to compensate the impact of the zero sequence components.

The proposed per-phase control strategies allow the grid forming inverters to provide balanced output voltages under severe load unbalance conditions. Even when the inverter has to supply power through two phases and absorb through the other one, due to the presence of a single-phase PV inverter, its output voltages remain balanced. The superior performance of the proposed control strategies were demonstrated by means of simulation and experimental studies under various scenarios.

CHAPTER 4

BESS OPERATION IN DIESEL HYBRID MINI-GRID

Traditionally, remote communities worldwide consist of autonomous power systems (mini-grids) supplied almost exclusively by diesel-engine generator sets (gensets) at relatively high costs. Integration of renewable energy sources (RESs) such as PV and wind can substantially reduce the cost of electricity generation and emissions in these remote communities. The highly variable load profile of the remote communities and the fluctuating characteristics of the RESs, cause frequent operation of the diesel genset at low loading condition, at low efficiency points. It results in carbon build up in the diesel engine, what increases maintenance cost and significantly affects the life time of the genset. A minimum load of about 0.4 pu is usually recommended by genset manufacturers. These issues can be mitigated with a battery energy storage system (BESS). In the *genset support mode*, as a basic feature, it can provide minimum loading for the genset and supplement it under peak load conditions. In cases when the power demand from the genset is low, due to high supply of RESs and/or low load consumption, the genset can be shut-down and the BESS operates in the *grid forming mode*, regulating voltage and frequency.

Another important aspect to consider in the diesel hybrid mini-grid is load unbalance. Diesel gensets supplying unbalanced loads experience overheating in the synchronous generator and vibration in the shaft. If a BESS is used in a diesel-hybrid mini-grid, it can help minimize this problem and also provide additional ancillary

services to reduce operating costs and improve power quality. Besides, mini-grid most often operate with variable frequency to convey information of the shortage (low frequencies) or surplus (high frequencies) of power/energy in the mini-grid to distributed controllable sources and loads. Therefore the BESS should be capable of working with frequency variation in grid forming and genset support modes in the diesel hybrid mini-grid. The main objective of this chapter is to provide a complete solution to overcome the operational and power quality issues in diesel hybrid mini-grid as discussed in section 1.2. Therefore, this chapter deals with a proposed multi-functional control system of a BESS for a variable frequency diesel hybrid mini-grid with high penetration of RESs and highly unbalanced loads.

4.1 Description of the System

The power circuit of the system under consideration is shown in Fig. 4.1. In the left-hand side, there is a three-phase diesel genset that operates with variable frequency using the power vs. frequency droop control strategy, and that can be disconnected from the system in case of need or convenience. Besides, there is also a three-phase BESS, which is connected in parallel to the genset at the point of common coupling (PCC). The BESS is based on a three-phase voltage source inverter (VSI) with an LC output filter. A distribution system is employed to connect the diesel power plant and the BESS to residential rooftop type PV systems and loads. Normally residential roof-top type PVs (capacity below 10 kW) are connected to the distribution system using current controlled single-phase voltage source inverters.

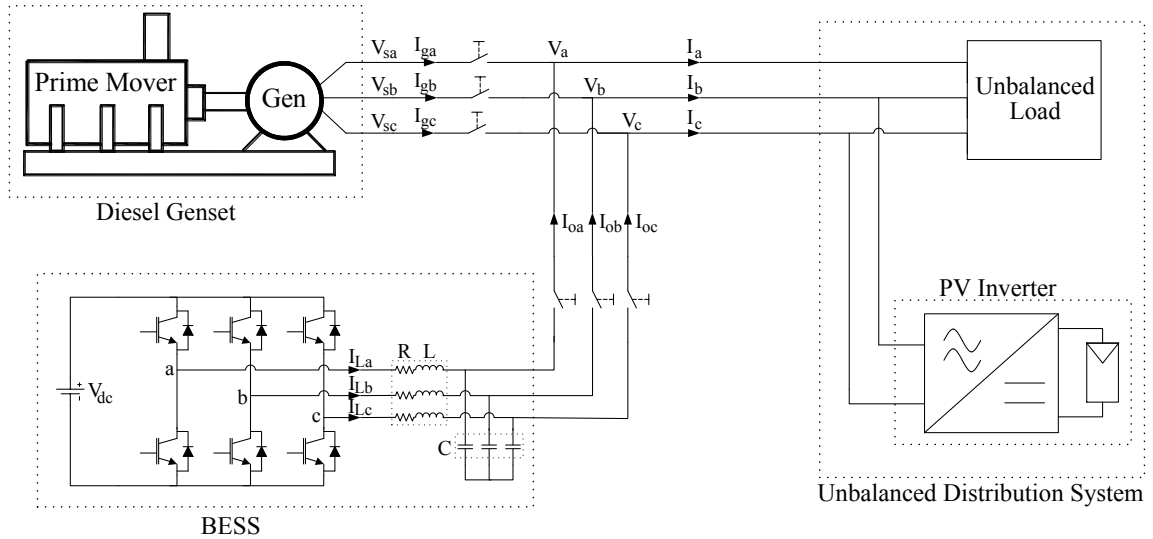


Fig. 4.1. Circuit diagram of a three-phase three-wire diesel-hybrid mini-grid with battery inverter, single-phase RES and unbalanced load.

The BESS has two basic operation modes: genset support, when the genset forms the grid, and grid forming, when the genset is off and the BESS regulates voltage and frequency. In the first mode it operates as a three-phase independently controllable current source. It balances the load by injecting the negative sequence of the load current, provides load reactive power so that the genset operates with unity power factor (UPF), supplies the reactive current for the output filter capacitors of the BESS and controls active power so as to force the genset to operate within an ideal output power range. If the output power of the genset falls below a certain value (P_{min}), typically 0.4 pu, the BESS absorbs active power to provide minimum loading for the genset. Conversely, the BESS will supply active power when the output power of the genset exceeds another value ($P_{max} = 0.9$ pu). The BESS should not deal any average active power when the genset operates in the ideal power range.

In the second mode, the BESS forms the grid what requires operation as a three-phase voltage source. One major challenge in this case is to provide balanced voltage to an unbalanced load. This should not have a significant impact in terms of voltage unbalances when a diesel genset with a low impedance synchronous generator forms the grid. On the other hand, when a battery inverter, with a relatively larger output impedance of the low pass filter, forms the grid, larger voltage unbalances might appear. In such a case, appropriate control loops have to be used so as to guarantee that even under highly unbalanced output currents, the grid forming battery inverter can supply balanced voltages to the distribution grid.

Finally a “Mode Selection and Transition System (MSTS)” is used to operate the BESS in either genset support or grid forming mode and make transition between the modes. The operation mode of the BESS depends on system conditions, e.g., a) Genset at minimum loading with load demand being less than 0.4 pu, while the BESS has enough energy to supply the light load which will result in a transition from genset support to grid forming mode, b) The BESS does not have enough energy in the grid forming mode anymore and the genset has to be brought in to supply the load which will result in a transition from grid forming to genset support mode, c) During daytime with high penetration of PV power generation, the genset can be turned off, so most of the power comes from PV while the remaining can be supplied or absorbed by the BESS, etc. Normally an energy management algorithm with the above information should decide the operating mode of the BESS. However, it would require typical daily load profile of the mini-grid, information about the state-of charge (SOC) of the battery etc. to choose the optimized operating mode of the BESS, which is beyond the scope of this work.

Therefore, in this work, the operation of the BESS in either mode and smooth transition of the BESS between the modes are mainly analyzed. The MSTS is proposed to select and operate the BESS in the desired mode and make smooth transition of the BESS between the modes.

4.2 Control Circuit of the BESS

The general block diagram of the control circuit of the BESS is shown in Fig. 4.2. It consists of a per-phase dq controller, a reference current generator for the genset support mode, a PLL+ICA (Phase Locked Loop + Intelligent Connection Agent) module and a “Mode Selection and Transition System (MSTS)” module. These components are discussed in the following sub-sections.

As mentioned before, the BESS will operate either as a controlled current source, for genset support, or as voltage source, forming the grid. In such a case, it is convenient to employ the conventional two loop cascaded control scheme with an inner current loop and an outer voltage loop. The key element is the per-phase dq control block, including the voltage and current loops, that is used for the generation of the gating signals of the three phases with SPWM. A switch controlled by the operating mode of the BESS is used to select the reference current for the inner current loop, which can be either the output of the voltage control loop, when the BESS forms the grid, or an external signal, when the BESS is supporting the genset.

During the genset support mode, the BESS will employ only the inner current loop and the reference will be provided by the external signal from “*I_{ref} Generator in Genset Support Mode*” block. The external signal from the reference current generator contains

the required current components for the BESS to: 1) Balance the load for the genset; 2) Compensate for the reactive power consumed by the output filter capacitors; 3) Supply the load reactive power and 4) Inject/absorb the active power needed to keep the genset operating within the desired range. For these function to be implemented, additional blocks are required and will be described in details in the following subsections.

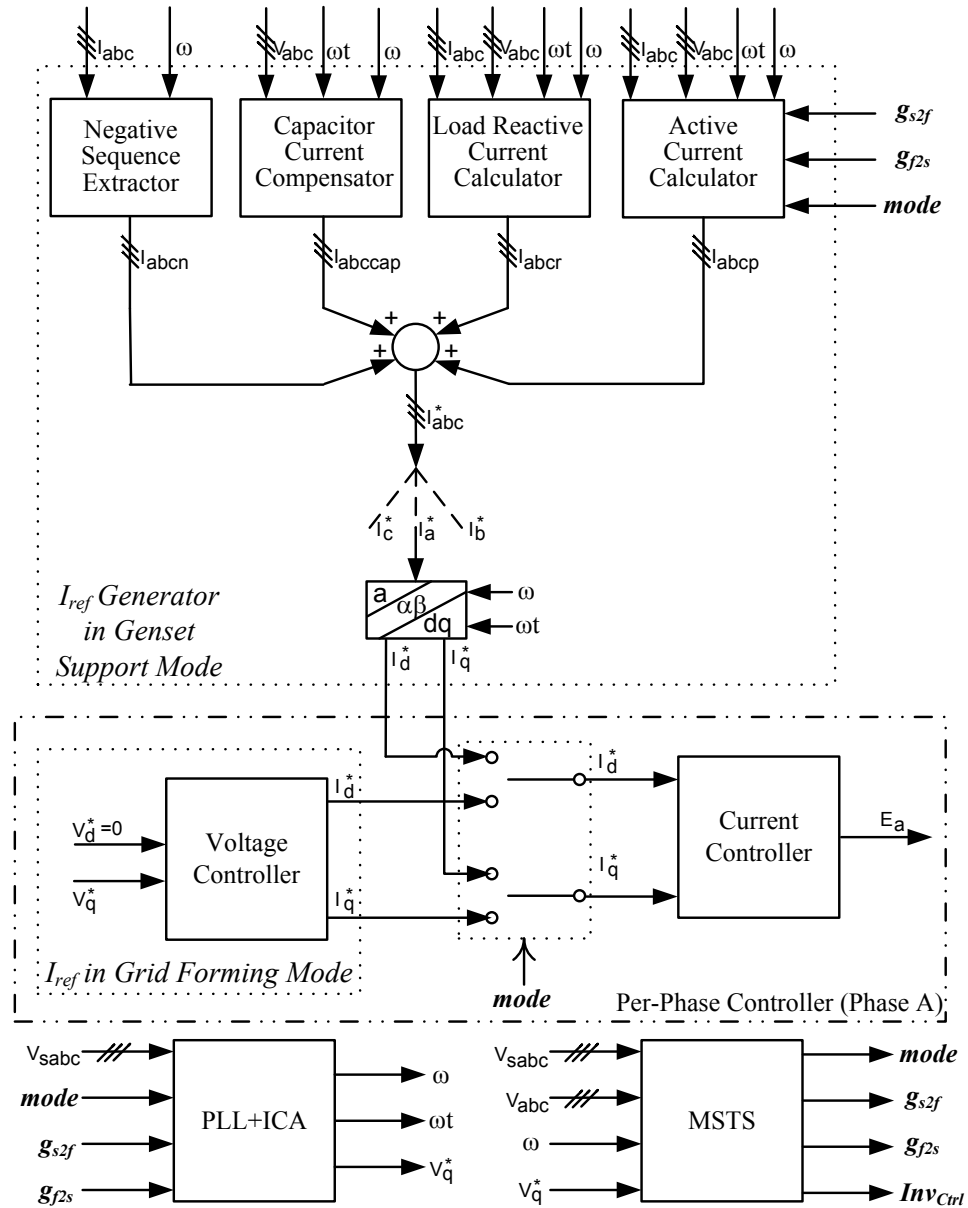


Fig. 4.2. Schematic diagram of the proposed control circuit for the BESS.

The per-phase dq controller requires the phase angle and angular frequency for the Park and Inverse Park transformation during both modes, which are extracted using PLL+ICA module. During the genset support mode, the PCC voltage will be the reference for phase angle and frequency while during the grid forming mode, the desired rated mini-grid voltage will be the reference voltage. Besides, the PLL+ICA will also provide these quantities for smooth transition during connection and disconnection events of the genset.

Finally the MSTS block is used to control the operation of the BESS either in genset support mode or in grid forming mode depending on the condition of the system as described in previous section. Besides it also performs the controlled smooth transition between the two operating modes. For these purposes, this block generates several control signals which will be discussed in later subsections.

4.2.1 The Per-Phase Cascaded DQ Control Block

The per-phase dq control strategy proposed in section 3.1 is used for the BESS with some modifications that allow operation in both modes. The block diagram of the modified per-phase dq control strategy for phase “a” of the BESS is shown in Fig. 4.3. The three phase legs of the BESS are controlled independently from each other, as single-phase units with per-phase dq control strategy, so as to regulate the (phase) voltage with cascaded inner current and outer voltage loops in the grid forming mode or to provide the desired current using only the inner current loop in the genset support mode.

During the genset support mode, the voltage regulation loop is disabled by the \overline{mode} signal coming from the MSTS module (during genset support, $mode = 1$ and vice versa) and the reference currents are provided through the external signal coming from

reference current generator (I_{dqext}^*). During the grid forming mode, the BESS operates with the cascaded control loop, i.e., the outer voltage control loop generates the reference current for the inner current loop.

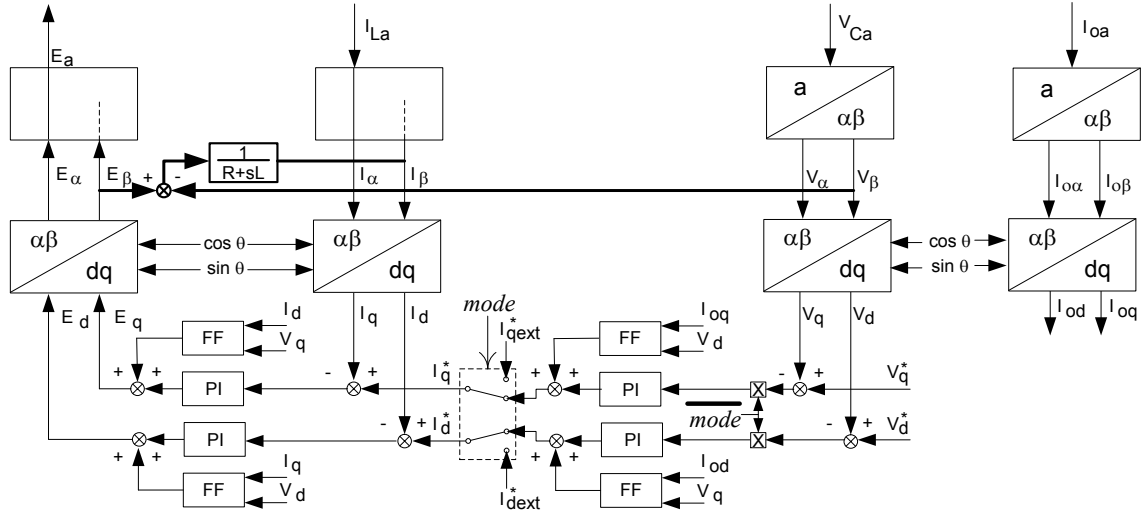


Fig. 4.3. Schematic diagram of the per-phase cascaded control block for the BESS.

The angular frequency (ω) used in the SOGIs for orthogonal signal generation is provided by the PLL+ICA block. Besides, the $\sin\theta$ and $\cos\theta$ terms required for the Park and inverse Park transformations are also obtained from the phase angle provided by the PLL+ICA block.

Similar per-phase controllers also apply for phase “b” and phase “c” with the three θ angles being 120° apart. The reference voltages for the three phases have the same magnitude and are phase shifted by 120° in the grid forming mode. V_q^* is set at the peak value of the reference phase voltage as determined by the PLL+ICA block while V_d^* is set at 0 V for the three per-phase controllers in the grid forming mode.

4.2.2 Reference Current Generation in Genset Support Mode

During the genset support mode, the reference current for the inner current loop is generated externally from the “ I_{ref} Generator in Genset Support Mode” block as shown in Fig. 4.2. It consists of four components and the generation of each component is described below.

4.2.2.1 Negative Sequence Component Extraction from Load Current

Any sets of unbalance voltages or currents can be expressed as three symmetrical components of positive, negative and zero sequence. In the absence of a neutral wire, like in the case considered in this study, there are no zero sequence components. The negative sequence current components can be extracted as follows. Clark transformation is used for transforming the variables in between abc and $\alpha\beta$ frames as shown in equation (4.1) and (4.2).

$$\begin{bmatrix} X_\alpha \\ X_\beta \end{bmatrix} = \sqrt{\frac{2}{3}} \begin{bmatrix} 1 & -\frac{1}{2} & -\frac{1}{2} \\ 0 & \frac{\sqrt{3}}{2} & -\frac{\sqrt{3}}{2} \end{bmatrix} \begin{bmatrix} X_a \\ X_b \\ X_c \end{bmatrix} \quad (4.1)$$

$$\begin{bmatrix} X_a \\ X_b \\ X_c \end{bmatrix} = \sqrt{\frac{2}{3}} \begin{bmatrix} 1 & 0 \\ -\frac{1}{2} & \frac{\sqrt{3}}{2} \\ -\frac{1}{2} & -\frac{\sqrt{3}}{2} \end{bmatrix} \begin{bmatrix} X_\alpha \\ X_\beta \end{bmatrix} \quad (4.2)$$

The positive and negative sequence $\alpha\beta$ components of the three-phase unbalanced signals can be obtained with equation (4.3).

$$\begin{bmatrix} X_{\alpha}^{+} \\ X_{\beta}^{+} \\ X_{\alpha}^{-} \\ X_{\beta}^{-} \end{bmatrix} = \frac{1}{2} \begin{bmatrix} 1 & 0 & 0 & 1 \\ 0 & 1 & -1 & 0 \\ 1 & 0 & 0 & -1 \\ 0 & 1 & 1 & 0 \end{bmatrix} \begin{bmatrix} X_{\alpha} \\ X_{\beta} \\ jX_{\alpha} \\ jX_{\beta} \end{bmatrix} \quad (4.3)$$

In order to use equation (4.3) to obtain the positive and negative sequence components in $\alpha\beta$ frame, one needs to implement the j operator that corresponds to a 90° phase shift. Therefore, one can use the SOGI as shown in Fig. 2.16, where the β component corresponds to a $-j$ term and which also allows precise calculation due to the frequency adaptive characteristics in case of frequency variation in the mini-grid. Therefore, in this case, at first the load currents (i_{abc}) are converted in $\alpha\beta$ frame ($i_{\alpha\beta}$) by equation (4.1), then equation (4.3) is used to extract the negative sequence components of the load current in $\alpha\beta$ frame ($i_{\alpha\beta}^{-}$) and finally inverse Clark transformation is applied to obtain the reference negative sequence current in abc frame (i_{abcn}) which the BESS needs to inject into the mini-grid for load balancing.

4.2.2.2 BESS Capacitor Current Compensation

In the genset support mode the BESS acts as a controlled current source. The purpose of the output capacitor is to reduce switching frequency harmonics mainly during the grid forming mode. The BESS can supply the reactive currents of the capacitors in the grid support mode. If v_{α} and v_{β} are the $\alpha\beta$ voltage components for a phase, then the amplitude of each phase voltage is calculated as,

$$|V| = \sqrt{v_{\alpha}^2 + v_{\beta}^2} \quad (4.4)$$

Therefore, the amplitude of the required reactive current of the capacitor is given by,

$$|I| = \frac{|V|}{X_C} \quad (4.5)$$

Where, X_C is the capacitive reactance and it should be updated depending on the value of the angular frequency (ω). Similarly, the amplitude of the required reactive currents of other phases can be calculated. Using the phase angle and amplitude the required reactive current reference are generated for the three phases to compensate the capacitor current as given in equation (4.6).

$$\left. \begin{aligned} i_{acap} &= |I| \sin\left(\omega t + \frac{\pi}{2}\right) \\ i_{bcap} &= |I| \sin\left(\omega t + \frac{\pi}{2} - \frac{2\pi}{3}\right) \\ i_{ccap} &= |I| \sin\left(\omega t + \frac{\pi}{2} + \frac{2\pi}{3}\right) \end{aligned} \right\} \quad (4.6)$$

4.2.2.3 Load Reactive Power Compensation

The BESS should also supply the reactive power of the load, so that the genset operates with unity power factor. Note that in system with a *small* genset, if this has to balance all active power, it is better to “save” all its apparent power for active power control. The total positive sequence reactive power of the load can be calculated as,

$$Q^+ = v_{\beta}^+ i_{\alpha}^+ - v_{\alpha}^+ i_{\beta}^+ \quad (4.7)$$

Equations (4.1) and (4.3) is applied on the PCC voltage and the load currents to obtain the positive sequence $\alpha\beta$ components ($v_{\alpha\beta}^+$ and $i_{\alpha\beta}^+$) required for using equation (4.7) to determine the load positive sequence reactive power. Though the positive sequence power is a DC quantity resulting from balanced positive sequence voltages and currents, still a low pass filter with a cut off frequency of 10 Hz is used on this signal to minimize the effect of sudden load disturbances.

The power calculated from equation (4.7) is used to calculate the peak value of the reference reactive component of the current of the BESS for load reactive power compensation as follows,

$$I_{ar} = -\frac{Q^+}{3} \frac{2}{V^+} \quad (4.8)$$

Where, V^+ is the peak value of the positive sequence voltage components. The negative sign indicates that the BESS supplies reactive power while the load is consuming. The instantaneous reference reactive currents (i_{abcr}) of the BESS for load reactive power compensation will have the same magnitude and is generated using the cosine of the phase angle with abc phase sequence.

4.2.2.4 BESS' Active Component Current Calculation to Operate the Genset within the Desired Range

In order to avoid the carbon build-up phenomenon as well as low efficiency of the genset, it should typically run above a power capacity of $P_{min} = 0.4$ pu. The BESS can absorb power to provide minimum loading for the genset and also supply extra power when the genset is about to operate at its maximum capacity ($P_{max} = 0.9$ pu). This logic can be implemented using the information of the minigrid load power demand. Since the BESS is providing the negative sequence components of the load during the genset support mode, therefore, it should supply or absorb positive sequence power in order to ensure the operation of the genset within the desired range. The total positive sequence power of the load can be calculated as,

$$P^+ = v_{\alpha}^+ i_{\alpha}^+ + v_{\beta}^+ i_{\beta}^+ \quad (4.9)$$

Equations (4.1) and (4.3) are applied on the PCC voltage and the load currents to obtain the positive sequence $\alpha\beta$ components ($v_{\alpha\beta}^+$ and $i_{\alpha\beta}^+$) required for using equation (4.9) to determine the load positive sequence power. Though the positive sequence power is a DC quantity resulting from balanced positive sequence voltages and currents, still a low pass filter with a cut off frequency of 10 Hz is used on this signal to minimize the effect of sudden load disturbances.

The power calculated from equation (4.9) is passed to a look-up table to determine the reference positive sequence power command for the BESS. The characteristics of the look-up table describing the relationship between the BESS positive sequence power (P_{BESS}^+) and the load positive sequence power (P^+) is given by,

$$P_{BESS}^+ = \begin{cases} P_{min} - P^+ & ; P^+ < P_{min} \\ 0 & ; P_{min} \leq P^+ \leq P_{max} \\ P^+ - P_{max} & ; P^+ > P_{max} \end{cases} \quad (4.10)$$

Therefore the peak value of the reference positive sequence active component of the current of the BESS is given by,

$$I_{ap} = \frac{P_{BESS}^+}{3} \frac{2}{V^+} \quad (4.11)$$

Where, V^+ is the peak value of the positive sequence (phase) voltage components. The instantaneous reference active currents ($i_{abc p}$) of the BESS will have the same magnitude and is generated using the sine of the phase angle with abc phase sequence.

4.2.3 Mode Selection and Transition System (MSTS) Module

The Mode Selection & Transition System (MSTS) Module is proposed to select and operate the BESS in the desired mode which can be either genset support or grid forming depending on the status/condition of the system as mentioned in section 4.2. Besides, MSTS also performs the controlled smooth transition between the two operating modes. For these purposes, it generates the following four control signals:

- ‘*mode*’ signal: It is mainly used to operate the BESS either in genset support or grid forming mode. During the genset support, $mode = 1$ while during the grid forming, $mode = 0$.
- ‘ g_{sf} ’ signal: It performs the controlled transition of the BESS from genset support to grid forming mode (when $g_{sf} = 1$).
- ‘ g_{gs} ’ signal: It performs the controlled transition of the BESS from grid forming to genset support mode (when $g_{gs} = 1$).
- ‘ Inv_{ctrl} ’ signal: This signal is used for controlling the breaker of the BESS. $Inv_{ctrl} = 1$ in normal operation of the BESS. In case of maintenance of the BESS, MSTS makes $Inv_{ctrl} = 0$ to open the BESS breaker from the minigrid system. After the maintenance the BESS can be connected to the diesel hybrid mini-grid system in genset support mode with $Inv_{ctrl} = 1$, since the BESS is synchronized with the PCC voltage and reference current is still generated from the external reference current generator block.

The objectives and functions served by these signals during two operating modes and transitions are described in details below.

4.2.3.1 '*mode*' Signal

This signal indicates the operating mode of the BESS in the mini-grid system. The BESS operates in genset support mode when $mode = 1$, and operates in grid forming mode when $mode = 0$. It has several control functions. During the grid forming mode, the genset breaker opens and the BESS forms the grid for the mini-grid distribution system. Again the BESS supports the genset when the genset forms the grid with the genset breaker being closed. The $mode$ signal controls the genset breaker directly depending on the operating mode of the BESS.

The $mode$ signal also selects the control loop for the per-phase controllers, i.e., when $mode = 1$, then the inner current loop takes the reference from the reference current generator block in the genset support mode and when $mode = 0$ then takes the reference current from the output of the voltage controller in grid forming mode. Besides, the error signal of the voltage controller is also multiplied by the \overline{mode} signal, so that during genset support mode the output of the PI controller of the voltage loop is kept at zero which ensures minimal transition for the voltage during the mode transfer. Besides, the $mode$ signal is used in the PLL+ICA module to generate the appropriate phase angle and angular frequency (and reference voltage) for the per-phase controllers. This signal is also used in the reference current generator block in both modes and also during the smooth transition processes as will be discussed in next section. During the transition from grid forming to genset support mode of the BESS, the genset should be loaded slowly with the positive sequence power, therefore, the $mode$ signal is also used to initiate the transfer of the current slowly from BESS to the genset as will be shown later in this section.

4.2.3.2 ' g_{s2f} ' Signal and the Corresponding Transition Process

This signal is used for planned transition from genset support to grid forming mode. The MSTS module monitors the system status and when necessary performs this transition. It initiates the transition by making $g_{s2f} = 1$ and keeps this value during the whole transition process. This signal is used in the reference current generator block and the PLL+ICA module to make the smooth transition. The proposed transition process is shown in Fig. 4.4. It takes place through the following events.

- a) Initially the genset is supplying positive sequence current component to the mini-grid system in the genset support mode. At first the BESS should unload the genset in order to prevent the sudden current change in the genset. So the BESS takes over all the positive sequence current of the load while still supplying the required negative sequence component, reactive current component of the load and the output capacitor current. This is done by changing the reference positive sequence active power of the BESS from the output of the look up table to the full load positive sequence active power as shown later in section 4.2.3.4. And this process is initiated by the g_{s2f} signal.
- b) The MSTS system monitors the PCC voltage in terms of frequency and magnitude of the phase voltage. When the genset is unloaded, the PCC voltage of the minigrid will be operating with the no-load frequency and voltage of the genset. The MSTS module monitors the system status and as soon the system reaches steady state taken as 15 cycles, it changes the *mode* signal from 1 to 0, so the genset breaker will open and the BESS starts operating in grid forming mode.
- c) As the mode changes, the frequency, phase angle and the reference voltage for the per-phase controllers is kept the same as it was during the grid support mode. So the

parameters of the PLL+ICA module are changed to achieve this. This ensures that the the mini-grid distribution system does not experience any voltage disturbance at the PCC during the mode transfer.

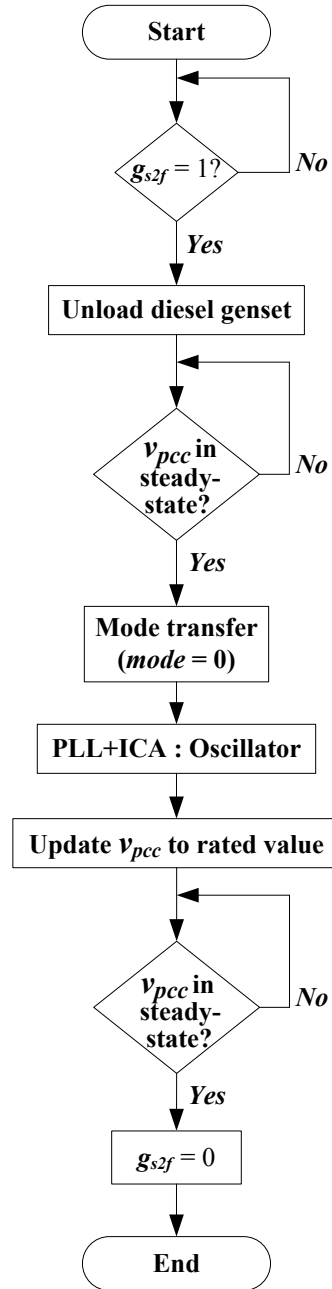


Fig. 4.4. Flow chart for the transition from genset support to grid forming mode.

- d) Since the grid forming unit is operating with the last no-load voltage and frequency of the genset and it is not the rated value of the mini-grid distribution system, so the PLL+ICA module will change the frequency and voltage magnitude to the rated values.
- e) Finally the MSTS makes $g_{sf} = 0$ when the grid forming BESS operates with steady state rated values (for voltage magnitude and frequency) for 15 cycles (~ 0.25 s.) The MSTS waits 0.25 s in order to keep safe margin from the changes in frequency and amplitude of the grid forming BESS.

4.2.3.3 ' g_{fs} ' Signal and the Corresponding Transition Process

This signal is used for planned transition from grid forming to genset support mode. The MSTS module monitors the system status and when necessary performs this transition. It initiates the transition by making $g_{fs} = 1$ and keeps this value during the whole transition process. This signal is used in the reference current generator block and the PLL+ICA module to make the smooth transition. The flow chart indicating the transition process from grid forming to genset support mode is presented in Fig. 4.5. The proposed transition process takes place through the following events.

- a) Initially the grid forming BESS is operating with fixed rated frequency and voltage of the minigrid system. When the genset is ready to be reconnected, the reference voltage of the grid forming unit should be synchronized with the genset (no-load) output voltage. It is done by changing the parameters of the PLL+ICA module to a slow synchronization value. When g_{fs} signal is made '1', then at first, the angular frequency and phase angle are synchronized with the genset output voltage. Then the

reference peak value of the voltage for the grid forming unit will be made equal to the peak value of the genset output voltage.

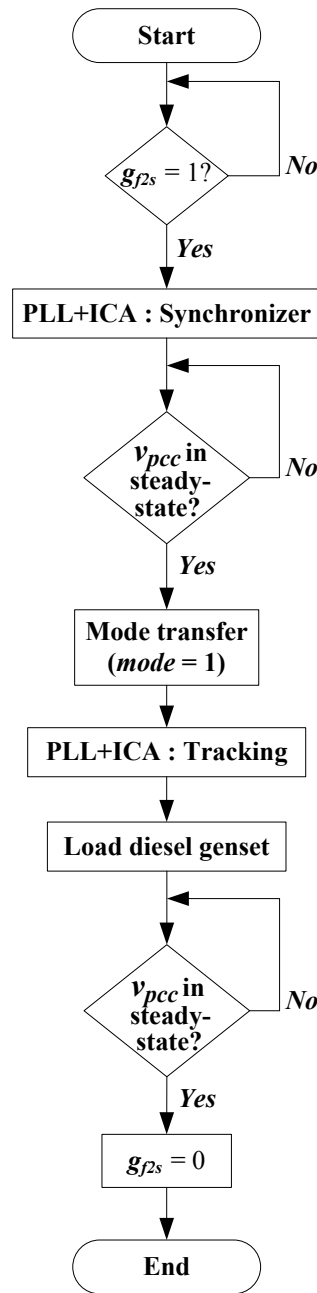


Fig. 4.5. Flow chart for the transition from grid forming to genset support mode.

- b) The MSTS module monitors this synchronization process. It checks the frequency and voltage magnitude of the PCC and also the voltage difference between the genset

- output and the PCC. As soon the system reaches steady state (for 15 cycles), the MSTS changes the *mode* signal from 0 to 1, so the genset breaker will close and the BESS starts working in genset support mode.
- c) The parameters of the PLL+ICA module will be changed to the normal tracking values when the *mode* signal changes from 0 to 1, so that the BESS tracks the PCC voltage as set by the genset.
 - d) During this mode transfer, the genset should not be loaded suddenly. So to achieve smooth transition of the positive sequence current from the BESS to the genset, the positive sequence reference current of the BESS should be decreased slowly by the reference current generator block, resulting in slow loading of the genset during this mode transfer. This is done by changing the reference positive sequence active power of the BESS from the full load positive sequence active power to the output of the look up table as shown in the next section. And this process is initiated by the *mode* signal.
 - e) The MSTS module monitors the system status and as soon the system reaches steady state (for 15 cycles), it makes $g_{fs} = 0$ to end the transition process.

4.2.3.4 Loading & Unloading of Genset Current during Transition Processes

During the grid support mode, the BESS supply or absorb positive sequence (or average) active power if the genset operates with mini-grid load of above $P_{max} = 0.9$ pu or below $P_{min} = 0.4$ pu respectively. It ensures maximum or minimum loading of the genset. If during the transition processes the *mode* signal is changed suddenly without prior attention to the genset output power then it will have a large impact on the genset

transient. Therefore, a smooth transition of the active power should be adopted between the genset and BESS.

Fig. 4.6 shows the generation of the positive sequence active power command for the BESS as adopted in this study. The switches used in the model use a threshold of 0.5, therefore when the control signal is more than 0.5, then it passes the top input and vice-versa. During the genset support mode, the output of the look up table provides the reference value for the BESS. During the transition from the genset support to grid forming mode, the BESS has to take all positive sequence power slowly from the genset. So when the g_{s2f} signal becomes 1 then the reference value of the positive sequence active power for the BESS is directly set as the load positive sequence power instead of the the command from the look up table as shown in Fig. 4.6. However this step change is passed through a rate limiter, so the positive sequence power transfers slowly from the genset to the BESS and the genset is finally unloaded before the mode transfer.

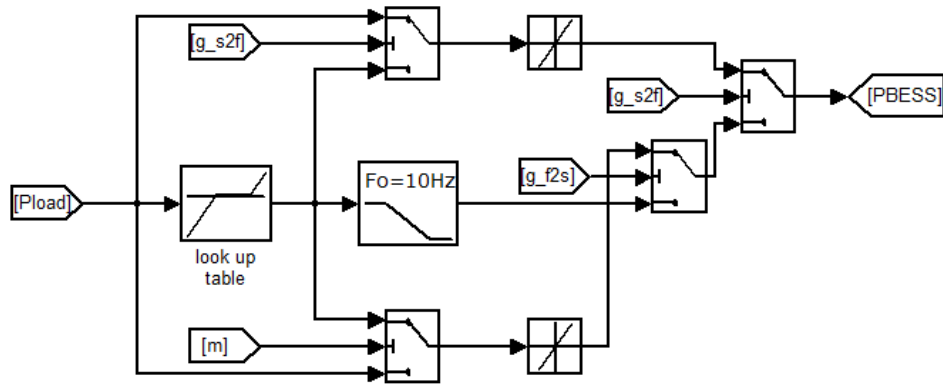


Fig. 4.6. Generation of positive sequence active power command for the BESS.

Again during the transition from grid forming to genset support, the genset should be loaded slowly. So it is done on the reverse way controlled by the g_{f2s} signal. When $g_{f2s} = 1$, then the reference power command is the full load power in the grid forming mode

and as the signal $mode = 1$ is applied, the input power command changes to the output of the look up table as shown in Fig. 4.6. But this step change is passed through a rate limiter to transfer the power from the BESS to the genset smoothly.

4.2.4 PLL+ICA Module

The per-phase dq controller requires the phase angle and angular frequency for the Park and Inverse Park transformation in both modes and also during the transition between the modes. Besides, the external reference current generator also uses these quantities to generate the reference current in the genset support mode. During the genset support mode, the BESS should be synchronized to the PCC voltage, while during the grid forming mode it should be synchronized with a desired reference output voltage. The PLL+ICA (Phase Locked Loop + Intelligent Connection Agent) as shown in Fig. 4.2 can perform these tasks. During the grid forming mode, the PLL+ICA module will also provide the reference voltage command for the per-phase controller. This module can also change this reference value as well as angular frequency and phase angle during transition between the modes to achieve smooth operation of the mini-grid system with the requirement proposed in MSTs. Besides, the angular frequency and magnitude of the PCC voltage provided by this module are also used as feedback signals in the MSTs to manage its control signals.

Frequency locked loop (FLL) based grid synchronization methods use adaptive filters, implemented by means of dual SOGIs (DSOGIs), which are self-tuned to the grid frequency through the action of the FLL [86]. With a simple change in its configuration, it can be transformed into an oscillator, which makes it a good choice to operate both as synchronization system or oscillator. However, the system proposed in [86], uses two

DSOGI-FLL structures to control an intelligent connection agent (ICA) based on a voltage source inverter for smooth transition of a microgrid between grid connected and islanded mode. During the grid connected mode, it just monitors the grid and does not do any grid feeding or grid support operation and in case of fault in the grid side, it disconnects the microgrid by a controlled switch operated by the ICA system. After disconnection it works as an oscillator and controls the VSI as a grid forming unit to control the voltage of the isolated microgrid. Again during the reconnection process of the microgrid with the network, the two DSOGI-FLL structures has been used to detect the normal grid condition and synchronize the grid forming unit with the grid voltage and finally the microgrid was connected to the utility grid [86]. However in this study this concept is modified with only one DSOGI-FLL structure, which allows the operation of the BESS in both modes and also during the smooth transition between the modes.

The structure of SOGI for orthogonal signal generation is shown in Fig. 4.7, where ω_o is the SOGI resonant frequency and k_s is the damping factor. When the frequency of the input signal is equal to ω_o the output signal amplitude will be the same as input amplitude. If v is an input sinusoidal signal, then v' and qv' will be sinusoidal as well. Moreover, qv' will be always 90° lagging of v' , independent of both the frequency of v and the values of ω_o and k_s . The transfer functions describing the behavior between input v and the outputs v' and qv' are given by equations (4.12) and (4.13) respectively [72].

$$\frac{v'(s)}{v(s)} = \frac{k_s \omega_o s}{s^2 + k_s \omega_o s + \omega_o^2} \quad (4.12)$$

$$\frac{qv'(s)}{v(s)} = \frac{k_s \omega_o^2}{s^2 + k_s \omega_o s + \omega_o^2} \quad (4.13)$$

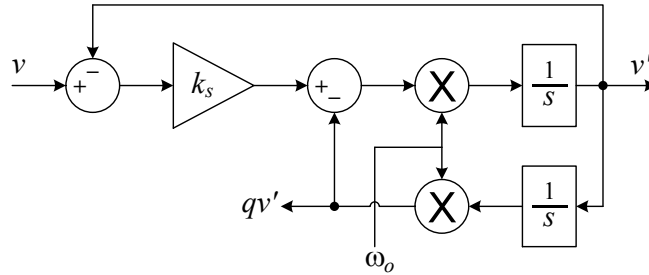
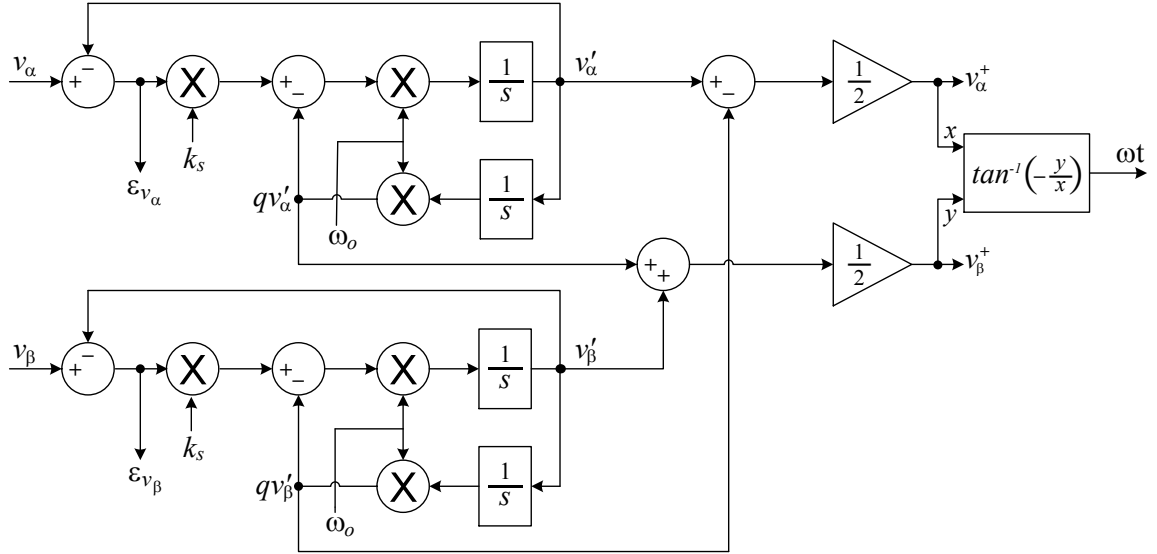


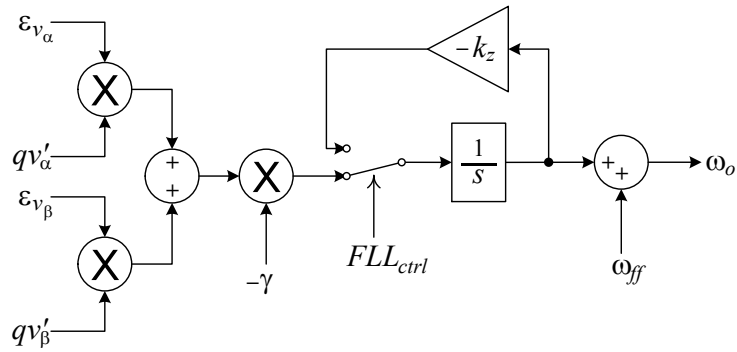
Fig. 4.7. Frequency adaptive SOGI block diagram for generation of an orthogonal component.

The dynamic response of the SOGI is defined by the damping factor, k_s . Low values of k_s result in more selective filtering response and a longer stabilization time, whereas high values result in faster and less damped responses [72]. A trade-off between stabilization time and overshoot limitation can be achieved with $k_s = \sqrt{2}$.

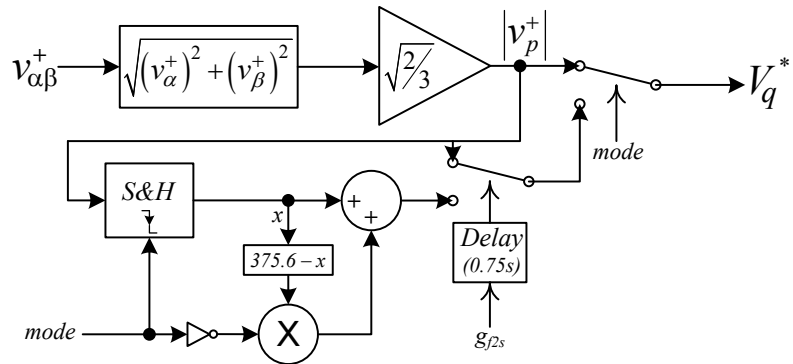
The block diagram for the proposed PLL+ICA module is shown in Fig. 4.8. In order to extract the positive sequence components during the genset support mode, the genset output voltages (v_{sabc}) are first transformed into $\alpha\beta$ frame ($v_{\alpha\beta}$) using Clark transformation: equation (4.1). Then, the positive sequence components, in $\alpha\beta$ frame, can be extracted using equation (4.3). Finally, the phase angle and peak amplitude can be extracted from the positive sequence components. The extraction of the phase angle from the positive sequence components (PSC) is shown in Fig. 4.8(a). The resonant frequency of the DSOGI is provided by the FLL. Fig. 4.8(b) shows the structure of the FLL. In this system, γ is an integration gain and ω_{ff} is the rated center frequency, which is used as feed-forward. The extraction of the peak amplitude from the positive sequence components during the genset support mode is shown in Fig. 4.8(c) (upper path with $mode = 1$).



(a) Diagram of the DSOGI and the PSC.



(b) FLL for frequency estimation.



(c) Magnitude of the PCC voltage generation or extraction.

Fig. 4.8. Basic components of the PLL+ICA module.

During the transition from genset support to grid forming mode, it is expected that the PCC voltage and its angular frequency and phase angle should be the same just before disconnection of the genset from the mini-grid system. The damping factor k_s defines the dynamics of the SOGI as described in equations (4.12) and (4.13). If k_s is set to zero, the output positive sequence component will oscillate indefinitely with frequency ω_o regardless of its input [86]. When the genset is disconnected, then the PLL+ICA module makes $k_s = 0$; so the SOGI will operate with the same frequency as ω_o . Therefore it is possible to change the frequency and phase angle in this mode (grid forming) by changing ω_o . However the amplitude of the output positive sequence voltage components does not keep the same value and it changes in this mode [86]. Therefore, careful measures should be taken account for controlling the PCC voltage by the BESS. The phase angle of the system is extracted using the positive sequence $\alpha\beta$ components in the grid forming mode also. It corresponds to the desired operating frequency of this DSOGI-FLL system.

Again, as the mode changes from genset support to grid forming, the parameter γ changes to 0. Therefore, it will keep the same frequency value after disconnection as it was during genset support mode. As mentioned in the MSTs section, the genset is unloaded before disconnection from the mini-grid system; therefore, the mini-grid system operates with the no-load frequency of the genset (due to the droop characteristic). Since the rated frequency of the mini-grid system is 60 Hz, so the frequency should be changed to the rated value. As the center frequency for the FLL is 60 Hz, so the desired rated frequency can be achieved with “discharging” the integrator of the FLL with a negative

feedback loop as shown in Fig. 4.8(b), where the integrator resetting depends on k_z , and its settling time is given by,

$$t_{s_{FLL}} = \frac{4}{k_z} \quad (4.14)$$

For this work, $k_z = 80$ has been selected which results in a settling time of 0.05 s. The input to the DSOGI-FLL block is still the genset voltage but since the parameters of the DSOGI-FLL are zero, it does not affect the output frequency and phase angle. When the genset is ready to be reconnected to the mini-grid system, then the frequency and phase angle should be synchronized. So, at the beginning of the synchronization process and in order to avoid large transients, conservative values of k_s and γ are chosen [86], making the reference/output voltage of the grid forming unit synchronize with the genset output voltage. When the magnitude of the voltage is also updated, then the genset can be reconnected to the mini-grid system and the BESS can go back to the support mode. After the reconnection, the parameters of the DSOGI-FLL can be updated to the desired ones [86]. Table 4.1 shows the logic used for selecting the parameters of the DSOGI-FLL system in different modes and during the transition processes as adopted in this work.

Table 4.1. Look-Up Table Used for the Parameters' Value of DSOGI-FLL.

mode	g_{f2s}	k_s	γ
1	0/1	$\sqrt{2}$	0.411
0	0	0	0
0	1	$\sqrt{2}/5$	0.411/100

The generation of reference q axis voltage (V_q^*) during different modes and transition between the modes, is shown in Fig. 4.8(c). This quantity also represents the magnitude of the PCC voltage when the genset is connected to the mini-grid system. V_q^*

for the per-phase voltage controller is kept the same as the peak value of the positive sequence component of the PCC voltage during the genset support mode (when $mode = 1$) as shown in Fig. 4.8(c). When the variable $mode$ changes from 1 to 0, indicating grid forming mode, the last value of the PCC voltage is held by a sample and hold (S&H) block. Then, at the beginning of the grid forming mode, the amplitude is changed to the rated value (375.6 V peak for the phase voltage), as shown in Fig. 4.8(c). The grid forming unit continues operating with this value as V_q^* . When the genset is to be reconnected, V_q^* for the grid forming BESS should be the same as the peak value of the genset output voltage. However, the peak value provided by the DSOGI and PSC is not the correct one just before the reconnection signal g_{f2s} becomes 1. Therefore, when g_{f2s} becomes 1 with $k_s = \sqrt{2}/5$ and $\gamma = 0.411/100$, it takes almost 0.3 s (worst case) for the DSOGI and PSC to reach the steady state peak value of the genset output voltage [86]. In order to keep some margin, a delay of 0.75 s is considered before updating the value of V_q^* from the instant g_{f2s} becomes 1. As soon as the mode transfer is done, it again keeps following the peak value of the positive sequence component of the PCC voltage with $k_s = \sqrt{2}$ and $\gamma = 0.411$.

4.3 Diesel Genset Model

A 30 kW diesel genset has been considered for analyzing the transient response of a diesel hybrid mini-grid. The diesel genset model consists of two main elements: A synchronous generator (SG) and the prime mover (diesel engine) as shown in Fig. 4.9. The SG is implemented with the 31.5 kVA/460 V, 1800 RPM/ 60 Hz "synchronous machine" block available in SimPower Systems library of Simulink. The SG is connected to the mini-grid distribution system by means of a three-phase breaker block. The SG

also has a measurement block to measure its output currents (I_g) and voltage (V_s). The mechanical input for the SG is selected to be "speed ω ," thus making the inertia constant H of the block to be disregarded. The mechanical shaft of the genset is represented by a first order transfer function with the moment of inertia of the engine and SG lumped together as shown in Fig. 4.9.

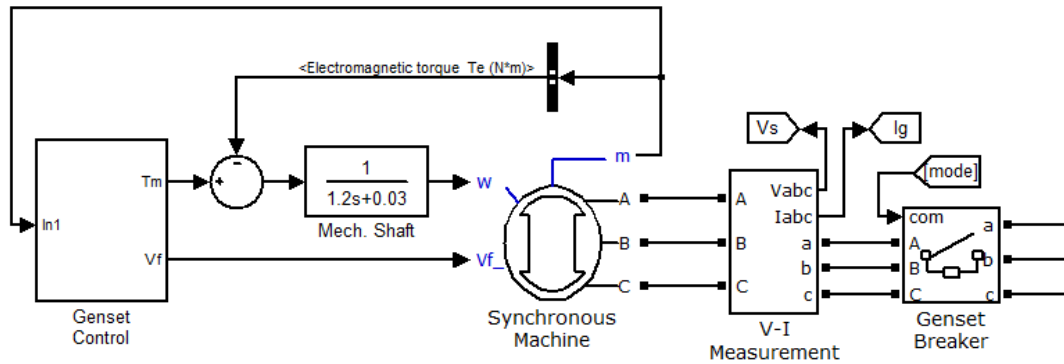


Fig. 4.9. SIMULINK implementation of diesel generator.

The “Genset control” block contains the speed and voltage controllers, which are shown in Fig. 4.10. The field voltage (V_f) of the SG is provided by a PI type voltage regulator with 5% droop and its input is the rated voltage of the generator as no-load reference voltage as shown in (lower part of) Fig. 4.10. The fuel injection actuator is represented by a first order transfer function while a delay block models the time interval between fuel injection and torque developed in the mechanical shaft of the diesel engine. The governor of the genset is of the PI type with a 5% droop ($P-\omega$ Droop) and its input is the no-load speed of the genset as shown in (upper part of) Fig. 4.10. Further details of this genset model are shown in [87] and the parameters are presented in the Appendix.

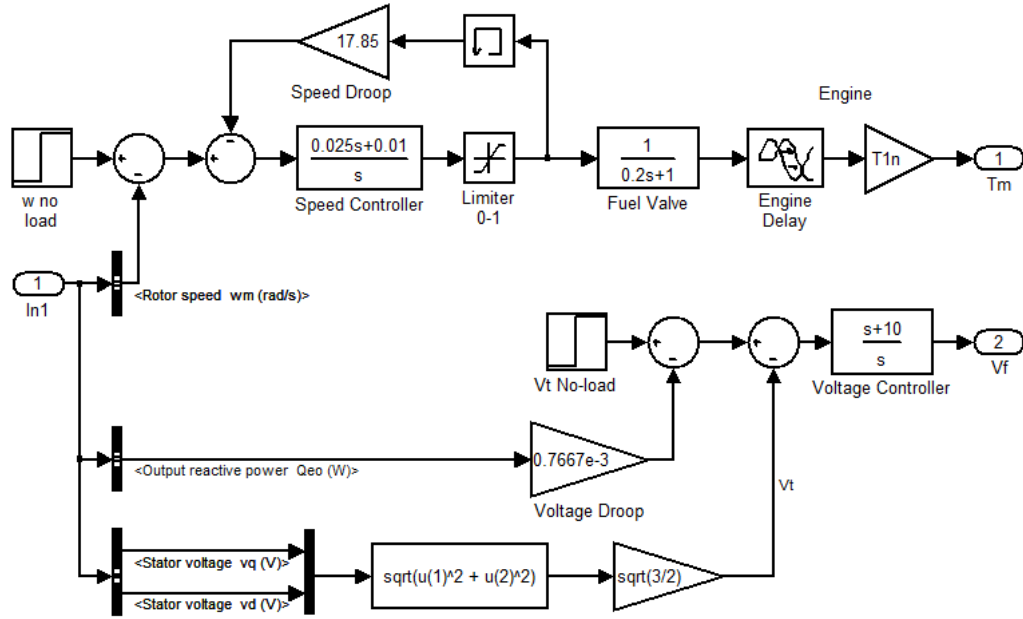


Fig. 4.10. SIMULINK implementation of genset controller.

4.4 Performance Verification

The performance of the proposed control strategy of the BESS is verified by means of simulation using SIMULINK. The three-phase BESS operates with SPWM at 5 kHz from a 1000 V DC bus and the rated output voltage is 460 V_{L-L} at 60 Hz. The current and voltage sensors are assumed to be ideal with a unity gain. The inductance and resistance of the output filter inductor are equal to 3 mH and 0.1 Ω. The capacitance is 25 μF. PI controllers were employed in both current and voltage control loops of the per-phase controllers. The inner current control loop was designed for a bandwidth (f_x) of 1200 Hz and $\xi = 1.2$, yielding $k_p = 19.54$ and $k_i = 86 \times 10^3$. The outer voltage loop was designed for a bandwidth of 120 Hz and $\xi = 0.707$, yielding $k_p = 0.016$ and $k_i = 7.106$.

4.4.1 BESS Supporting the Diesel Genset

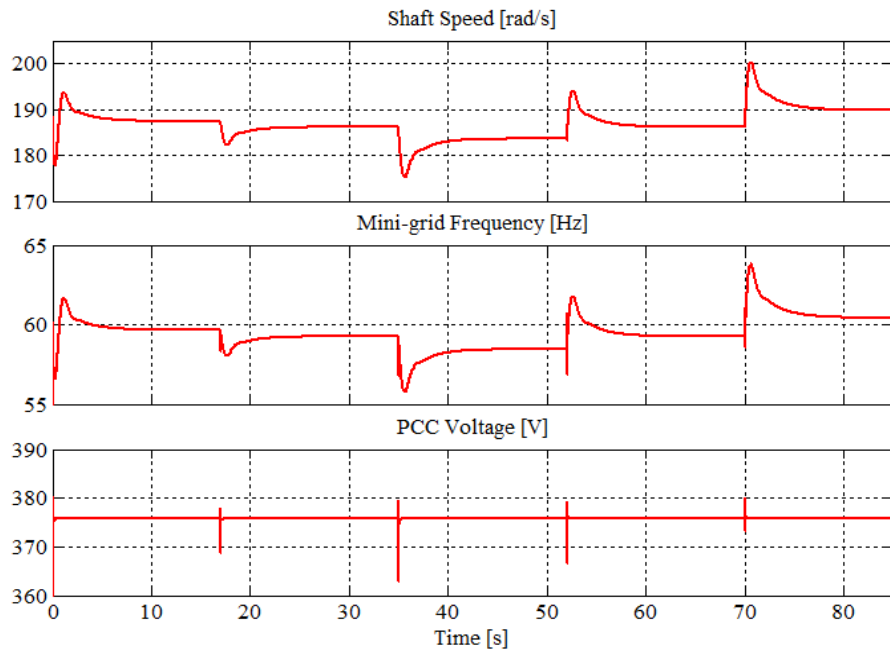
In this case, the genset forms the grid and the BESS provides support by compensating the load unbalance, the equivalent load power factor, supplying the output

capacitor currents and injecting/absorbing active power if the genset is about to operate outside its ideal power range. The limits for the genset are chosen as $P_{min} = 12$ kW and $P_{max} = 27$ kW. Table 4.2 shows the loads for different time instants connected in the mini-grid during the grid support mode. The load values are rated at 460 V and 60 Hz.

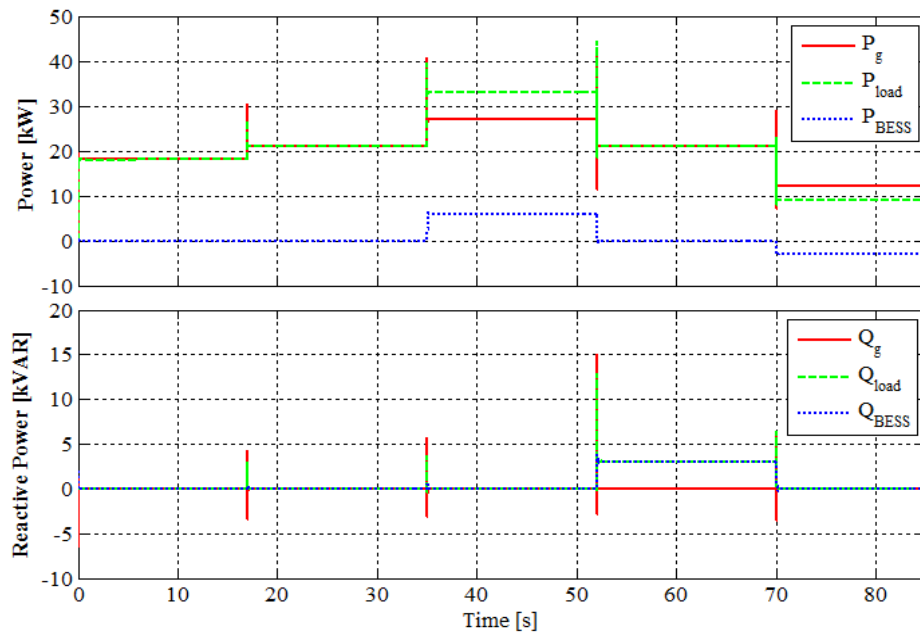
Table 4.2. Loads in Diesel Mini-Grid during Genset Support Mode of BESS.

No.	Time (s)	Load between 'a' and 'b'	Load between 'b' and 'c'	Load between 'c' and 'a'
1	0 – 17	6 kW	6 kW	6 kW
2	17 – 35	9 kW	6 kW	6 kW
3	35 – 52	12 kW	12 kW	9 kW
4	52 – 70	9 kW & 3 kVAR (lag)	6 kW	6 kW
5	70 – 85	2.25 kW	2.25 kW	4.5 kW

Fig. 4.11 shows some waveforms during load variations with the BESS in the genset support mode. As the load demand changes, the genset speed and mini-grid frequency vary as per the droop characteristics of the genset as shown in Fig. 4.11(a). During heavy load (load#3) these quantities have the minimum value while during light load (load#5) condition, these have the maximum values. The magnitude of the peak value (of the positive sequence component) of the PCC voltage is not affected as shown in Fig. 4.11(a), though the genset operates with Q-E droop characteristics. It happens because the load reactive power demand is provided by the BESS. Fig. 4.11(b) shows the three-phase average or positive sequence real and reactive power of the genset, load and BESS in the genset support mode. The BESS supplies active power during load#3 as the load demand is more than P_{max} and also absorbs active power when the load demand is less than P_{min} as seen with load#5. Besides, when an inductive load (load#4) is connected to the system, its reactive power is supplied by the BESS.



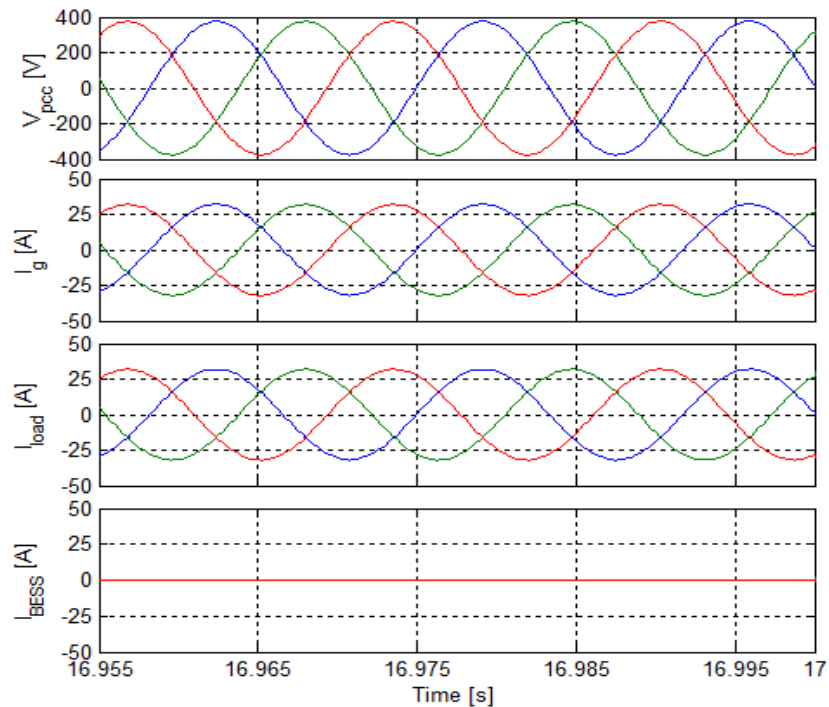
(a)



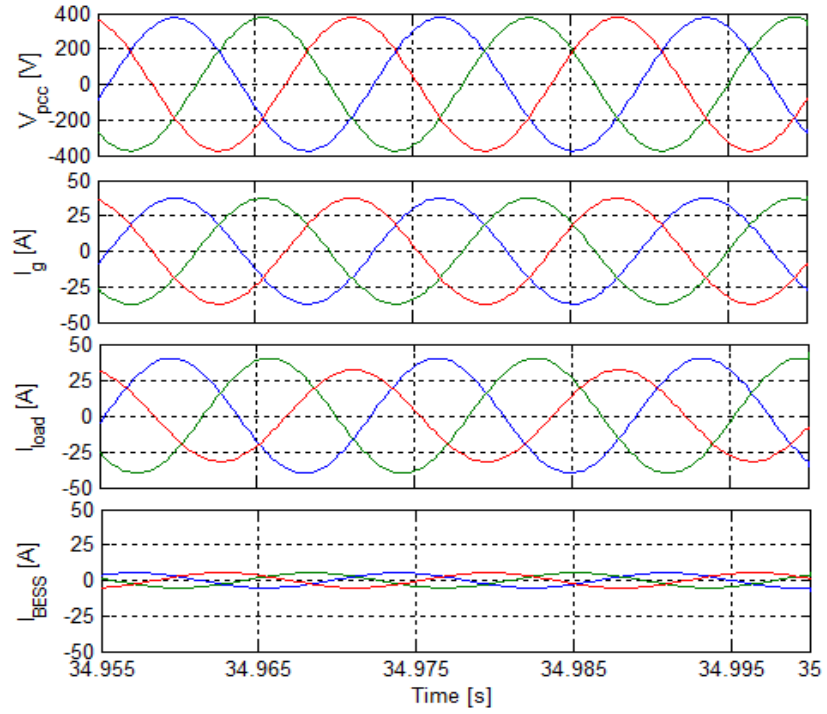
(b)

Fig. 4.11. Waveforms for the genset support mode. (a) Genset shaft speed, mini-grid frequency and peak value of the positive seq. voltage; (b) Real and reactive power of the genset, load and BESS.

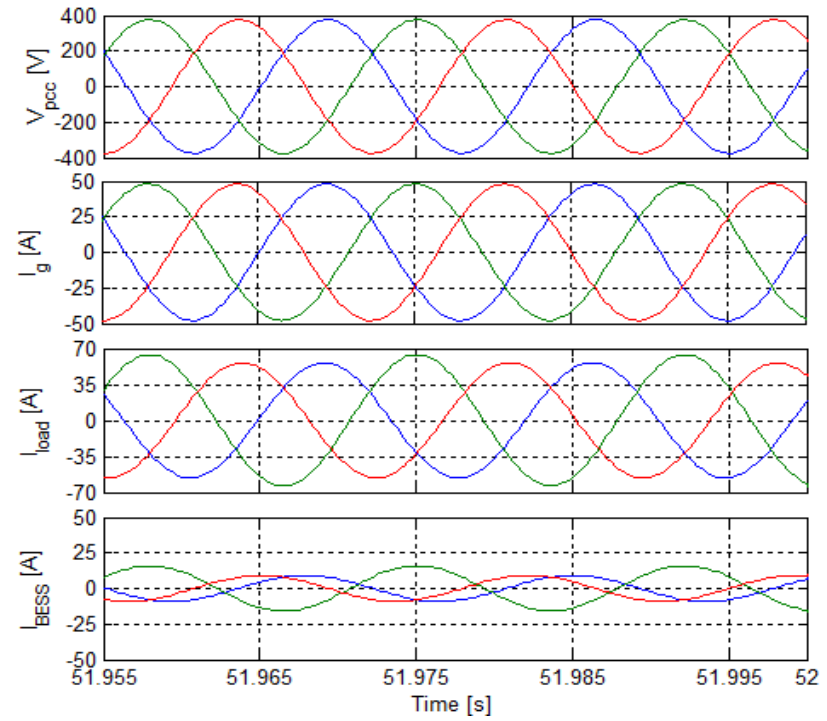
Fig.4.12 shows the steady state waveforms of the PCC voltages, genset currents, load currents and the BESS output currents in the genset support mode. Depending on the load demand, the BESS supplies/absorbs active component of the current, does load compensation by supplying the negative sequence currents and compensates the PF so that the genset operates with UPF. Due to all these actions, the PCC voltage is balanced and fixed at the rated value. Also it ensures the genset current to be balanced and limited to 48 A (peak) corresponding to a genset power of 27 kW, while the load current in the three phases are in the range of 56 to 64 A (peak) during load#3. It also ensures the minimum current to be 21.3 A (peak) for the genset corresponding to the genset minimum power of 12 kW, while the load current in the three phases are in the range of 12 to 18 A (peak).



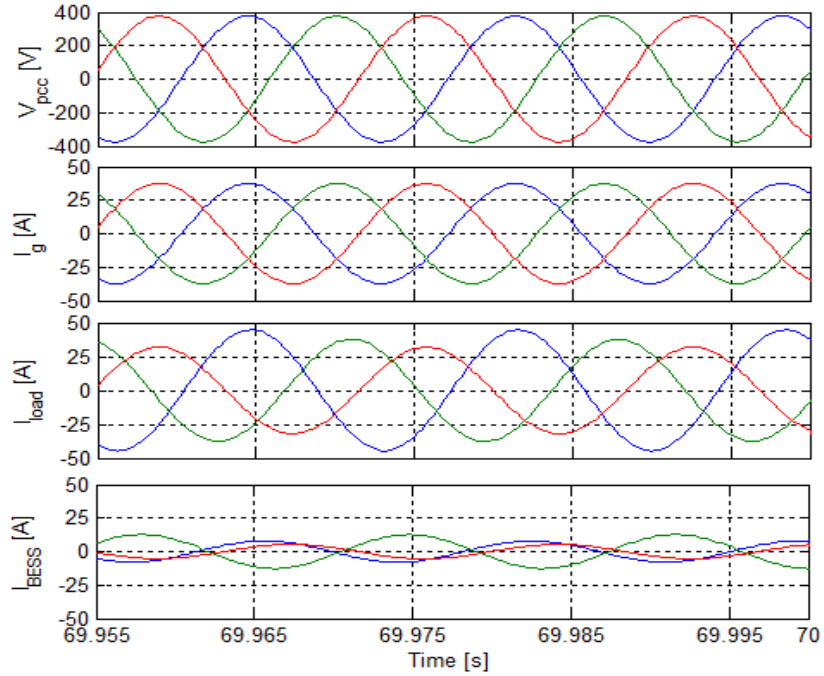
(a)



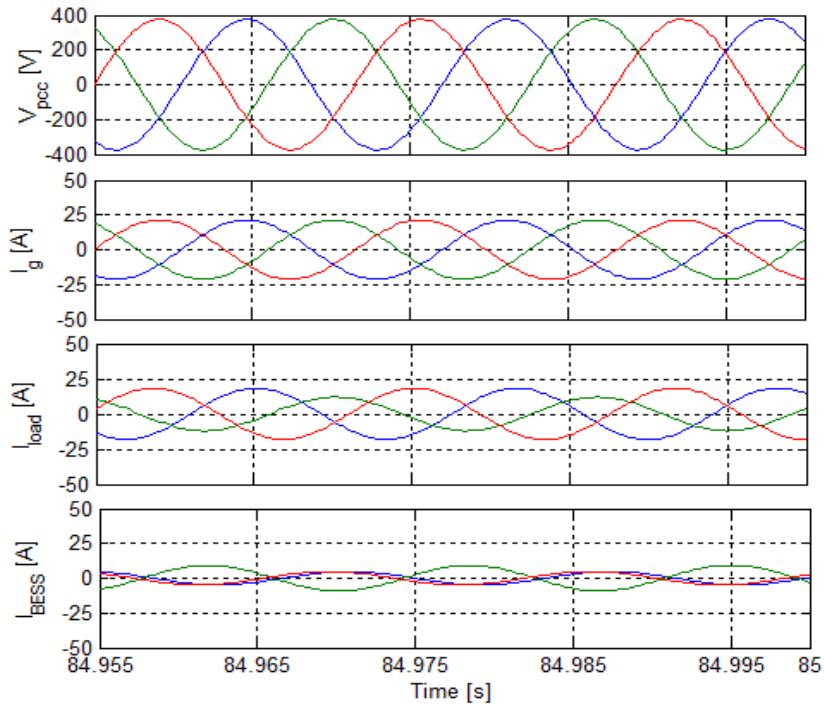
(b)



(c)



(d)



(e)

Fig.4.12. Steady-state waveforms of the PCC voltages, genset currents, load currents and BESS currents for different loads.

4.4.2 BESS Acting as Grid Forming Unit

The desired load voltage for the BESS in grid forming mode is 460 V_{L-L} at 60 Hz. Initially the grid forming BESS is supplying a 7.5 kW three-phase balanced load (2.5 kW/phase). At $t = 0.2 \text{ s}$, the load demand increases to 5 kW in between lines A-B and at $t = 0.3 \text{ s}$, the load demand changes to 3 kW at 0.8 PF lagging in between lines C-A. Finally, at $t = 0.4 \text{ s}$ a single-phase PV inverter connected between lines B-C, starts supplying 3.5 kW with UPF. The resulting three-phase load voltages and load currents are shown in Fig. 4.13 for the proposed control scheme. The load voltages remain balanced in steady-state for all the various load unbalances considered in this study. The proposed method presents a very fast response regulating the load voltages almost instantaneously, even under highly unbalanced loads.

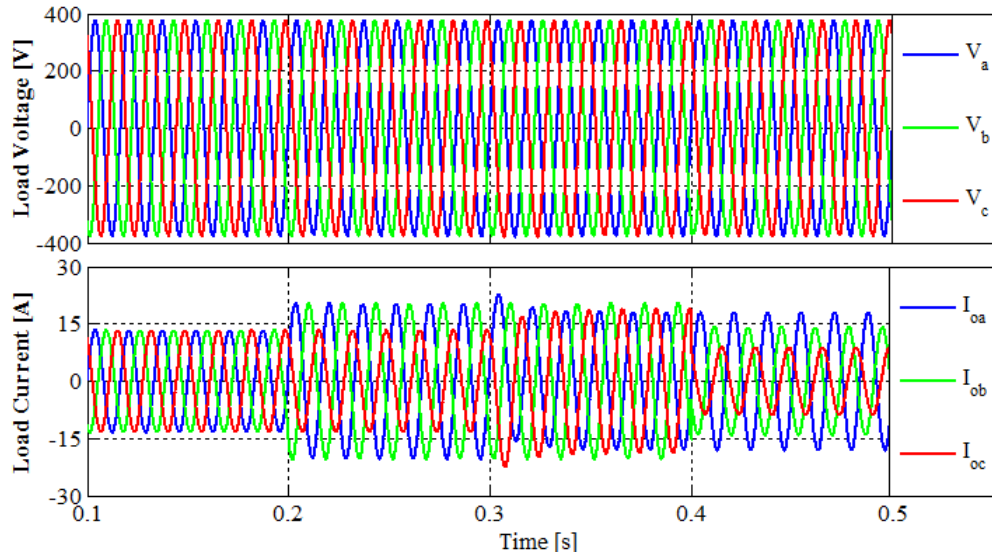
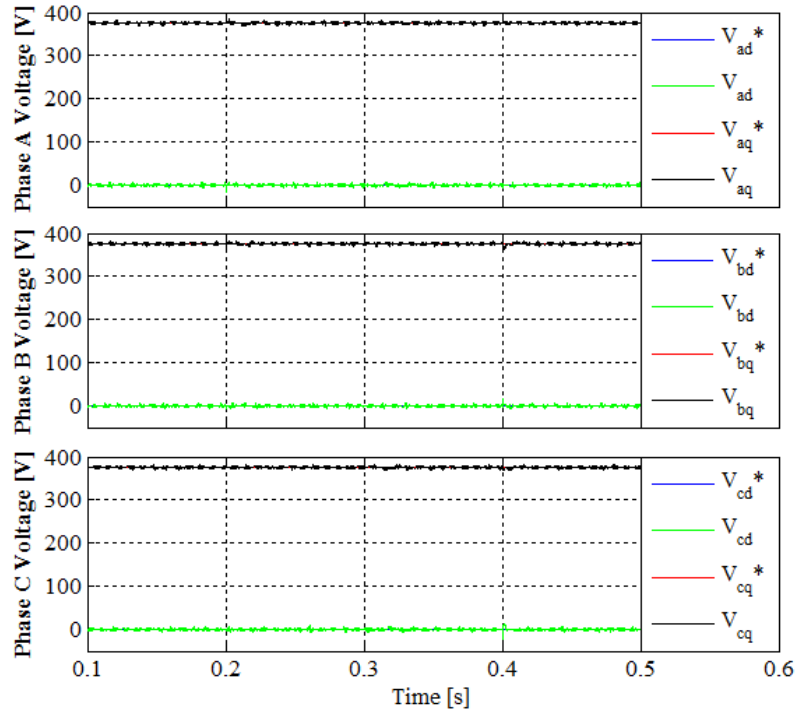
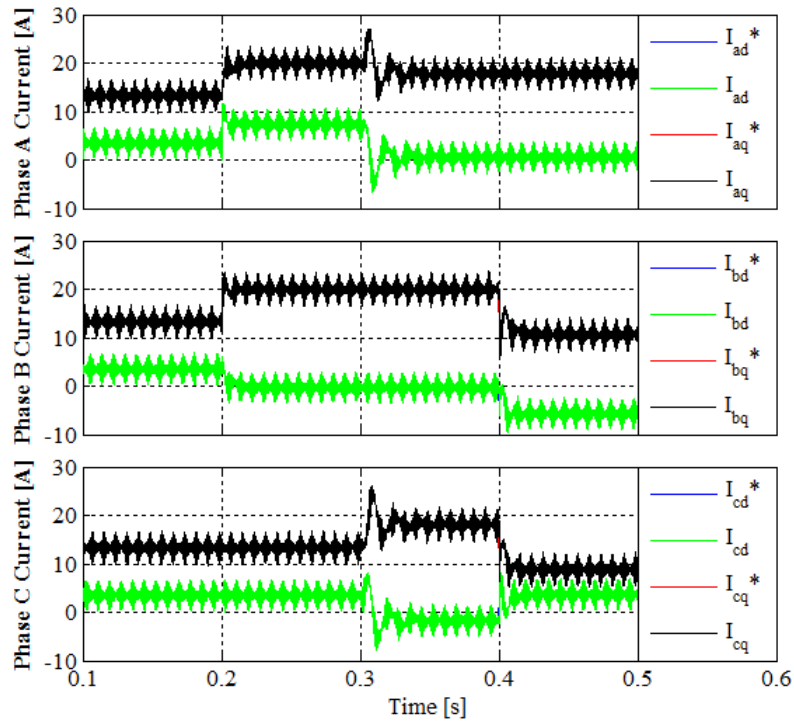


Fig. 4.13. Output voltages and currents of the grid forming BESS for varying loads.

Fig. 4.14 shows the reference and actual voltages and currents for the grid forming BESS in the dq frame with the proposed control scheme. There, one clearly sees that the deviations in the voltage signals are small and short with the proposed per-phase scheme.



(a)



(b)

Fig. 4.14. Waveforms of the control loops of the grid forming BESS in dq frames. a)

Reference and actual voltages; b) Reference and actual currents.

The current reference signals for the proposed scheme reacts fast to load variations and voltage errors to regulate the output voltage as shown in Fig. 4.14. Variations in the reference currents to compensate for voltage unbalances take place fast and only in the phases directly related to the load variations, while the other is unaffected.

4.4.3 Transition between the Modes

This section analyzes the behavior of the BESS during the transitions between the genset support and grid forming modes. The load connected to the mini-grid system is represented by the active power demand of $P_{ab} = P_{bc} = 3.712$ kW and $P_{ca} = 5.29$ kW, which are rated at 460 V and 60 Hz. The load is kept constant during this analysis. The goal is to achieve soft transitions during the mode transfer. Some time-domain results during the transitions are shown in Fig. 4.15, Fig. 4.16 and Fig. 4.17. The frequency of the genset and BESS, peak amplitude of the PCC voltage and the average or positive sequence active power of the genset, BESS and load are shown in Fig. 4.15. Fig. 4.16 shows the PCC voltage, the voltage difference between the genset output and PCC and the currents of genset, load and BESS. The actual currents of the three phases of the BESS in dq frame during this transition process are shown in Fig. 4.17.

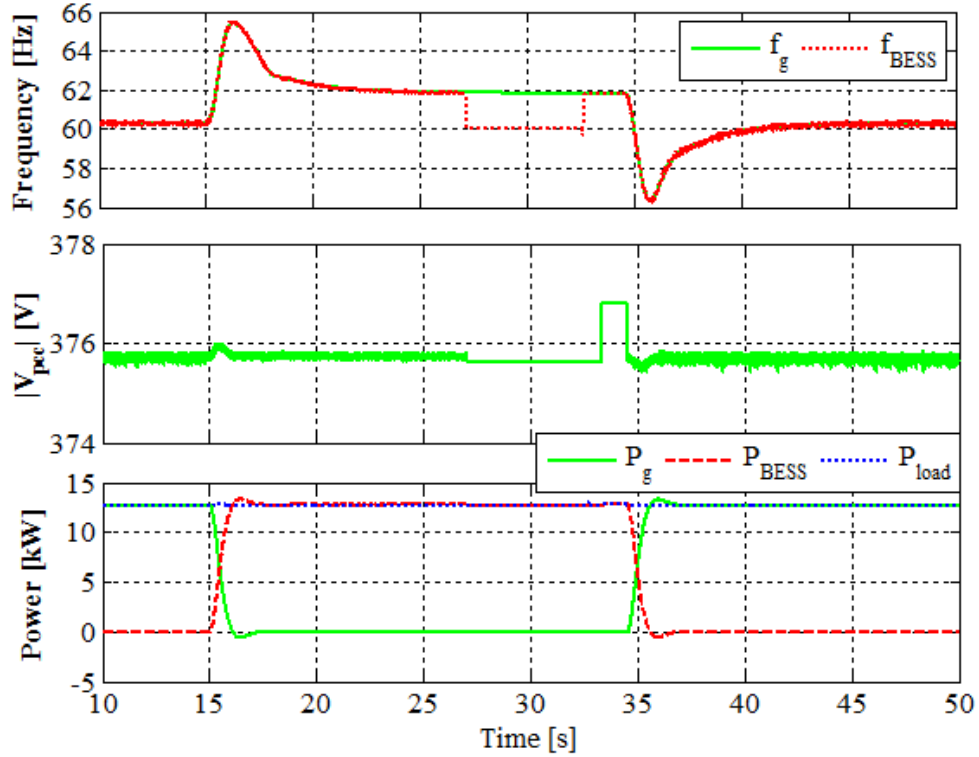
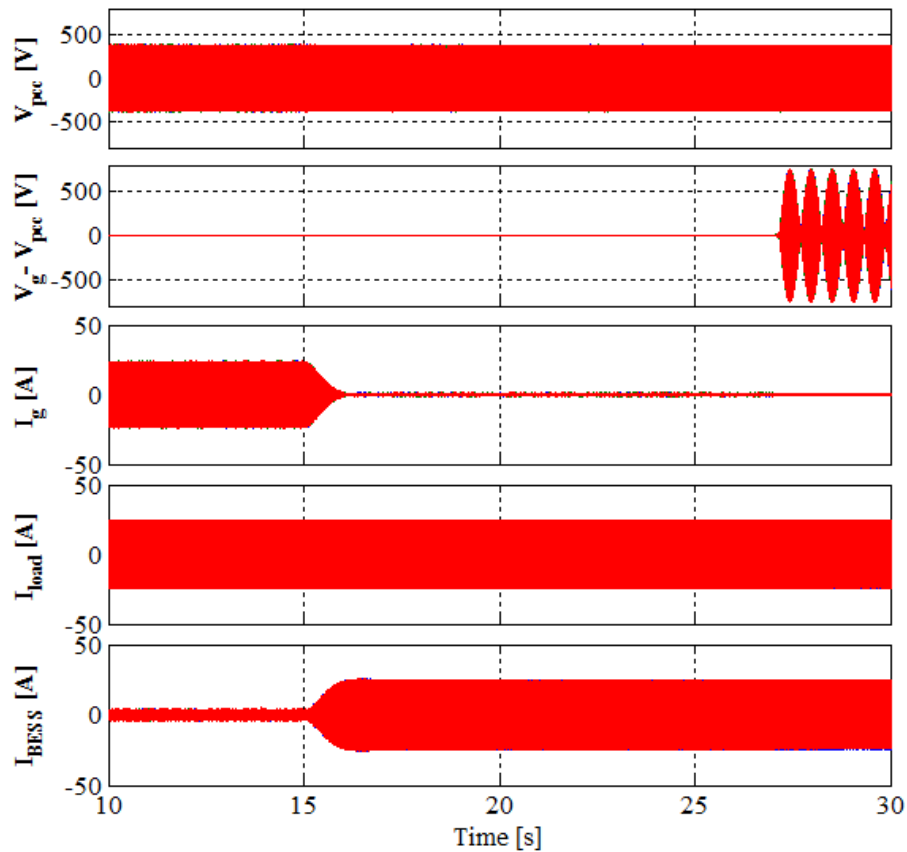


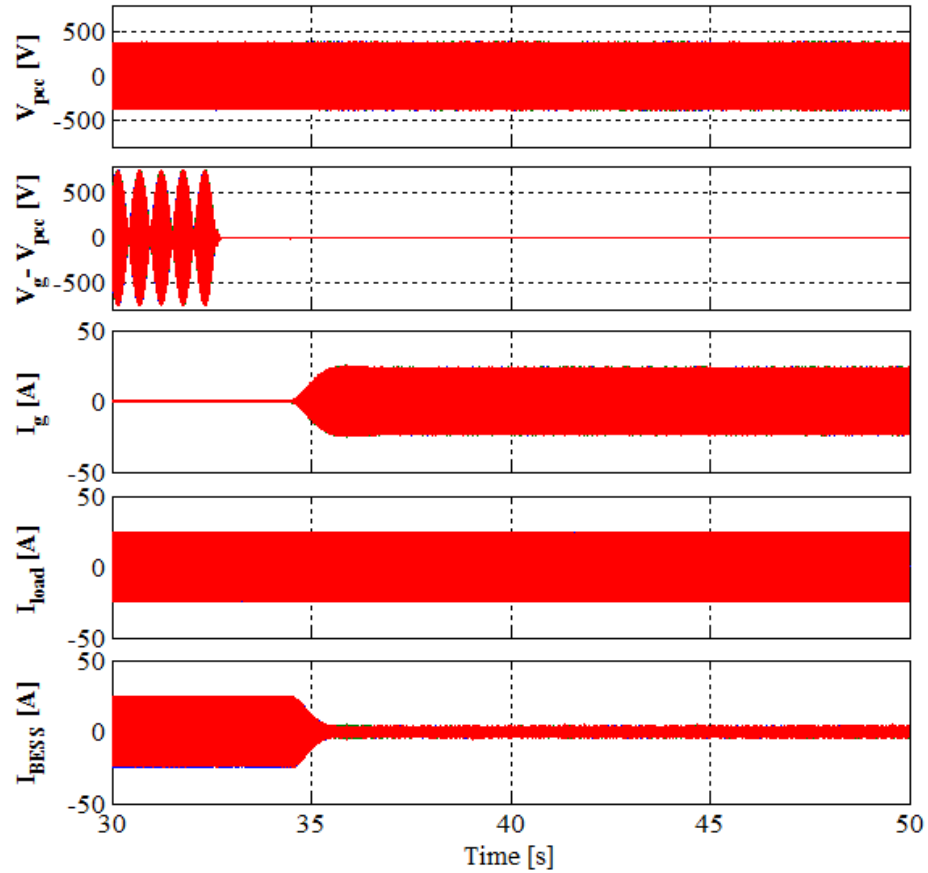
Fig. 4.15. Waveforms during transition between the modes. (From top to bottom: Frequency of the genset and BESS; Peak value of the PCC phase voltage; Active power of the genset, BESS and load.)

Initially the system operates in the grid support mode. The genset voltage is the input to the DSOGI-FLL block. During steady state in the genset support mode, the DSOGI-FLL operates with $k_s = \sqrt{2}$ and $\gamma = 0.411$. The system is in steady state as shown in Fig. 4.15, Fig. 4.16(a) and Fig. 4.17 in between $t = 10$ s and 15 s. The MSTs module activates the transition by setting $g_{s2f} = 1$ at $t = 15$ s and it will be active during this transition process from genset support to grid forming. At first, the genset should be unloaded. When the g_{s2f} becomes active, the BESS starts to take over all the power of the load slowly, making the genset output power become zero. The change of the power between the genset and the BESS can be observed in Fig. 4.15. The three-phase currents

of the genset drop to zero slowly and the BESS takes over all the positive sequence current as shown in Fig. 4.16(a), while the load currents are virtually unaffected during this current transfer. As only the positive sequence power component supplied by the BESS is changed, the q-axis currents for the three phases increase to supply the required load demand, while the d-axis currents are not affected as shown in Fig. 4.17. This unloading process of the genset is done by changing the reference active power command of the BESS from the output of the look up table to the full positive sequence power of the load. Still, it keeps supplying the load negative sequence component and reactive power. So the whole load demand is provided by the BESS as shown in Fig. 4.15, Fig. 4.16(a) and Fig. 4.17.



(a) Transition from genset support to grid forming



(b) Transition from grid forming to genset support

Fig. 4.16. Waveforms during the transitions. (Top to bottom: PCC voltage, difference between genset voltage and PCC voltage, genset current, load current and BESS current)

Since the genset is unloaded, the genset (or mini-grid system) starts operating with the no-load frequency (of the genset) after a transient as shown in Fig. 4.15. The MSTs block monitors the system status and, as soon as the system reaches steady state (in terms of frequency and magnitude of PCC voltage), it changes the *mode* signal from 1 to 0 at $t = 27$ s. Therefore, the BESS starts operating in grid forming mode. The BESS should be working with the same frequency, phase angle and peak value of the PCC phase voltage after the genset is disconnected. As soon as the *mode* signal changes, the DSOGI-FLL starts working with $k_s = 0$ and $\gamma = 0$ in the oscillator mode. Therefore it keeps initially the

same frequency and phase angle in the grid forming mode. Again, it is required to set the reference value for the per-phase voltage controllers before the disconnection of the genset. The DSOGI-FLL block tracks the peak value of the (positive sequence) PCC phase voltage and this value is set as V_q^* for the per-phase voltage controllers while V_d^* is set to 0 in the genset support mode. It should be the same after the disconnection to have minimal transient on the load which is achieved by a sample and hold block controlled by the *mode* signal. As the operating mode of the BESS changes, the voltage controller of each per-phase controller is enabled and it provides the reference current for the inner current loop after the disconnection of the genset from the mini-grid system. Therefore, the magnitude of the PCC voltage remains the same as shown in Fig. 4.15. Then, the BESS keeps supplying the same dq-currents in the three phases to meet the load demand after the disconnection of the genset as shown in Fig. 4.17.

Since the system was operating with the no-load frequency (62 Hz) and the voltage of the genset, which is not the same as the rated value in the grid forming mode, the BESS can be made to work at rated frequency (60 Hz) and voltage. Therefore, the V_q^* is updated by the PLL+ICA module to the rated value of 460 V (L-L) at $t = 27$ s. The PLL+ICA module starts updating the reference frequency to the desired 60 Hz at $t = 27$ s as shown in Fig. 4.15. In this way, the grid forming unit keeps working with the rated values. Finally, when the steady state is reached for 15 cycles, the MSTS module makes $g_{s2f} = 0$ at $t = 28.5$ s indicating the end of the transition. The BESS keeps operating in grid forming mode. The next transition from grid forming to genset support is described next.

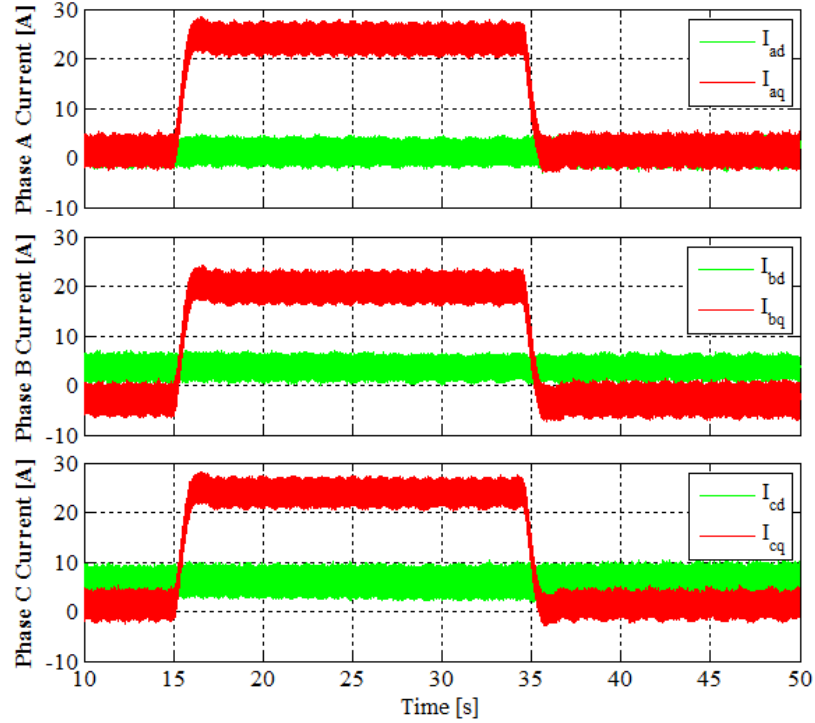


Fig. 4.17. Dq current waveforms for the three phases of the BESS during the transitions.

The MSTS block initiates the transition by making the signal $g_{fs} = 1$ at $t = 32.6$ s and keeps it active during the whole transition process. First, the reference voltage of the grid forming unit should be synchronized with the genset output voltage. The phase angle, frequency and amplitude can be synchronized using the PLL+ICA module. The signal g_{fs} makes $k_s = \sqrt{2}/5$ and $\gamma = 0.411/100$ and also enables FLL block to slowly synchronize the phase angle and angular frequency of the BESS with the genset output voltage. The frequency update of the BESS from rated value to the no-load frequency of the genset can be observed in Fig. 4.15 which takes approximately 0.05 s. Then, V_q^* for the BESS is updated to the peak value of the genset output (no-load) voltage at $t = 33.35$ s as shown in Fig. 4.15, which is controlled by the delayed g_{fs} signal (of 0.75 s). Therefore, the output voltage of the BESS is synchronized with the genset output voltage, which can be visualized by observing the voltage difference shown in Fig. 4.16(b).

The MSTS module makes the transition of the BESS from grid forming to genset support by making $mode = 1$ at $t = 34.7$ s; which in turn closes the genset breaker, connecting it to the mini-grid system. As the $mode$ signal changes to 1, the DSOGI changes the parameter to $k_s = \sqrt{2}$ and $\gamma = 0.411$ and keeps tracking the PCC voltage. At the same time, it disables the voltage controller of the per-phase controllers by \overline{mode} signal and the reference input for the current loop is set to the reference current generator by the $mode$ signal. During this mode transfer, the genset should not be loaded suddenly. To achieve smooth transition of the positive sequence current from the BESS to the genset, the positive sequence reference current of the BESS is changed slowly. This current change from the BESS to the genset can be observed in Fig. 4.16(b), while the load is not affected at all by this transition. Besides, the positive sequence current component affect the q-axis current for the three phases of the BESS as shown in Fig. 4.17, which reduces to the initial value shown in between $t = 10$ s and $t = 15$ s. The MSTS finds the steady state condition by monitoring the frequency and magnitude of the PCC voltage of the mini-grid system. When steady state is reached, the MSTS makes $g_{f2s} = 0$ at $t = 48.05$ s ending the transition process.

It should be mentioned that, since the BESS provides the reactive power of the mini-grid system in genset support mode, the magnitude of the PCC voltage remains at the rated (no-load) value. Also, during the grid forming mode, the voltage is maintained at the rated value. Therefore, the magnitude of the PCC voltage almost remains the same during operation in either mode or during the transition between the modes as shown in Fig. 4.15.

4.5 Summary of Chapter 4

A multi-functional control system of a BESS for a variable frequency diesel hybrid mini-grid with high penetration of PV and highly unbalanced loads has been presented in this chapter. In the genset support mode, the BESS provides load balancing, reactive power compensation and active power control of the genset. Therefore, the diesel genset operates in balanced condition within a desired power range with UPF and high efficiency. In this way, the BESS avoids the impact of unbalanced operation and carbon build up in the diesel engine which in turn also reduces operational and maintenance cost of the diesel genset. Due to the reactive power compensation by the BESS, the diesel genset can use most of its capacity for active power control in the mini-grid system. Again, in cases during the net low load of the mini-grid system due to the high supply of RESs and/or low load consumption, the BESS operates as grid forming unit while the genset is shut-down. In this mode, the BESS provides balanced regulated voltages to the mini-grid distribution system, even when supplying power in two phases and absorbing in the other one, due to the presence of unbalanced loads and renewable generation. The BESS employed a frequency adaptive emulation based per-phase dq-control strategy to obtain zero error in steady-state and fast dynamic response for the output voltage/current. During the grid forming mode, the BESS employed the cascaded control scheme to provide balanced regulated voltage across the unbalanced distribution system, while during the genset support mode, it employs only the inner current loop to provide the desired compensation currents of the mini-grid.

In order to define the operating mode of the BESS in the diesel hybrid mini-grid and to make smooth transitions between the operating modes, the MSTTS module has been

proposed in this chapter. It generates several control signals to choose the operating mode of the BESS, control the genset breaker and coordinate the smooth transition between the modes. It ensures slow loading/unloading of the genset during the transition processes. Besides, the synchronization of the BESS with the genset and the disconnection of the genset from the mini-grid system are done by the proposed PLL+ICA module; the control signals generated by the MSTs are used to perform these processes. The proposed PLL+ICA module tracks the PCC voltage during the genset support mode and works as an oscillator to provide the desired mini-grid voltage during the grid forming mode. For this purpose, it provides/extracts the proper phase angle, angular frequency and the reference voltage for the per-phase dq controllers and the reference current generator (in the genset support mode). It also ensures minimal disturbance at the PCC voltages during the transitions.

The effectiveness of the proposed multi-functional control scheme of the BESS operating in variable frequency diesel hybrid mini-grid has been verified by simulation. The results are presented to justify the operation of the BESS in diesel hybrid mini-grid in order to achieve the objectives as stated in the beginning of this thesis.

CHAPTER 5

CONCLUSION

5.1 Summary

The main focus of this Ph.D. thesis is on diesel based hybrid mini-grids. A brief background on diesel hybrid mini-grids was provided, discussing the main operation (fuel)/maintenance costs and power quality issues in the system. Regarding operation/maintenance costs, in diesel hybrid mini-grids, the highly variable residential load characteristics in conjunction with non-dispatchable RETs makes gensets operate at low load conditions more often, what reduces the efficiency and can cause carbon build-up in the diesel engine. In terms of power quality, unbalanced operation of the diesel genset is the main concern in the system. A BESS can be adopted to mitigate the above mentioned issues. However, it requires a suitable control strategy to operate as an unbalanced unit both in genset support and grid forming modes. A means for achieving a smooth transition between the two modes of the BESS is also necessary. Besides, a fast acting current control loop for single-phase PV inverters interfaced to utility or microgrid/mini-grid system as well as three-phase BESS in hybrid mini-grids, even for operation with variable frequency is important for dynamic operation of the system. Some possible solutions for these problems were assessed and proposed in this thesis.

In order to reduce operating cost, fuel consumption and environmental impact of diesel genset, roof-top type PVs are usually incorporated into the mini-grid using current controlled single-phase VSIs to supply part of the load. The conventional single-phase

vector current control strategy can provide regulated current to the fixed frequency grid but has some limitations, i.e., slow dynamic response, unsuitable for variable frequency mini-grid system, etc. Therefore, a new vector (dq) current control strategy for single-phase inverters was presented in this thesis which was based on a fictive axis circuit emulation and provided regulated current with high dynamic performance, like its three-phase counterpart, and was also capable of operating in variable frequency mini-grid systems. Simulation and experimental results were presented to justify the performance of the proposed vector current control technique. This newly developed control strategy also served as the basis for the proposed frequency adaptive per-phase vector control strategy of three-phase inverter operating with unbalanced system.

Stand-alone hybrid mini-grid systems typically present three-phase unbalanced distribution systems with single-phase and three-phase loads and renewable energy sources. Besides, frequency variation is commonly used for active power sharing in the mini-grid system. Therefore, a BESS system with an appropriate control strategy should be capable of operating with unbalance voltage/current in the variable frequency diesel hybrid mini-grid system in both genset support and grid forming modes. In this regard, this Thesis presented a new frequency adaptive per-phase dq control strategy of three-phase grid forming battery inverter for operation with unbalanced loads. The conventional control strategies of grid forming battery inverters usually employ symmetrical components calculators, which are implemented using filters. However, the dynamics of these filters are usually neglected in the design of controllers which results in slow dynamic response. Besides, these filters were usually designed for operation with a specific frequency. Therefore, these techniques are not suitable for operation in variable

frequency mini-grids. The proposed per-phase dq control strategy employs fictive axis circuit emulation in the inner current loop and frequency adaptive SOGI in the outer voltage loop to obtain the orthogonal components. As a result, the proposed per-phase control strategy is fast and frequency adaptive, with zero error in steady-state unlike the conventional control methods. The use of cascaded control loops also allowed such system to be used as BESS in a three-phase diesel hybrid mini-grid system.

For a three-phase three-wire system, a per-phase dq controlled three-leg VSI was used to indirectly regulate the positive sequence component of the output voltage and cancel the negative sequence voltage drop on the inverter output filter. Recall that the zero sequence components do not appear in three-wire systems. Then, the research work focused on three-phase four-wire systems, which provide more flexibility for loads and DGs in terms of voltage levels. It was shown that the control scheme devised for the three-wire system can also be used with a Δ -Y transformer in the output of the inverter. Although the zero sequence component in the secondary of the transformer is not reflected to the line current of the Δ windings, the phase shift introduced by the transformer was taken into account in the proposed regulation of the output voltage with the three-leg VSI currents. Finally, the per-phase control strategy was also adapted for use in the more flexible and performing four-leg inverter. In this case, a new coupled fictive axis circuit emulation for the inner current loop was proposed. The superior performance of the proposed per-phase control strategies for the grid forming inverters, with respect to the conventional techniques, was demonstrated by means of simulation and experimental studies under severe load unbalance conditions.

Finally, a complete multi-functional control system of a BESS for a three-phase variable frequency diesel hybrid mini-grid with high penetration of PVs and highly unbalanced loads was presented in this thesis. The BESS operated mainly in two modes; genset support mode and grid forming mode. In the genset support mode, when the genset formed the grid, the BESS was operated as a three-phase independently controllable current source; it balanced the load, by injecting the negative sequence of the load current, provided load reactive power, so that the genset operates with UPF, supplied the reactive current for the output filter capacitors of the BESS and controlled active power so as to provide minimum loading for the genset to avoid carbon build up and supplement it under peak load conditions. Therefore, the diesel genset operated in balanced condition within a desired power range with UPF and high efficiency, thus avoiding the impact of unbalanced operation and carbon build up in the diesel engine. Due to the reactive power compensation by the BESS, the diesel genset could use most of its capacity for active power supply in the mini-grid system.

Again, during the time when the net load of the mini-grid system was low, due to the high penetration of PVs and/or low load consumption, the genset could be shut-down while the BESS operated as grid forming unit. In this mode, the BESS acted as three-phase controllable voltage source and provided balanced regulated voltages to the highly unbalanced mini-grid distribution system. The control strategy of the BESS was required to provide fast dynamic response for the output voltage/current with zero error in steady-state and should also be capable of working in the variable frequency diesel hybrid mini-grid. Therefore, the proposed frequency adaptive per-phase dq control strategy with cascaded control loops was employed for the BESS. During the grid forming mode, the

BESS employed the cascaded control scheme to provide balanced regulated voltage across the unbalanced distribution system. While during the genset support mode, the proposed external reference current generator provided the reference current for the BESS and it employed only the inner current loop to provide this desired compensation currents for the diesel hybrid mini-grid.

Moreover, an approach for executing the transition of one operating mode to another in a smooth way was desired. This and other management tasks were carried out by the proposed Mode Selection and Transition System (MSTS) module. This module generated several control signals to define the operating mode of the BESS in the diesel hybrid mini-grid, control the genset breaker and coordinate the smooth transition between the modes. It also ensured slow loading/unloading of the genset during the transition processes. The synchronization of the BESS with the genset for transition from grid forming to genset support mode and the disconnection process of the genset from the mini-grid system during genset support to grid forming mode were done by a proposed PLL+ICA module; the control signals generated by the MSTS were used to perform these processes. Detailed techniques were developed in this thesis to achieve the desired smooth transitions between the modes.

For proper functionality of the per-phase dq controllers, external reference current generator block and MSTS module of the BESS, some variables were required. The per-phase dq controllers required the phase angle, angular frequency and reference q-axis voltage in both modes and also during the transitions. The external reference current generator also used these quantities to generate the reference current in the genset support mode. Besides, angular frequency and amplitude of the PCC voltage were also used by

the MSTS module to initiate the steps during the transition processes between the modes. These quantities were generated or extracted by the proposed PLL+ICA module. It acted as a PLL during the genset support mode and extracted the required variables. During the grid forming mode, it acted as an oscillator and generated these variables for the desired output voltage across the distribution system. Besides, the proposed control strategy for this block provided these variables to achieve smooth transitions, so that the load connected to the mini-grid did not experience large transient in their supply voltage.

5.2 Suggestions for Future Work

Some suggestions for future studies related to the concepts developed in this thesis are presented below.

5.2.1 Analysis of Energy Management for the BESS Based Diesel Hybrid Mini-grid

A more elaborate energy management system for the diesel hybrid mini-grid system could be developed. For this regard the following issues could be considered.

- A more detail model of an appropriate battery could be adopted in the dc side of the BESS. Therefore the SOC information can be directly included in the energy management system,
- Typical unbalanced load profile with renewable energy generation for the diesel hybrid mini-grid system should be collected and considered for the energy management system, etc.

The energy management system would have information about the SOC of the battery and forecasted net load of the distribution system, therefore, would be able to decide the operating mode of the BESS more efficiently. Besides, the load profile will also facilitate to size the battery and the inverter system used in the BESS.

5.2.2 Further Investigation of Power Quality Issues in the Diesel Hybrid Mini-grid

The control system of the BESS could be further investigated for more power quality issues in the diesel hybrid mini-grid, i.e., harmonic compensation for non-linear loads, frequency improvement during the transients of the mini-grid system, etc. In case of non-linear loads connected to the mini-grid, the BESS could supply the harmonic components in the genset support mode and compensate for the effects of harmonic at the PCC voltage in the grid forming mode. For small diesel dominated hybrid mini-grid systems, the kinetic energy stored in the rotating machines is small, which leads to larger and faster frequency variations following a sudden power mismatch due to load or PV power variations. This transient variation of frequency in the mini-grid system can be improved by adopting virtual inertia in the control system of the BESS.

5.2.3 Fault Study of the BESS Based Diesel Hybrid Mini-grid

The impact of different faults in the mini-grid system could be assessed. This could include the performance analysis of the system during both modes. Depending on this analysis, appropriate protection features could be adopted in the BESS system.

5.2.4 Impact of Secondary Controllable Loads

Load management is an interesting option for diesel hybrid mini-grid systems. Controllable secondary loads, such as water heaters, water pumps, ice making plants, etc., can be turned on or off without major issues for the consumers and so can be dispatched to balance power generation and consumption in the mini-grid. In the absence of dedicated fast communication link for dispatch, these loads can be equipped to automatically react, turning on-off or even changing the amount of power they consume

as a function of the mini-grid frequency. The impact of these loads could be assessed for the proposed BESS based diesel hybrid mini-grid system.

5.2.5 Alternative Options for Energy Storage System

Ideal battery was considered in the dc side of the three-phase inverter in this Thesis. The requirement for this storage unit to operate in the considered diesel hybrid mini-grid system was to have bidirectional power flow capability with fast dynamic response. Therefore, other alternative storage units or combination of source and storage could be assessed; e.g., one alternative could be to analyze a system composed of fuel cell (FC), ultracapacitor (UC) and electrolyzer. The FC can provide power but cannot store it and also the response is slow. Therefore UC can supply/absorb power during the transient condition. The electrolyzer would be used for storage purposes, generating the fuel (hydrogen) required by the FC.

BIBLIOGRAPHY

- [1] H. Farhangi, "The Path of the Smart Grid," *IEEE Power and Energy Magazine*, vol. 8, No. 1, pp. 18-28, 2010.
- [2] G. M. Masters, *Renewable and Efficient Electric Power Systems*. Hoboken, NJ: John Wiley & Sons, 2004.
- [3] N. Hatziargyriou, H. Asano, R. Iravani, and C. Marnay, "Microgrids," *IEEE Power and Energy Magazine*, vol. 5, No. 4, pp. 78-94, 2007.
- [4] F. Katiraei, R. Iravani, N. Hatziargyriou, and A. Dimeas, "Microgrids Management," *IEEE Power and Energy Magazine*, vol. 6, No. 3, pp. 54-65, 2008.
- [5] S. Pelland, D. Turcotte, G. Colgate, and A. Swingler, "Nemiah Valley Photovoltaic-Diesel Mini-Grid: System Performance and Fuel Saving Based on One Year of Monitored Data," *IEEE Transactions on Sustainable Energy*, vol. 3, No. 1, pp. 167-175, 2012.
- [6] K. Mauch, G. Bopp, M. Vandenberg, and J.-C. Marcel, "PV Hybrids in Mini-Grids - New IEA PVPS Task 11," in *Proceeding of 17th Photovoltaic Solar Energy Conference*, Fukuoka, Japan, pp. 1-4, 2007.
- [7] L. A. C. Lopes, F. Katiraei, K. Mauch, M. Vandenberg, and L. Arribas, "PV Hybrid Mini-grids: Applicable Control Methods for Various Situations," International Energy Agency (IEA) : Photovoltaic Power Systems (PVPS) Programme, IEA-PVPS T11-07:2012, 2012.
- [8] P. Kundur, N. J. Balu, and M. G. Lauby, *Power System Stability and Control*. New York: McGraw-Hill, 1994.

- [9] B. Wichert, "PV-Diesel Hybrid Energy Systems for Remote Area Power Generation — A Review of Current Practice and Future Developments," *Renewable and Sustainable Energy Reviews*, vol. 1, No. 3, pp. 209-228, 1997.
- [10] J. Ayoub and L. D. Bailey, "Photovoltaic Technology Status and Prospects - Canadian Annual Report 2007," CANMET Energy Technology Centre - Varennes, CETC Number 2008-027 / 2008-08-13, 2008.
- [11] F. Katiraei, D. Turcotte, A. Swingler, and J. Ayoub, "Modeling and Dynamic Analysis of a Medium Penetration PV-Diesel Mini-Grid System," presented at the *4th European Conference on PV-Hybrid and Mini-Grid*, Greece, 2008.
- [12] L. M. Tolbert, W. A. Peterson, T. J. Theiss, and M. B. Scudiere, "Gen-sets," *IEEE Industry Applications Magazine*, vol. 9, No. 2, pp. 48-54, 2003.
- [13] Caterpillar Inc., "Caterpillar® Marine Auxiliary Engine 3512," TMI Reference No.: DM 1896-07 (6-15-01), 2001.
- [14] R. Pena, R. Cardenas, J. Proboste, J. Clare, and G. Asher, "Wind-Diesel Generation Using Doubly Fed Induction Machines," *IEEE Transactions on Energy Conversion*, vol. 23, No. 1, pp. 202-214, 2008.
- [15] Cummins Inc., "Generator-Drive Engine Exercising," Cummins Application Engineering Bulletin AEB 10.17, January 2004.
- [16] R. Tonkoski, L. A. C. Lopes, and D. Turcotte, "Active Power Curtailment of PV Inverters in Diesel Hybrid Mini-grids," in *Proceeding of 2009 IEEE Electrical Power & Energy Conference (EPEC)*, pp. 1-6, 22-23 Oct., 2009.

- [17] N. C. Scott, D. J. Atkinson, and J. E. Morrell, "Use of Load Control to Regulate Voltage on Distribution Networks with Embedded Generation," *IEEE Transactions on Power Systems*, vol. 17, No. 2, pp. 510-515, 2002.
- [18] Y. W. Li, D. M. Vilathgamuwa, and P. C. Loh, "A Grid-Interfacing Power Quality Compensator for Three-Phase Three-Wire Microgrid Applications," *IEEE Transactions on Power Electronics*, vol. 21, No. 4, pp. 1021-1031, 2006.
- [19] M. W. Davis, R. Broadwater and J. Hambrick, "Modeling and Testing of Unbalanced Loading and Voltage Regulation," Joint Project from DTE Energy Company, Electrical Distribution Design Inc., Virginia Polytechnic Institute and State University, and National Renewable Energy Laboratory (U.S.), (2007).
- [20] "IEEE Standard for Interconnecting Distributed Resources With Electric Power Systems," *IEEE Standard 1547-2003*, pp. 1-16, 2003.
- [21] "Voltage Characteristics of Electricity Supplied by Public Distribution Systems," *EN 50160:2000*.
- [22] J. M. Guerrero, J. Matas, L. G. de Vicuna, M. Castilla, and J. Miret, "Wireless-Control Strategy for Parallel Operation of Distributed-Generation Inverters," *IEEE Transactions on Industrial Electronics*, vol. 53, No. 5, pp. 1461-1470, 2006.
- [23] B. Singh, A. Adya, A. P. Mittal, and J. R. P. Gupta, "Application of Battery Energy Operated System to Isolated Power Distribution Systems," in *Proceeding of 7th IEEE International Conference on Power Electronics and Drive Systems (PEDS '07)*, pp. 526-532, 27-30 Nov., 2007.

- [24] F. Shahnia, R. Majumder, A. Ghosh, G. Ledwich, and F. Zare, "Operation and Control of a Hybrid Microgrid Containing Unbalanced and Nonlinear Loads," *Electric Power Systems Research*, vol. 80, No. 8, pp. 954-965, 2010.
- [25] B. Singh and S. Sharma, "Design and Implementation of Four-Leg Voltage-Source-Converter-Based VFC for Autonomous Wind Energy Conversion System," *IEEE Transactions on Industrial Electronics*, vol. 59, No. 12, pp. 4694-4703, 2012.
- [26] S. J. Chiang, S. C. Huang, and C. M. Liaw, "Three-Phase Multifunctional Battery Energy Storage System," *IEE Proceedings of Electric Power Applications*, vol. 142, No. 4, pp. 275-284, 1995.
- [27] B. Singh, J. Solanki, A. Chandra, and K. A. Haddad, "A Solid State Compensator with Energy Storage for Isolated Diesel Generator Set," in *Proceeding of 2006 IEEE International Symposium on Industrial Electronics*, vol. 3, pp. 1774-1778, 9-13 July, 2006.
- [28] U. Borup, P. N. Enjeti, and F. Blaabjerg, "A New Space-Vector-Based Control Method for UPS Systems Powering Nonlinear and Unbalanced Loads," *IEEE Transactions on Industry Applications*, vol. 37, No. 6, pp. 1864-1870, 2001.
- [29] R. Cárdenas, R. Peña, P. Wheeler, J. Clare, and C. Juri, "Control of a Matrix Converter for the Operation of Autonomous Systems," *Renewable Energy*, vol. 43, No. 1, pp. 343-353, 2012.
- [30] M. Dai, M. N. Marwali, J. Jin-Woo, and A. Keyhani, "A Three-Phase Four-Wire Inverter Control Technique for a Single Distributed Generation Unit in Island Mode," *IEEE Transactions on Power Electronics*, vol. 23, No. 1, pp. 322-331, 2008.

- [31] E. Demirkutlu and A. M. Hava, "A Scalar Resonant-Filter-Bank-Based Output-Voltage Control Method and a Scalar Minimum-Switching-Loss Discontinuous PWM Method for the Four-Leg Inverter Based Three-Phase Four-Wire Power Supply," *IEEE Transactions on Industry Applications*, vol. 45, No. 3, pp. 982-991, 2009.
- [32] R. A. Gannett, J. C. Sozio, and D. Boroyevich, "Application of Synchronous and Stationary Frame Controllers for Unbalanced and Nonlinear Load Compensation in 4-Leg Inverters," in *Proceeding of 2002 IEEE Applied Power Electronics Conference and Exposition (APEC-2002)*, vol. 2, pp. 1038-1043, 2002.
- [33] C. Il-Yop, L. Wenxin, D. A. Cartes, E. G. Collins, and M. Seung-II, "Control Methods of Inverter-Interfaced Distributed Generators in a Microgrid System," *IEEE Transactions on Industry Applications*, vol. 46, No. 3, pp. 1078-1088, 2010.
- [34] H. Karimi, A. Yazdani, and R. Iravani, "Robust Control of an Autonomous Four-Wire Electronically-Coupled Distributed Generation Unit," *IEEE Transactions on Power Delivery*, vol. 26, No. 1, pp. 455-466, 2011.
- [35] K.-H. Kim, N.-J. Park, and D.-S. Hyun, "Advanced Synchronous Reference Frame Controller for Three-phase UPS Powering Unbalanced and Nonlinear Loads," in *Proceeding of IEEE 36th Power Electronics Specialists Conference (PESC '05)*, pp. 1699-1704, June, 2005.
- [36] A. Mohd, E. Ortjohann, N. Hamsic, W. Sinsukthavorn, M. Lingemann, A. Schmelter, and D. Morton, "Control Strategy and Space Vector Modulation for Three-Leg Four-Wire Voltage Source Inverters under Unbalanced Load Conditions," *IET Transactions on Power Electronics*, vol. 3, No. 3, pp. 323-333, 2010.

- [37] E. Ortjohann, A. Arias, D. Morton, A. Mohd, N. Hamsic, and O. Omari, "Grid-Forming Three-Phase Inverters for Unbalanced Loads in Hybrid Power Systems," in *Proceeding of IEEE 4th World Conference on Photovoltaic Energy Conversion*, vol. 2, pp. 2396-2399, May, 2006.
- [38] I. Vechiu, O. Curea, and H. Camblong, "Transient Operation of a Four-Leg Inverter for Autonomous Applications With Unbalanced Load," *IEEE Transactions on Power Electronics*, vol. 25, No. 2, pp. 399-407, 2010.
- [39] E. Ortjohann, A. Mohd, N. Hamsic, and M. Lingemann, "Design and Experimental Investigation of Space Vector Modulation for Three-Leg Four-Wire Voltage Source Inverters," in *Proceeding of 13th IEEE European Conference on Power Electronics and Applications (EPE '09)*, pp. 1-6, 8-10 Sept., 2009.
- [40] H.-S. Song and K. Nam, "Dual Current Control Scheme for PWM Converter under Unbalanced Input Voltage Conditions," *IEEE Transactions on Industrial Electronics*, vol. 46, No. 5, pp. 953-959, 1999.
- [41] Y. Suh, V. Tijeras, and T. A. Lipo, "A Control Method in dq Synchronous Frame for PWM Boost Rectifier under Generalized Unbalanced Operating Conditions," in *Proceeding of IEEE 33rd Annual Power Electronics Specialists Conference (PESC'02)*, vol. 3, pp. 1425-1430, 2002.
- [42] M. P. Kazmierkowski and L. Malesani, "Current Control Techniques for Three-Phase Voltage-Source PWM Converters: A Survey," *IEEE Transactions on Industrial Electronics*, vol. 45, No. 5, pp. 691-703, 1998.

- [43] D. N. Zmood, D. G. Holmes, and G. H. Bode, "Frequency-Domain Analysis of Three-Phase Linear Current Regulators," *IEEE Transactions on Industry Applications*, vol. 37, No. 2, pp. 601-610, 2001.
- [44] M. Reyes, P. Rodriguez, S. Vazquez, A. Luna, R. Teodorescu, and J. Carrasco, "Enhanced Decoupled Double Synchronous Reference Frame Current Controller for Unbalanced Grid-Voltage Conditions," *IEEE Transactions on Power Electronics*, vol. 27, No. 9, pp. 3934-3943, 2012.
- [45] I. Etxeberria-Otadui, U. Viscarret, M. Caballero, A. Rufer, and S. Bacha, "New Optimized PWM VSC Control Structures and Strategies Under Unbalanced Voltage Transients," *IEEE Transactions on Industrial Electronics*, vol. 54, No. 5, pp. 2902-2914, 2007.
- [46] L. Quan and P. Wolfs, "A Review of the Single Phase Photovoltaic Module Integrated Converter Topologies With Three Different DC Link Configurations," *IEEE Transactions on Power Electronics*, vol. 23, No. 3, pp. 1320-1333, 2008.
- [47] H. Akagi, "Active Harmonic Filters," *Proceedings of the IEEE*, vol. 93, No. 12, pp. 2128-2141, 2005.
- [48] M. M. Jovanovic and Y. Jang, "State-of-the-Art, Single-Phase, Active Power Factor Correction Techniques for High Power Applications - An Overview," *IEEE Transactions on Industrial Electronics*, vol. 52, No. 3, pp. 701-708, 2005.
- [49] F. Blaabjerg, R. Teodorescu, M. Liserre, and A. V. Timbus, "Overview of Control and Grid Synchronization for Distributed Power Generation Systems," *IEEE Transactions on Industrial Electronics*, vol. 53, No. 5, pp. 1398-1409, 2006.

- [50] R. R. Pereira, C. H. da Silva, L. E. M. Cavalcanti, L. E. B. da Silva, G. Lambert-Torres, S. U. Ahn, J. O. P. Pinto, and B. K. Bose, "A Simple Full Digital Adaptive Current Hysteresis Control with Constant Modulation Frequency for Active Power Filters," in *Proceeding of 42nd IEEE IAS Annual Meeting*, pp. 1644-1648, 23-27 Sept., 2007.
- [51] D. N. Zmood and D. G. Holmes, "Stationary Frame Current Regulation of PWM Inverters with Zero Steady-State Error," *IEEE Transactions on Power Electronics*, vol. 18, No. 3, pp. 814-822, 2003.
- [52] R. Teodorescu, F. Blaabjerg, M. Liserre, and P. C. Loh, "Proportional Resonant Controllers and Filters for Grid-Connected Voltage-Source Converters," *IEE Proceedings of Electric Power Applications*, vol. 153, No. 5, pp. 750-762, 2006.
- [53] T. Erika and D. G. Holmes, "Grid Current Regulation of a Three-Phase Voltage Source Inverter with an LCL Input Filter," *IEEE Transactions on Power Electronics*, vol. 18, No. 3, pp. 888-895, 2003.
- [54] R. Zhang, M. Cardinal, P. Szczesny, and M. Dame, "A Grid Simulator with Control of Single-Phase Power Converters in D-Q Rotating Frame," in *Proceeding of IEEE 33rd Annual Power Electronics Specialists Conference (PESC'02)*, vol. 3, pp. 1431-1436, 2002.
- [55] U. A. Miranda, M. Aredes, and L. G. B. Rolim, "A DQ Synchronous Reference Frame Current Control for Single-Phase Converters," in *Proceeding of IEEE 36th Power Electronics Specialists Conference (PESC '05)*, pp. 1377-1381, June, 2005.
- [56] J. Salaet, S. Alepuz, A. Gilabert, and J. Bordonau, "Comparison between Two Methods of DQ Transformation for Single Phase Converters Control. Application to

- a 3-Level Boost Rectifier," in *Proceeding of IEEE 35th Annual Power Electronics Specialists Conference (PESC'04)*, vol. 1, pp. 214-220, 20-25 June, 2004.
- [57] R.-Y. Kim, S.-Y. Choi, and I.-Y. Suh, "Instantaneous Control of Average Power for Grid Tie Inverter using Single Phase D-Q Rotating Frame with All Pass Filter," in *Proceeding of 30th Annual Conference of IEEE Industrial Electronics Society (IECON 2004)*, vol. 1, pp. 274-279, 2-6 Nov., 2004.
- [58] B. Saritha and P. A. Jankiraman, "Observer Based Current Control of Single-Phase Inverter in DQ Rotating Frame," in *Proceeding of IEEE International Conference on Power Electronics, Drives and Energy Systems (PEDES '06)*, pp. 1-5, 12-15 Dec., 2006.
- [59] A. Roshan, R. Burgos, A. C. Baisden, F. Wang, and D. Boroyevich, "A D-Q Frame Controller for a Full-Bridge Single Phase Inverter Used in Small Distributed Power Generation Systems," in *Proceeding of 22nd Annual IEEE Applied Power Electronics Conference (APEC 2007)*, pp. 641-647, Feb. 25 - Mar. 1, 2007.
- [60] D. Dong, T. Thacker, R. Burgos, D. Boroyevich, and F. Wang, "On Zero Steady-State Error Voltage Control of Single-Phase PWM Inverters with Different Load-Types," *IEEE Transactions on Power Electronics*, vol. 26, No. 11, pp. 3285 - 3297, 2011.
- [61] N. A. Ninad and L. A. C. Lopes, "A Vector-Controlled Single-Phase Voltage Source Inverter Based Grid Interface Suitable for Variable Frequency Operation in Autonomous Microgrids," *Electric Power Components and Systems*, vol. 40, No. 11, pp. 1266-1284, 2012.

- [62] N. A. Ninad, L. A. C. Lopes, and A. Rufer, "A Vector Controlled Single-Phase Voltage Source Inverter with Enhanced Dynamic Response," in *Proceeding of 2010 IEEE International Symposium on Industrial Electronics (ISIE 2010)*, pp. 2891-2896, 4-7 July, 2010.
- [63] N. A. Ninad and L. A. C. Lopes, "Per-Phase Vector Control Strategy for a Four-Leg Voltage Source Inverter Operating with Highly Unbalanced Loads in Stand-Alone Hybrid Systems," submitted in *Electrical Power and Energy Systems*, IJEPES-D-12-00893, 2012. (under review)
- [64] N. A. Ninad and L. A. C. Lopes, "Per-Phase Vector (dq) Controlled Three-Phase Grid-Forming Inverter for Stand-Alone Systems," in *Proceeding of 2011 IEEE International Symposium on Industrial Electronics (ISIE)*, pp. 1626-1631, 27-30 June, 2011.
- [65] N. A. Ninad and L. A. C. Lopes, "Unbalanced Operation of Per-Phase Vector Controlled Four-Leg Grid Forming Inverter for Stand-Alone Hybrid Systems," in *Proceeding of Annual IEEE Industrial Electronics Conference (IECON-2012)*, Montreal, QC, Canada, pp. 3500-3505, 25-28 October, 2012.
- [66] N. A. Ninad and L. A. C. Lopes, "Control of Δ -Y Transformer Based Grid Forming Inverter for Unbalanced Stand-Alone Hybrid Systems," in *Proceeding of 2012 IEEE Electrical Power & Energy Conference (EPEC-2012)*, London, ON, Canada, pp. 176-181, 10-12 October, 2012.
- [67] B. Bahrani, A. Rufer, S. Kenzelmann, and L. A. C. Lopes, "Vector Control of Single-Phase Voltage-Source Converters Based on Fictive-Axis Emulation," *IEEE Transactions on Industry Applications*, vol. 47, No. 2, pp. 831-840, 2011.

- [68] P. Liu, J. Xiong, Y. Kang, H. Zhang, and J. Chen, "Synchronous Frame Based Control Method Of Voltage Source Converter For Prototype Super-conducting Magnetic Energy Storage (SMES)," in *Proceeding of 3rd IEEE International Power Electronics and Motion Control Conference (IPEMC)*, vol. 2, pp. 537-541, 2000.
- [69] N. A. Ninad and L. A. C. Lopes, "A Low Power Utility Interactive Inverter for Residential PV generation with Small DC Link Capacitor," in *Proceeding of 3rd Canadian Solar Building Conference*, Fredericton, Canada, pp. 28-36, August, 2008.
- [70] F. Katiraei and M. R. Iravani, "Power Management Strategies for a Microgrid With Multiple Distributed Generation Units," *IEEE Transactions on Power Systems*, vol. 21, No. 4, pp. 1821-1831, 2006.
- [71] P. Rodriguez, A. Luna, I. Candela, R. Mujal, R. Teodorescu, and F. Blaabjerg, "Multiresonant Frequency-Locked Loop for Grid Synchronization of Power Converters Under Distorted Grid Conditions," *IEEE Transactions on Industrial Electronics*, vol. 58, No. 1, pp. 127-138, 2011.
- [72] P. Rodriguez, A. Luna, R. Munoz-Aguilar, I. Etxeberria-Otadui, R. Teodorescu, and F. Blaabjerg, "A Stationary Reference Frame Grid Synchronization System for Three-Phase Grid-Connected Power Converters Under Adverse Grid Conditions," *IEEE Transactions on Power Electronics*, vol. 27, No. 1, pp. 99-112, 2012.
- [73] R. Sebastian, "Modelling and Simulation of a High Penetration Wind Diesel System with Battery Energy Storage," *Electrical Power & Energy Systems*, vol. 33, No. 3, pp. 767-774, 2011.

- [74] M. Monfared and H. Rastegar, "Design and Experimental Verification of a Dead Beat Power Control Strategy for Low Cost Three Phase PWM Converters," *Electrical Power & Energy Systems*, vol. 42, No. 1, pp. 418-425, 2012.
- [75] M. N. Marwali and A. Keyhani, "Control of Distributed Generation Systems-Part I: Voltages and Currents Control," *IEEE Transactions on Power Electronics*, vol. 19, No. 6, pp. 1541-1550, 2004.
- [76] P. Li, B. Dan, K. Yong, and C. Jian, "Research on Three-Phase Inverter with Unbalanced Load," in *Proceeding of IEEE Applied Power Electronics Conference and Exposition (APEC '04)*, vol. 1, pp. 128-133, 2004.
- [77] D. Soto, C. Edrington, S. Balathandayuthapani, and S. Ryster, "Voltage Balancing of Islanded Microgrids using a Time-Domain Technique," *Electric Power Systems Research*, vol. 84, No. 1, pp. 214-223, 2012.
- [78] F. Zhang and Y. Yan, "Selective Harmonic Elimination PWM Control Scheme on a Three-Phase Four-Leg Voltage Source Inverter," *IEEE Transactions on Power Electronics*, vol. 24, No. 7, pp. 1682-1689, 2009.
- [79] N. A. Ninad and L. A. C. Lopes, "Per-Phase DQ Control of a Three-Phase Battery Inverter in a Diesel Hybrid Mini-grid Supplying Single-Phase Loads," in *Proceeding of 2011 IEEE International Conference on Industrial Technology (ICIT-2011)*, pp. 204-209, 14-16 March, 2011.
- [80] H. Kim and S. K. Sul, "Compensation Voltage Control in Dynamic Voltage Restorers by Use of Feed Forward and State Feedback Scheme," *IEEE Transactions on Power Electronics*, vol. 20, No. 5, pp. 1169-1177, 2005.

- [81] R. Zhang, V. H. Prasad, D. Boroyevich, and F. C. Lee, "Three-Dimensional Space Vector Modulation for Four-Leg Voltage-Source Converters," *IEEE Transactions on Power Electronics*, vol. 17, No. 3, pp. 314-326, 2002.
- [82] M. A. Perales, M. M. Prats, R. Portillo, J. L. Mora, J. I. Leon, and L. G. Franquelo, "Three-Dimensional Space Vector Modulation in abc Coordinates for Four-Leg Voltage Source Converters," *IEEE Power Electronics Letters*, vol. 1, No. 4, pp. 104-109, 2003.
- [83] J.-H. Kim and S.-K. Sul, "A Carrier-Based PWM Method for Three-Phase Four-Leg Voltage Source Converters," *IEEE Transactions on Power Electronics*, vol. 19, No. 1, pp. 66-75, 2004.
- [84] N.-Y. Dai, M. Wong, F. Ng, and Y. Han, "A FPGA-Based Generalized Pulse Width Modulator for Three-Leg Center-Split and Four-Leg Voltage Source Inverters," *IEEE Transactions on Power Electronics*, vol. 23, No. 3, pp. 1472-1484, 2008.
- [85] "IEEE Standard Test Procedure for Polyphase Induction Motors and Generators," *IEEE Standard 112*, 1991.
- [86] J. Rocabert, G. M. S. Azevedo, A. Luna, J. M. Guerrero, J. I. Candela, and P. Rodriguez, "Intelligent Connection Agent for Three-Phase Grid-Connected Microgrids," *Power Electronics, IEEE Transactions on*, vol. 26, No. 10, pp. 2993-3005, 2011.
- [87] M. Torres and L. A. C. Lopes, "Frequency Control Improvement in an Autonomous Power System: An application of Virtual Synchronous Machines," in *Proceeding of IEEE 8th International Conference on Power Electronics and ECCE Asia (ICPE & ECCE)*, pp. 2188-2195, May 30 - June 3, 2011.

LIST OF APPENDIX

Appendix-A : Diesel Genset Parameters

Table A.1. Parameters of Diesel Genset.

Rated capacity	31.5 kVA
Rated speed	1800 rpm
Rated voltage	460 V
Number of poles	4
Moment of inertia	1.2 kg.m ²
Droop factor (5%)	-7.5 kW/Hz
	-0.7667 V/kVAR
Friction losses coefficient	0.03 kg.m ² /s
Fuel injection time constant	0.2 s
Diesel engine delay	0.022 s
Speed controller (PI) parameters	0.025 – 0.4 s
Voltage controller (PI) parameters	1 – 10 s